MODELLING AND ECONOMIC ASSESSMENT OF MULTIPLE POWER ELECTRONIC BASED COMPENSATORS ALLOCATION IN ACTIVE POWER DISTRIBUTION NETWORKS

Vamsi Priya Goli

MODELLING AND ECONOMIC ASSESSMENT OF MULTIPLE POWER ELECTRONIC BASED COMPENSATORS ALLOCATION IN ACTIVE POWER DISTRIBUTION NETWORKS

A thesis submitted to
Indian Institute of Technology Guwahati
for the award of the degree of

DOCTOR OF PHILOSOPHY

by

Vamsi Priya Goli
(206102108)

under the guidance of

Dr. Sanjib Ganguly

DEPARTMENT OF ELECTRONICS AND ELECTRCAL ENGINEERING
INDIAN INSTITUTE OF TECHNOLOGY GUWAHATI
GUWAHATI - 781039, INDIA

January 2025

Certificate

This is to certify that the thesis entitled "**Modelling and economic assessment of multiple power electronic based compensators allocation in active power distribution networks**" submitted by **Vamsi Priya Goli** (206102108), to the Indian Institute of Technology Guwahati for the award of the degree of Doctor of Philosophy is a bona fide record of the research work done by her under my supervision. The contents of this thesis, in full or in parts, have not been submitted to any other Institute or University for the award of any degree or diploma.

Date:

Place: Guwahati

Dr. Sanjib Ganguly

Associate Professor

Dept. of Electronics and Electrical Engg.,

Indian Institute of Technology Guwahati,

Guwahati - 781 039, Assam, India.

Declaration

I certify that:

1. The work contained in this thesis is original and has been done by me under the guidance of my supervisor.
2. The work has not been submitted to any other Institute for any degree or diploma.
3. I have followed the guidelines provided by the Institute in preparing the thesis.
4. I have conformed to the norms and guidelines given in the Ethical Code of Conduct of the Institute.
5. Whenever I have used materials (data, theoretical analysis, figures, and text) from other sources, I have given due credit to them by citing them in the text of the thesis and giving their details in the references.

Date:

Place: Guwahati **Vamsi Priya Goli**

This Thesis is dedicated to

My Parents

Dr. Ravi Kumar Goli and Sunitha Goli

My Friend

Ratnakar Babu Bollipo

and

My Supervisor

Dr. Sanjib Ganguly

Acknowledgement

I would like to express my deepest gratitude to my supervisor, Dr. Sanjib Ganguly, for his invaluable guidance, support, and mentorship throughout my research journey. His insightful feedback and timely advice have been crucial in shaping the direction of my work and helping me overcome the challenges of my doctoral studies.

I am also sincerely thankful to the Indian Institute of Technology Guwahati for providing the financial, academic, and technical support that made this research possible. I extend my heartfelt thanks to the Head of the Department of Electronics and Electrical Engineering for facilitating the resources necessary to carry out my work.

I extend my gratitude to Dr. Sisir Kumar Nayak, Dr. Chandan Kumar, and Dr. Ravindranath Adda for their invaluable insights and constructive criticism as members of my Doctoral Committee. Additionally, I am deeply grateful to the entire faculty and staff, especially those in the Power & Control Lab-II, for their encouragement and assistance throughout this journey.

I would also like to thank Mr. Ratnakar Babu Bollipo for his constant support and encouragement. His unwavering presence during critical moments played a crucial role in the development and refinement of my work. I am also profoundly grateful to my friends, B. Srikanth and Y. Satya Narayana, for their support and encouragement throughout my journey.

I am deeply grateful to my parents, Dr. Ravi Kumar Goli and Mrs. Sunitha Goli, whose unconditional love and belief in me have been a constant source of inspiration.

Their unwavering support and the freedom they provided for me to pursue my aspirations have been truly invaluable.

I would like to express my gratitude to my friends from the National Institute of Technology Goa for their love and encouragement throughout this journey. I am also profoundly thankful to all my family members and friends for their unwavering support, patience, and understanding.

Date:

Place: Guwahati

Vamsi Priya Goli

Abstract

The integration of photovoltaic (PV) systems into distribution networks has been increased due to government policies promoting renewable energy schemes. However, this increased integration presents challenges, such as over-voltage and current harmonics. The thesis explores the strategic placement of power electronic (PE) based compensators in PV-rich power distribution networks to address these issues and enhance overall system performance.

The optimal placement of these compensators significantly reduces energy losses and improves the voltage profile of the network. The modeling and allocation planning of Series Compensators (SECs) and Shunt Compensators (SHCs) are presented to mitigate voltage sag/swell and current harmonics, respectively. In addition to the technical aspects, the thesis conducts a comprehensive economic evaluation of multiple SHC allocations in highly PV-integrated networks. The solution strategy chosen is Particle Swarm Optimization (PSO), meta-heuristics-based optimization algorithm. Over a 20-year planning horizon, profit maximization is performed by considering factors, such as PV integration, load growth, seasonal load variations, and intermittent PV generation profiles.

An operational optimization approach is proposed to determine the time-varying reactive power injection set-points for SHCs, considering varying load and PV generation scenarios. This approach shows that injecting time-varying reactive power into the networks reduces the annual energy loss costs. Due to the time-varying nature of load and PV generation, the objective function for annual energy loss costs involves many variables. A novel multi-swarm surrogate-assisted PSO algorithm has been developed to address this high-dimensional optimization problem. This new PSO variant combines the Gaussian Process Regression (GPR) technique with PSO in a multi-swarm framework, utilizing parallel computing. This approach demonstrates substantial capability in solving high-dimensional optimization problems.

An optimization approach is proposed to maximize PV hosting capacity (PVHC) and minimize energy losses. PVHC is defined as the maximum PV capacity a network can accommodate without degrading its operational performance. This process involves optimizing the time-varying reactive power injection set-points for SHCs and the time-varying charging and discharging set points for Battery Energy Storage Systems (BESS) in response to time-varying load and PV generation. A multi-objective planning approach is developed to address the conflicting objectives of maximizing PVHC and minimizing energy loss. This approach simultaneously optimizes these two objectives using the Strength Pareto Evolutionary Algorithm-2 (SPEA2)-based Multi-Objective GPR assisted PSO (SPEA2-MO-GPRS-PSO). The solution provides a set of options from which utilities can choose based on their preferences. Additionally, the proposed SEC and PV-integrated SHC (PV-SHC) allocation aims to minimize network power losses, the rating of compensators, and the number of undervoltage nodes. A multi-objective planning approach is also developed to optimally allocate SEC and PV-SHCs in distribution networks using the SPEA2-MO-GPRS-PSO.

The proposed planning models are validated using the 33-bus and 69-bus test distribution networks.

Contents

List of Acronyms

AEL	Annual energy losses
ALO	Ant lion optimization
aRBF-NFO	Radial basis functions neighborhood field optimizer
BESS	Battery energy storage system
BESS-SHC	BESS integrated SHC
BFO	Bacterial foraging optimization
CPD	Custom power devices
CSA	Cuckoo search algorithm
DG	Distributed generation
DG-CPD	DGintegrated CPD
DGCC	DGs connected to the DC link of CPDs
DGCNC	DGs and CPDs are not directly connected
DGHC	DG hosting capacity
DNO	Distribution Network Owner
DP	Dynamic programming

ESS	Energy storage system
FBS	Forward-backward Sweep
GA	Genetic algorithm
GPR	Gaussian process regression
IF	Inflation rate
IR	Interest rate
LP	Linear programming
LSA	Lightning search algorithm
LSADE	Lipschitz surrogate-assisted differential evolution
MGP-SLPSO	Multiobjective infill criterion driven gaussian process-assisted SL-PSO
MILP	Mixed-integer LP
MINLP	Mixed-integer NLP
MNRE	Ministry of new and renewable energy
MO-GPRS-PSO	Multi-objective GPR surrogate assisted PSO
MSCPSO	Multi-swarm self-adaptive and cooperative PSO
NLP	Non-linear programming
NSGA-II	Non-dominated sorting genetic algorithm-II
OM	Operational and maintenance
PAF	Pareto approximate front

Parallel-MS-GPRS-PSO	Parallel multi-Swarm GPR surrogate-based PSO
PE	Power electronics
PSO	Particle swarm optimization
PSO-GPR	PSO with GPR surrogate model
PSO-LDIW	PSO with linearly decreasing inertia weight
PV	Photovoltaic
PVHC	PV hosting capacity
PV-SHC	PV-integrated SHC
PWF	Present worth factor
QP	Quadratic programming
SACOSO	Surrogate-assisted cooperative swarm optimization
SAEA-HAS	Surrogate-sssisted evolutionary algorithm with hierarchical surrogate technique and adaptive infill strategy
SOC	State of charge
SEC	Series compensator
SHC	Shunt compensator
SL-PSO	Social learning-based PSO
SPEA2	Strength pareto evolutionary algorithm-2
SPEA2-MO-GPRS-PSO	SPEA2 based multi-objective GPR surrogate assisted PSO
THD	Total harmonic distortion

TLBO	Teaching–learning based optimization
VA	Volt-ampere
VAr	Volt-ampere reactive
VSM-PSO	Variable surrogate model-based PSO
WE	Wind energy

List of Symbols

δ	Phase angle between V_{S} and V_{R}
$(AEL)_{BCS}$	AEL for base-case distribution network
$(AEL)_{wPS}$	AEL obtained after placing PV and SHC
$(IN)_{OM}^{PV}$	Total operation and maintenance cost of PV system (in \$)
$(IN)_{PV}$	Total investment of PV (in \$)
$(IN)_{SHC}$	Total investment of SHC (in \$)
$(Q_{sh})_{total}$	Total reactive power rating of the SHCs
$(RP_{PV})_n$	Real power produced by PV in n^{th} year
$(S_{sh})_{total}$	Total VA rating of the SHCs
$(Saved\ AEL)_n$	Saved AEL in n^{th} year
$\aleph$	Set of all downstream buses
β^{T_p}	Present worth factor for planning period 'T_p'
β_n	Present worth factor for n^{th} year
δ''	Phase angle between V_{S} and V_{R} after compensation during the sag condition

δ'	Phase angle between V_{S} and V_{R} before compensation during the sag condition
η	set of daily load and PV generation profiles
$\mathcal{A}$	Set of all buses in the distribution network
$\mathcal{I}$	Set of all BESS units in the distribution network
$\mathcal{Z}$	set of all branches in the distribution network
ϕ_L	Phase angle between V_{L} and I_{L}
CUF_{PV}	Capacity utilisation factor of PV
θ_L	Phase angle between I_L and I_{sh}
$\varnothing$	Phase angle between V_{S} and V_{R} at the location of the SEC
C_{EL}	Cost of energy loss (in \$/kWh)
$C_{initial}^{PV}$	Initial cost of PV unit (in \$/kW)
C_{OM}^{PV}	Operation and maintenance cost of PV unit (in \$/kW/year)
C_{P}^{SHC}	Initial cost of SHC (in \$/KVA)
CS_{EL}	Cost savings obtained due to energy loss reduction (in \$)
EL_s	Daily energy losses for season 's'
EP_{PV}	Electricity price of PV power (in \$/kWh)
EP_{sl}	Energy price for load level l in season s
FR_{PV}	Financial returns obtained due to active power produced by PV (in \$)
H_S	Total number of hours in season s

I_{L}	Load current at the location of SHC
I_{S}	Sending end current at the location of SEC
$I_{\max}(ef,t)$	Thermal limit for branch ef in the distribution network at time t
I_{PV}	Current compensation by PV
I_L''	Line current compensated by PV-SHC
$I_L^{'}$	Line current at the location of SHC
I_L^{dis}	Distorted component of I_{L}
I_L^{fun}	Fundamental component of I_{L}
I_{mn}	Line current of branch mn
I_m	Load current at bus m
I_{sh}	Shunt compensating current injected by SHC
I_{sh}'	Shunt compensating current injected by PV-SHC
I_{sh}^{dis}	Distorted component of I_{sh}
I_{sh}^{fun}	Fundamental component of I_{sh}
K_{PV}	Fraction of line current provided by PV
L_{SHC_i}	Location of SHC_i
LC_n	Load curve for the n^{th} month
N_i	Binary variable that represents an undervoltage node, either 1 or 0
$P_i'(t)$	Modified real power demand at bus i and time t
$P_i(t)$	Real power demand at bus i and time t

P_L	Real power demand at load bus
P_{BCPL}	Real power of the base-case peak load in the distribution network
$P_{BESS(i)}(t)$	Real power provided/absorbed by BESS unit at bus i and time t
$P_{loss}(t)$	Real power losses in the distribution network at time t
P_m	Real power load at bus m
$P_{PV(i)}(t)$	Total real power provided by PV at bus i and time t
$P_{PV-SHC(i)}(t)$	Real power provided by PV-SHC at bus i and time t
P_{PV-SHC}	Real power rating of PV-SHC
$P_{PV}(t)$	Real power provided by PV units at time t
P_{PV}^{rating}	Total installed capacity of PV system
$P_{SS}(t)$	Real power provided by substation at time t
$PL_{ef(c)}$	Power losses on branch ef for scenario c
PL_{hl}	Real power losses at hour h and load level l
PV_i	Total capacity of PV units installed at bus i
$Q_i'(t)$	Modified reactive power demand at bus i and time t
$Q_i(t)$	Reactive power demand at bus i and time t
Q_L	Reactive power demand at load bus
$Q_{\text{SHC\_max(i)}}$	Maximum allowable reactive power injection limit of SHC_i
$Q_{loss}(t)$	Reactive power losses in the distribution network at time t
Q_m	Reactive power load at bus m

$Q_{PV-SHC(i)}(t)$	Reactive power provided by PV-SHC at bus i and time t
Q_{PV-SHC}	Reactive power rating of PV-SHC
Q_{sh_i}	Reactive power rating of SHC_i
$Q_{sh}(i)$	Reactive power provided by SHC_i
$Q_{sh(i)}(t)$	Reactive power supplied by SHC_i at time t
$Q_{SHC}(t)$	Reactive power provided by SHCs at time t
$Q_{SS}(t)(t)$	Reactive power provided by substation at time t
S_{se}	VA rating of SEC
S_P^{SHC}	Rating of SHC (in kVA)
S_{sh_i}	VA rating of SHC_i
SHC_i	i^{th} SHC
$SOC_{\max}$	Maximum allowable SOC of the BESS
$SOC_{\min}$	Minimum allowable SOC of the BESS
t_c	Time duration during scenario 'c'
t_{oh}	Operating hours of PV
THD_L	THD of I_{L}
THD_{sh}	THD of I_{sh}
V_{L}	Load voltage at the location of SHC
V_{R1}	Receiving end voltage after injecting voltage using SEC during healthy conditions

V_{R}	Receiving end voltage after injecting voltage using SEC during sag conditions
V'_{R}	Receiving end voltage without SEC during sag conditions
$V_{\mathrm{se}}^{\mathrm{hel}}$	Voltage injected by SEC during healthy condition
$V_{\mathrm{se}}^{\mathrm{sag}}$	Voltage injected by SEC during sag condition
V_{S}	Sending end voltage at the location of SEC
$V_i(t)$	Voltage at bus i and time t
V_{max}	Maximum allowable bus voltage of the distribution network
V_{min}	Minimum allowable bus voltage of the distribution network
Z_{mn}	Impedance of branch mn
$SOC_b(t_{ed})$	SOC of BESS b at the end of the day
$SOC_b(t_{sd})$	SOC of BESS b at the beginning of the day
$(IN)_{initial}^{PV}$	Total initial cost of PV system (in \$)

List of Figures

List of Tables

Chapter 1

Introduction and Literature Review

1.1 Introduction

The increasing demand for electricity rapidly depletes traditional energy sources, while continued reliance on fossil fuels significantly contributes to environmental degradation. As India's growth continues, its demand for energy and resources is projected to rise substantially. Energy use has doubled in the past 20 years and is expected to grow by at least another 25% by 2030 [1]. Transitioning to renewable energy is essential to meet these growing energy needs.

To promote sustainable energy and ensure a greener future, the Government of India has introduced a plan to integrate 450 GW of renewable energy capacity by 2030, including 140 GW of wind power and 280 GW of solar photovoltaic (PV) generation [1]. Over the past decade, due to India's policies, the country's solar installed capacity has significantly increased, growing from 160 MW in the financial year 2014-15 to 74,310 MW in 2023-24 [2]. However, as the world's most populous country with 1.42 billion people and a high population density, India faces challenges in securing vacant land for PV installations. Therefore, large-scale integration of rooftop PV systems, particularly at the distribution

network level, is essential [2].

To address these issues and to achieve the 280 GW target for PV integration, the Government of India has launched several initiatives. One notable scheme under the Ministry of New and Renewable Energy (MNRE) is the PM Surya Ghar: Muft Bijli Yojana, which promotes rooftop solar installations in rural areas and provides free electricity up to 300 units monthly for 10 million households. The scheme offers central financial assistance of 60% of the system cost for 2 kW installations and 40% for systems between 2 kW to 3 kW [3]. This policy is expected to reduce annual electricity costs by $7500 million while increasing renewable energy generation and reducing carbon emissions.

Rooftop solar PV systems are crucial in maximizing the use of limited land resources. These systems can connect to the local power grid or household loads, reducing grid dependency and easing the burden on the transmission and distribution system. Despite these advantages, high penetration of PVs into distribution networks can increase network power and energy losses. Therefore, it is crucial to determine the maximum PV capacity that a network can accommodate without compromising operational performance. This determination is known as PV hosting capacity (PVHC).

Various technologies and strategies are employed to manage these challenges effectively and ensure the reliable operation of distribution networks. The primary goal of distribution networks is to deliver high-quality power reliably, especially when integrating distributed generations (DGs), which can introduce additional challenges. Custom Power Devices (CPD) are integrated within DG-integrated distribution networks to deliver distortion-free and balanced electrical power [4]. These CPDs, based on Power Electronics (PE), are designed to mitigate voltage and current distortions. The CPDs in distribution networks include Series Compensators (SEC) and Shunt Compensators (SHC). The SEC is typically used to address voltage sags and swells [5]. Meanwhile, SHCs are connected in parallel with the system to provide Volt-Ampere reactive (VAr) support and mitigate current harmonics [6].

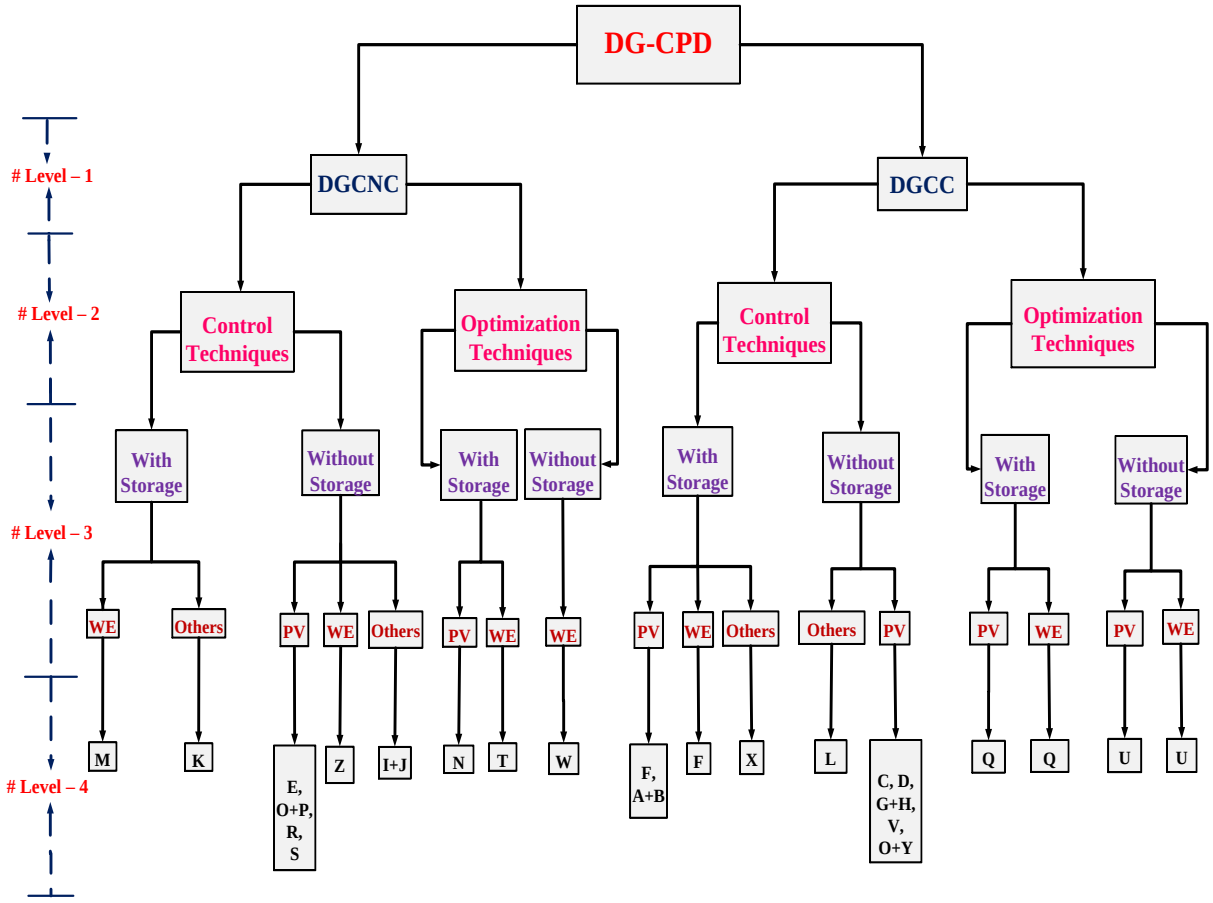

DG - Distributed Generations
CPD - Custom Power Decices
DG - CPD - DG integrated CPD
DGCNC - DG and CPD aren't connected each other
DGCC - DG connected parallel to DC link of CPD
PV - Photo Voltaic
WE - Wind Energy
Others - Various types of DGs

A : Self Tuning Filter
B : Unit Voltage Generator
C : Generalized Cascaded Delay Signal Cancellation
D : Synchronous Reference Frame
E : Adaptive Logarithmic Absolute
F : Fuzzy Logic Control
G : Dual Control Strategy
H : Feed Forward Control Loop
I : Hybrid Active Power Filter
J : Inductive Filtering Transformer
K : Islanding detection and Reconnection
L : Instantaneous single-phase P-Q Theory
M : Five Level Diode-clamped Multi Level converter
N : Multi Objective Particle Swarm Optimization
O : Unit Vector Template Algorithm
P : Hysteresis Current Control
Q : Atom Search Optimisation
R : Nine Level Multi Level Inverter
S : Sinusoidal Current Control Strategy
T : Adaptive Neuro Fuzzy Inference System
U : Biogeography-Based Optimization
V : Advanced Generalized Theory of Instantaneous Power
W : Modified Grey Wolf Optimization
X : Electric Vehicle Aggregator
Y : Instantaneous Reactive Power Theory
Z : Linear Quadratic Regulator

Fig. 1.1: Classification of existing DG-CPD models

Enhancing the voltage profile of DG-integrated networks involves various compensator models and techniques. The classification diagram of DG-integrated CPD (DG-CPD) is provided in Fig. 1.1. This classification primarily considers integrating DGs and CPDs into distribution networks in two ways. In the first approach, DGs are connected directly to the DC link of CPDs (DGCC) [7–9]. This setup facilitates real-time coordination, allowing the compensating device to adjust its operations based on the performance of the DG. In the second approach, DGs and CPDs are not directly connected (DGCNC) [10–12]. This method provides greater flexibility by optimizing each component independently, which can simplify the system design and reduce the complexity of interactions between DGs and CPDs. The second level of classification focuses on strategies explored in the literature to improve network performance. This research focuses on integrating CPD with appropriate control strategies and employing optimization techniques. Control algorithms monitor and adjust inverter operations in real-time to enhance network performance [13–15]. Meanwhile, optimization techniques aim to achieve objectives, such as minimizing CPD ratings, power and energy losses, investment costs, and maximizing factors like voltage stability and PVHC [16–18]. The third level of classification examines the types of DGs and storage technologies investigated in the research. Various combinations of PV, Wind Energy (WE), and energy storage systems (ESS), including Battery ESS (BESS), are explored [19–21]. BESS integration in distribution networks manages DG variability, particularly in PV systems. These BESS units store excess PV energy during off-peak periods and discharge stored energy when PV generation is low or during peak load hours. Lastly, the fourth level of classification presents the various control and optimization techniques applied in distribution networks.

1.2 Literature survey on the optimal integration of DG, ESS, and compensators in distribution networks

The integration of DG, ESS, and compensators such as SHCs has gained significant attention in recent years. This thesis focuses on the optimization techniques for integrating these components into distribution networks. The primary objective is to optimize the allocation, sizing, and operational strategies of DGs, ESS, and compensators to enhance system performance. These optimization algorithms address multiple constraints and objectives to improve overall system performance.

1.2.1 Objective functions considered in the literature

Studies on integrating DG, ESS, and compensators in distribution networks address various objective functions. These objectives typically include minimizing power and energy losses, improving voltage stability, and optimizing economic costs.

The objectives addressed in the literature are as follows:

- **Power loss minimization**: Minimizing power losses in the network is vital for enhancing distribution network performance. These losses result from the resistance in distribution lines and transformers, representing real power losses at any given moment, typically measured in kilowatts (kW). The goal is to optimize the network configuration, component ratings, and operating conditions. Several studies focus on reducing these power losses through strategically placing and sizing DGs and compensators [22,23]. It is essential to select the optimal locations and practical sizes for DGs and compensators, as improper placement or sizing can result in increased system losses. The authors in [24] proposed an approach to optimize the location and sizing of DGs and DHC, aiming to minimize power losses and improve voltage profiles in distribution networks under varying load conditions. Additionally, reference [25] employs an optimization technique to minimize power loss by integrating PV-BESS

with SEC and SHC.

- **Energy loss minimization**: Energy loss minimization aims to reduce the total energy lost over a specified period, often expressed in kilowatt-hours (kWh). Unlike power loss minimization, which addresses instantaneous losses, energy loss minimization accounts for cumulative losses over time, considering fluctuations in load and generation patterns. This approach targets reducing overall energy losses, leading to significant cost savings. The authors in [26] optimized single and double DG unit locations, sizes, and power factors, considering seasonal uncertainties in generation and consumption to minimize Annual Energy Losses (AEL) and voltage deviations. Reference [27] examines methodologies for optimizing network configurations and component sizes, focusing on the impact of time-varying voltage-dependent load models on wind DG planning to achieve lower energy losses. Moreover, studies such as [28] and [29] discuss energy loss reduction through the optimal allocation of SEC and SHC within the distribution network.

- **PVHC Maximization**: PVHC aims to maximize the benefits of integrating PV systems with hybrid configurations, such as battery storage or other complementary technologies. PVHC maximization involves optimizing the placement, sizing, and operational strategies of PV systems and their hybrid components to enhance energy utilization. Researches such as [30] and [31] explores strategies to optimize the PV generation planning to maximize the PVHC within distribution networks. Moreover, reference [32] proposes an equilibrium optimizer-based approach to enhance PVHC by effectively planning PV generation and addressing integration challenges. Similarly, reference [33] employs a hybrid optimization approach to estimate PVHC in distribution networks.

- **Voltage stability and deviation**: Maintaining an optimal voltage profile across the network is essential for the reliable operation of the network. Objective functions

that focus on minimizing voltage deviations ensure that voltage levels remain within acceptable limits, enhancing system stability. References [30] and [31] focus on improving voltage stability through optimal DG and ESS placement. Reference [34] reduces voltage deviation and improves voltage profiles by optimally placing SHCs in the network.

- **Economic cost optimization**: A key objective in distribution network optimization is minimizing the total operational and investment costs, which include expenses related to power losses, maintenance, and infrastructure investments. Many studies aim to design cost-efficient networks that enhance performance while keeping expenses low. References [35] and [23] present a day-ahead scheduling model that addresses uncertainties in PV energy, electricity prices, and load demands. This model incorporates demand response strategies to reduce microgrid operational costs while supporting the integration of renewable energy sources. In [36], the authors propose a hierarchical optimization model for distribution network planning, focusing on the grid connection of DERs. This model accounts for various factors, such as network loss, line investment, power purchase costs, carbon emission costs, and policy subsidies. The goal is to reduce investment costs through optimal DG placement. Similarly, reference [31] focuses on maximizing the investment benefits of DG placement by minimizing the cost associated with line losses.

- **Reliability enhancement:** Improving the reliability of distribution networks is a crucial objective, focusing on minimizing outages and ensuring the network's ability to recover from disturbances. Reliability-focused strategies aim to increase the network's resilience. In [37], the authors propose network reconfiguration techniques to optimize the operation of tie switches. This approach is designed to reduce power losses, enhance voltage profiles, and improve voltage stability, contributing to network reliability. Reference [38] analyses the effects of forced outage rates, peak load

variations, and the penetration of DGs and ESS on microgrid reliability. Further, reference [39] investigates the impact of electric vehicle charging stations on power loss, stability, and overall network reliability. Reference [40] uses Monte Carlo simulation to evaluate the reliability of two feeders within a distribution network. The study examines system adequacy and the impact of varying levels of DG penetration on network reliability.

1.2.2 Decision variables considered in the literature

In distribution network optimization, the variables include the optimal placement and sizing of DGs, ESS, and compensators. The decision variables considered in the literature include:

- **DG sizing and placement:** Decision variables related to the sizing and placement of DGs are essential for optimizing network performance. These variables help determine the DG unit's optimal capacity and location to maximize their benefits, such as reducing power losses and improving voltage stability [41]. The optimal integration of DGs is explored in studies like [42] and [43], which analyze the optimal allocation of PV and WE systems. References [44] and [35] consider the placement of multiple DGs to improve network performance.

- **Compensator placement and sizing:** Variables related to the placement and sizing of compensating devices, such as capacitors and CPDs, are essential for managing voltage levels and reactive power. These decision variables optimize the network's performance by minimizing voltage deviations and enhancing system stability [45]. The optimal allocation of compensators such as SEC and SHC is crucial. Reference [34] determine the optimal placement of SHC, while [23] and [24] explore the combined placement of SHC and DGs. Reference [46] focuses on optimizing the locations of SEC and SHC in the distribution network.

- **Load scheduling:** Load scheduling and demand response are essential for optimizing distribution network operations. Adjusting load timing and consumption helps balance supply and demand, reduce peak loads, and enhance efficiency [47]. Reference [48] formulates a nested optimization problem to ensure the simultaneous optimal planning and operation of DGs and hybrid ESS. This approach addresses uncertainties in DG generation, load demand, price-based demand response, and SHCs functionality while accounting for distribution network constraints.

- **ESS management:** Decision variables for managing ESS include the charging and discharging schedules and the sizing of storage units. These variables are essential for enhancing grid stability, managing intermittency, and improving load management [49]. References [44] and [35] consider the placement of multiple DGs and BESS to improve network performance.

Each of these decision variables is integral to formulating and solving distribution network optimization problems, with their selection and optimization adapted to the specific objectives and constraints of the network under study.

1.2.3 Constraints employed in the literature

In distribution network optimization, various constraints are considered to ensure that solutions are feasible and practical. These constraints represent the physical, operational, and regulatory boundaries within a distribution network. Some of the most commonly discussed constraints in the literature include:

- **Power balance constraints**: These constraints ensure that the total generated active and reactive power equals the total power demand, including system losses. They are crucial for ensuring supply consistently meets demand [50].

- **Voltage constraints**: Voltage levels at each bus in the network must remain within

specified limits to guarantee reliable operation. Exceeding these limits can result in equipment damage [51].

- **Thermal constraints**: These constraints relate to the thermal limits of distribution lines and transformers. Current flows must not exceed these thermal limits to prevent overheating and potential equipment failure, which is vital for maintaining network safety [52].
- **Reactive power constraints**: When reactive power compensators are installed in the network, it is essential to ensure that the reactive power supplied does not exceed the maximum rating of the compensators. This is essential for effective voltage control and loss minimization [53].
- **Capacity constraints**: These constraints involve the maximum capacities of DG units, ESS, compensators, and other network components. Capacity limits ensure that the optimization model does not suggest unrealistic or impractical expansions [54].

These constraints are essential in developing distribution network optimization models. The specific constraints selected and their incorporation into the optimization process depend on the unique objectives and characteristics of the distribution network considered.

1.2.4 Optimization models

In distribution network optimization, various mathematical models address complex decision-making processes. These models are the basis for formulating optimization problems, aiming to minimize or maximize a specific objective, such as reducing power losses, lowering operational costs, or improving system reliability while adhering to constraints. The selection of an appropriate model depends on the nature of the objective and the constraints, which can range from linear to highly non-linear relationships. Different optimization models to address specific types of problems are explained below.

- **Linear Programming (LP)**: LP involves optimizing a linear objective function subject to linear constraints. This method is particularly effective for problems where relationships between variables are linear. LP is well-suited for large-scale optimization problems due to its linear problem formulation and efficient solution techniques [55].

- **Non-linear Programming (NLP)**: NLP extends LP to handle cases where either the objective function or the constraints are non-linear. This is important in power systems, where power flow equations and other system dynamics are inherently non-linear. NLP allows for optimizing more complex objectives, such as reducing generation costs while considering non-linear system behaviors. However, NLP problems can be more challenging due to their non-convex nature [56].

- **Mixed-Integer LP (MILP)**: MILP incorporates continuous and discrete variables into the LP framework. This approach is helpful for problems involving discrete decisions, such as the placement and sizing of distributed generation units or the switching of network components. MILP combines the linearity of LP with the flexibility to handle integer constraints, making it suitable for combinatorial optimization problems [57].

- **Mixed-Integer NLP (MINLP)**: MINLP combines non-linear relationships with continuous and integer decision variables. This method is mainly for complex distribution network problems where the objective function and constraints are non-linear, and decisions involve discrete choices. Although MINLP offers a flexible solution for complex problems, it can be computationally expensive and typically needs advanced solving methods [58].

- **Quadratic Programming (QP)**: QP is a form of NLP where the objective function is quadratic and the constraints are linear. It is often used in optimal power flow problems to minimize a quadratic cost function, such as generation costs or power

losses. QP balances complexity and accuracy, providing a more refined representation of specific cost structures compared to linear models [59].

- **Dynamic Programming (DP)**: DP addresses optimization problems by breaking them into simpler, interrelated sub-problems. This approach is ideal for multi-stage decision problems where each stage depends on the previous outcomes. In distribution network optimization, DP can be used for sequential decisions, such as the placement of DG units or network reconfigurations. While highly effective, DP can be difficult to apply to large-scale problems due to its computational and memory requirements [60].

1.2.5 Solution strategies based on the type of optimization methods

The literature employs various solution strategies to address the optimization problems related to DG, ESS, and compensator integration. These strategies include metaheuristic methods and mathematical approaches.

1.2.5.1 Metaheuristic algorithms

Metaheuristic algorithms have proven to be highly effective in addressing the complexities of multi-dimensional optimization problems, particularly in optimizing DG and compensator placement in power systems. A brief overview of some commonly used metaheuristic algorithms is as follows:

- **Particle Swarm Optimization (PSO)**: PSO is an optimization technique inspired by the social behavior of birds flocking together. In this algorithm, each individual in the population, known as a particle, represents a potential solution. Particles move through the solution space by adjusting their positions based on their own experience and the experiences of neighboring particles. The movement is guided by the best-known positions in the swarm, leading to convergence towards optimal or near-optimal solutions. PSO is particularly effective in handling complex, non-linear problems [61].

- **Genetic Algorithm (GA)**: GA is based on natural selection and genetics principles. It starts with a randomly generated population of potential solutions, each encoded as a chromosome. The algorithm generates new offspring solutions through crossover (recombination of parent solutions) and mutation (random alterations). Over successive generations, the population evolves, with fitter solutions more likely to survive and reproduce, improving solution quality. GA is widely used for its ability to effectively explore a large solution space [62].

- **Ant Lion Optimization (ALO)**: ALO is inspired by the predatory behavior of ant lions in nature. In this algorithm, candidate solutions represent prey, while ant lions represent traps in the solution space. The positions of prey (solutions) are iteratively adjusted, simulating the process of being trapped by ant lions. As the algorithm progresses, the prey is guided towards better solutions, imitating the natural selection process where only the best solutions survive. ALO is particularly useful for solving optimization problems with complex landscapes [43].

- **Lightning Search Algorithm (LSA)**: LSA draws inspiration from the natural phenomenon of lightning, which follows an unpredictable yet directed path. The algorithm simulates this behavior by balancing exploration (searching new areas of the solution space) and exploitation (refining existing solutions). LSA uses a combination of local and global search strategies to effectively navigate the solution space, making it suitable for a wide range of optimization problems, especially those requiring a balance between finding and refining solutions [22].

- **Teaching–Learning Based Optimization (TLBO)**: TLBO is modeled after the educational process, where a teacher transmits knowledge to students. In this algorithm, the population of solutions is divided into learners, with the best solution acting as the teacher. The teacher improves the overall knowledge (quality) of the class (population) by guiding learners toward better solutions. The learning process

is divided into two phases: the teaching phase, where learners improve based on the teacher's guidance, and the learning phase, where learners improve by interacting with each other. TLBO is simple, efficient, and does not require algorithm-specific parameters, making it easy to implement [63].

- **Bacterial Foraging Optimization (BFO)**: BFO is inspired by the foraging behavior of bacteria, particularly their movement towards nutrient-rich areas. The algorithm simulates the chemotaxis process, where bacteria move toward increasing nutrient concentration, representing better solutions. The population of solutions undergo processes like reproduction (replication of the best solutions) and elimination-dispersal (removal of poor solutions and random generation of new ones) to explore the solution space efficiently. BFO is well-suited for optimization problems that involve complex, dynamic environments [34].

- **Cuckoo Search Algorithm (CSA)**: CSA is based on the brood parasitism of cuckoo birds, which lay their eggs in the nests of other birds. In this algorithm, each solution represents a cuckoo egg. Host birds attempt to discover and remove the alien eggs, representing a selection process where poor solutions are discarded. The algorithm employs Levy flights, a random walk strategy, to explore the solution space, ensuring that the search is global and diverse. CSA is effective for finding high-quality solutions in complex optimization problems due to its ability to balance exploration and exploitation [24].

- **Simulated annealing:** Simulated annealing is a probabilistic optimization algorithm inspired by the annealing process in metallurgy. It explores the solution space by accepting better and worse solutions with a probability that decreases over time, allowing the algorithm to escape local minima and search more broadly. This technique is useful for complex optimization problems where the search space is large and poorly understood, providing good approximations to global optima [64].

These algorithms are widely adapted to optimize DG and compensator placement due to their adaptability and ability to handle the high-dimensional, non-linear nature of power distribution systems.

1.2.5.2 Mathematical algorithms

Mathematical approaches to optimization are essential in solving distribution network problems, mainly due to their precision and ability to handle well-defined mathematical structures. These methods depend on formulating the optimization problem as a set of mathematical equations and inequalities, often involving objective functions that need to be minimized or maximized [65, 66]. An overview of various widely used mathematical algorithms is presented below:

- **Simplex algorithm:** The Simplex algorithm is widely used for solving LP problems, where both the objective function and constraints are linear. It operates by iteratively moving along the edges of the feasible region defined by the constraints to locate the optimal vertex. This method is efficient for large-scale problems, providing optimal solutions quickly by systematically improving the objective function value with each iteration [67].

- **Branch and bound:** The Branch and bound algorithm is used to solve integer programming and combinatorial optimization problems. It systematically explores branches of a decision tree, each representing a subset of potential solutions. The algorithm eliminates branches that cannot surpass the current best solution by applying bounds. This approach effectively narrows the search space and delivers accurate solutions for complex problems involving discrete choices [68].

- **Gradient descent:** Gradient descent is an iterative optimization technique used to find the minimum of a function by moving in the direction of the steepest descent, as indicated by the negative gradient. It is beneficial for optimizing non-linear functions

and is commonly employed in machine learning to minimize loss functions during model training. While effective, it may converge to local minima depending on the choice of step size (learning rate) and the function's characteristics [69].

- **Newton's method:** Newton's method is an iterative algorithm designed to find better approximations to the roots of a real-valued function by using both the first derivative (gradient) and the second derivative (Hessian). This method accelerates convergence compared to gradient descent by incorporating curvature information of the function. It is well-suited for smooth optimization problems but requires the computation of second-order derivatives, which can be computationally expensive [70].

- **Conjugate gradient method:** The Conjugate gradient method is used for solving large systems of linear equations and quadratic programming problems. It iteratively generates a sequence of approximations to the solution, using conjugate directions to improve efficiency. This method is particularly effective for large, sparse matrices where direct methods are impractical, requiring less memory and computational resources [71].

These mathematical approaches are essential in distribution network optimization, providing various methods to attain optimal solutions across different constraints and objectives. The selection of a particular approach depends on the specific characteristics of the problem, with each method presenting its strengths and limitations.

1.2.6 Solution strategies based on the number of objective functions

Optimization approaches are generally categorized into single-objective and multi-objective optimization depending on the number of objective functions involved in the problem.

1.2.6.1 Single-objective optimization

Single-objective optimization focuses on finding the optimal solution for a single objective function while meeting specific constraints [72]. This approach aims to identify the best possible solution that either maximizes or minimizes the given objective. It is advantageous when a clear and singular goal needs to be achieved.

In practice, single-objective optimization problems are typically structured as follows:

$$\text{Objective: Minimize (or Maximize)} \quad f(x) \tag{1.1}$$

$$\text{Subject to} \quad g_i(x) \leq 0 \quad \text{for } i = 1, 2, \ldots, m \tag{1.2}$$

$$h_j(x) = 0 \quad \text{for } j = 1, 2, \ldots, p \tag{1.3}$$

Here, $f(x)$ represents the objective function that aims to optimize, while $g_i(x)$ and $h_j(x)$ denote the constraints that must be satisfied, with $g_i(x)$ being inequality constraints and $h_j(x)$ being equality constraints.

Standard techniques to address single-objective optimization problems contain mathematical methods and various metaheuristic algorithms. These approaches are particularly effective for scenarios where the goal is clearly defined and singular, making them well-suited for providing practical solutions to complex issues.

1.2.6.2 Multi-objective optimization

Multi-objective optimization involves simultaneously optimizing two or more objective functions, subject to constraints. Unlike single-objective optimization, which focuses on finding the best possible solution for a single goal, multi-objective optimization generates a set of solutions representing trade-offs between different objectives [73]. The objective here is to balance competing goals and provide a range of solutions from which one can choose based on specific preferences or requirements. In this approach, solutions are often

visualized as a Pareto front, where no solution is superior in all objectives. Instead, solutions on this front are considered optimal because improving one objective leads to a trade-off with another.

In multi-objective optimization, the problem is formulated as follows:

$$\text{Objective: Minimize (or Maximize)} \quad f(x) = [f_1(x), f_2(x), \ldots, f_k(x)] \tag{1.4}$$

$$\text{Subject to} \quad g_i(x) \leq 0 \quad \text{for } i = 1, 2, \ldots, m \tag{1.5}$$

$$h_j(x) = 0 \quad \text{for } j = 1, 2, \ldots, p \tag{1.6}$$

Here, $f(x)$ denotes the vector of objective functions $[f_1(x), f_2(x), \ldots, f_k(x)]$ that need to be optimized simultaneously. The constraints $g_i(x)$ and $h_j(x)$ are similar to those in single-objective optimization, with $g_i(x)$ representing inequality constraints and $h_j(x)$ representing equality constraints.

The methods used in multi-objective optimization are as follows:

- **Weighted sum method**: This approach aggregates multiple objectives into a single composite objective function by assigning weights to each objective. The weighted sum is then optimized using standard single-objective optimization techniques. This method explores different trade-offs between objectives by varying the weights assigned to each objective. Changing the weights adjusts the relative importance of each objective, leading to a set of solutions representing different balances among the objectives. For example, increasing the weight of one objective will generally lead to solutions that favor that objective more while potentially compromising on others [74].

- **ϵ-constraint method**: In this method, one objective is chosen to be optimized as the

primary goal, while the other objectives are treated as constraints with predefined thresholds, or ϵ-values. Multiple single-objective optimization problems are solved by systematically varying these thresholds. Each ϵ-value represents a different constraint level, leading to various solutions that achieve various trade-offs between the objectives. As the constraints are varied, the algorithm produces a series of solutions, each providing a different balance between the primary objective and the constraints imposed on the other objectives [75].

- **Pareto-based optimization**: This approach identifies solutions that form the Pareto front, representing the trade-offs between objectives. Solutions on the pareto front are not dominated by any other solution in all objectives, meaning that improving one objective would worsen another. Multi-objective evolutionary algorithms, such as Non-dominated Sorting Genetic Algorithm II (NSGA-II) [76] and Strength Pareto Evolutionary Algorithm 2 (SPEA2) [77], are commonly used to explore and converge towards this front. These algorithms evolve a population of solutions over time, ensuring diversity and convergence to handle multiple objectives effectively. This approach helps to identify solutions that best meet the various goals set by decision-makers.

The above literature on DG, ESS, and compensator integration reveals a wide range of objectives and solution strategies to improve network performance. A summary of the various optimization methods explored in the literature is provided in Table 1.1. The development of advanced optimization techniques and compensator designs suggest the potential for enhancing the distribution network's performance and economic viability.

1.3 Motivation behind this thesis

Conventional distribution networks often experience poor energy efficiency and lower bus voltage magnitudes due to the high R/X ratio of distribution lines. Integrating DGs can enhance energy efficiency and bus voltages. However, integrating large-scale PV sys-

Table 1.1: Literature review on distribution network optimization

Ref. No.	Type of DER		Type of CPD		Objective function						Solution strategy	
	DG	ESS	SEC	SHC	Power Losses	Energy Losses	PVHC	Voltage stability	Cost	Reliability	Metaheuristic	Mathematical
[22]	✓	×	×	✓	✓	×	×	✓	×	×	✓	×
[23]	✓	×	×	✓	✓	×	×	✓	✓	×	✓	×
[24]	✓	×	×	✓	✓	×	×	✓	×	×	✓	×
[25]	✓	✓	✓	✓	✓	×	×	×	✓	×	✓	×
[28]	✓	✓	✓	✓	×	✓	×	×	✓	×	✓	×
[29]	×	×	✓	✓	×	✓	×	×	×	×	×	✓
[30]	✓	×	×	×	✓	×	×	✓	✓	×	×	✓
[31]	✓	✓	×	×	✓	×	×	✓	✓	×	✓	×
[32]	✓	×	×	×	×	×	✓	×	×	×	✓	×
[33]	✓	×	×	×	×	×	✓	×	×	×	×	✓
[34]	×	×	×	✓	✓	×	×	✓	×	×	✓	×
[35]	✓	✓	×	×	×	×	×	×	✓	×	✓	×
[36]	✓	×	×	×	✓	×	×	×	✓	×	✓	×
[37]	✓	✓	×	✓	✓	×	×	✓	×	✓	✓	×
[38]	✓	×	×	×	×	×	×	×	✓	✓	×	✓
[39]	✓	×	×	✓	✓	×	×	✓	×	✓	✓	×
[40]	✓	×	×	×	×	×	×	✓	✓	✓	×	✓
[41]	✓	×	×	×	×	✓	×	×	×	×	✓	×
[42]	✓	×	×	×	✓	×	×	✓	×	×	✓	×
[43]	✓	×	×	×	✓	×	×	✓	×	×	✓	×
[44]	✓	✓	×	×	×	✓	×	×	×	×	✓	×
[45]	×	×	✓	✓	✓	×	×	✓	✓	×	✓	×
[46]	×	×	✓	✓	×	×	×	×	✓	×	✓	×
[47]	✓	×	×	✓	✓	×	×	✓	×	×	✓	×
[48]	✓	✓	×	✓	×	×	×	✓	✓	×	×	✓
[49]	✓	✓	×	×	×	×	×	×	✓	×	✓	×
[50]	✓	×	×	✓	×	×	×	✓	✓	×	✓	×
[51]	×	×	×	✓	×	×	×	×	✓	×	✓	×
[52]	×	×	×	✓	×	✓	×	×	✓	×	✓	×
[53]	✓	×	×	✓	×	×	×	×	×	✓	✓	×
[54]	✓	×	×	×	✓	×	×	✓	×	×	✓	×
[59]	✓	×	×	✓	✓	×	×	✓	✓	×	×	✓
[62]	✓	×	×	✓	✓	×	×	×	×	×	✓	×
[63]	✓	×	×	×	×	×	×	×	✓	×	✓	×
[65]	×	×	×	✓	✓	×	×	✓	×	×	×	✓
[66]	✓	×	×	×	✓	×	×	✓	×	×	×	✓
[72]	✓	×	×	✓	✓	×	×	×	×	×	✓	×
[73]	✓	×	×	×	✓	×	×	✓	✓	×	✓	×
[74]	✓	×	×	×	✓	×	×	✓	×	×	✓	×
[76]	✓	✓	×	✓	×	×	×	✓	✓	✓	✓	×
[77]	✓	×	×	×	✓	×	×	×	✓	×	✓	×
[78]	✓	×	✓	✓	×	✓	✓	×	×	×	✓	×

tems into existing networks poses several challenges, even in a country like India, which is geographically well-suited for solar energy. Ground-mounted PV installations face significant challenges due to the scarcity of vacant or unused land in densely populated areas. Rooftop solar installations solve this problem by utilizing available rooftop space in residential households. This research is motivated by the potential to mitigate land scarcity issues through rooftop PV installations and their integration into distribution networks. In the coming years, rooftop PV installation capacities are expected to increase rapidly, driven by the Government of India's policies that encourage customers to integrate more rooftop PVs. However, injecting large PV generation into distribution networks can increase power losses and voltage and current harmonics. Improving PVHC can be achieved through various methods, including reactive power compensation.

This research addresses these issues using CPDs, such as SHCs, to ensure an energy-efficient power distribution system. Integrating PV systems and deploying SHCs require significant investment, motivating an economic analysis to explore financially viable solutions. Furthermore, PV generation depends on environmental conditions, such as solar irradiation, site coordinates, and shading objects, which can affect the continuous feeding of loads. Incorporating BESS alongside PV systems can address this issue by storing excess power generated during peak hours and supplying it during non-PV generating hours or peak load times. These challenges highlight the importance of appropriate solutions to overcome the challenges associated with PV integration, intermittency in PV generation, and economic feasibility, ultimately supporting a sustainable energy transition in India.

Existing literature on optimization goals focuses on minimizing converter rating requirements, reducing power and energy losses, and maximizing PVHC. The time-varying load and PV generation in distribution networks increase the number of variables, necessitating the assessment of real-time behavior for designed objective functions. Although similar multi-dimensional optimization problems have been addressed, there is a need for more efficient techniques. Consequently, research is required to develop new optimization variants

that effectively address high-dimensional objective functions.

1.4 Research gaps

Considering the issues highlighted above, the following research gaps have been identified:

- **Compensation to PV-rich distribution networks:** Studies have predominantly focused on integrating large PVs at specific network locations to minimize power losses. However, understanding the impact of distributing PV integration throughout the network and its effect on overall network performance is essential, especially considering space limitations for larger PV units in residential distribution networks.

- **Optimal allocation of multiple SHCs:** Previous studies have focused on optimizing the allocation of PVs and SHCs to minimize power losses. However, it is necessary to investigate the optimal placement of multiple SHCs within PV-rich distribution networks to minimize energy losses, particularly while considering time-varying PV generation and load profiles.

- **Comprehensive cost-effectiveness assessment:** Despite economic benefits explored for SHC deployment in passive networks, the potential advantages in active distribution networks with high PV penetration remain understudied. Conducting economic analyses to assess the benefits of SHC installation in active networks is crucial. The research studies should address the optimal allocation of multiple SHCs to maximize saved energy-derived profit.

- **Operational optimization of BESS and SHCs:** Previous studies have not explored the potential adaptation of BESS converters to supply reactive power despite their primary role in supplying active power to distribution networks. Moreover, practical strategies for charging/discharging BESS and managing the reactive power

of SHCs based on time-varying load and PV generation are necessary. Additionally, operational optimization of BESS and SHCs to maximize PVHC while minimizing energy losses requires further research.

- **Novel metaheuristic variants for distribution network optimization:** The objective functions of power distribution networks become multi-dimensional problems with more variables due to time-varying loads and PV generation. This complexity makes it challenging to converge on a solution using existing optimization techniques. Therefore, it is necessary to develop new metaheuristic variants capable of effectively managing high-dimensional optimization problems with more than 150-200 variables.

1.5 Organisation of the thesis

The thesis is organized as follows.

- In Chapter-2, the modeling of SHCs within PV-rich distribution networks is discussed. The chapter uses the forward-backward sweep load flow algorithm to determine network parameters and calculate energy losses. It also explains how PSO is employed to identify optimal locations for SHCs to minimize energy losses in the network. Additionally, the chapter addresses the importance of factors such as voltage, thermal limits, and power balance constraints in efforts to reduce energy losses. A performance comparison of the proposed planning approach with similar methods in literature is also provided.

- In Chapter-3, an economic evaluation is conducted on the combined placement of PV units and SHCs in distribution networks. The planning approach is designed to maximize profit by increasing revenue from PV generation and reducing network energy losses while accounting for the investment costs of SHCs and PVs. Additionally, the strategic placement of multiple SHCs across the network is examined to analyze economic and technical outcomes.

- In Chapter-4, the operational optimization of SHCs is proposed by determining the specific VAr injection for each hour to minimize AEL costs. The chapter introduces a Gaussian Probability Distribution methodology to predict monthly load curves for residential, commercial, and industrial sectors. The objective function of minimizing AEL cost accounts for the 24-hour time-varying nature of load and PV generation profiles over 12 months, resulting in a 288-variable objective function. A novel PSO variant called Parallel Multi-Swarm Gaussian Process Regression (GPR) Surrogate-based PSO (Parallel-MS-GPRS-PSO) is developed to address the challenges of optimizing this high-dimensional problem.

- In Chapter-5, a multi-objective planning approach is introduced, focusing on optimizing both PVHC and energy losses within distribution networks. This chapter presents an operational optimization strategy designed to determine the VAr compensation set-points for SHCs and the charging/discharging set-points for BESS in response to time-varying load and PV generation. The multi-objective method is proposed, utilizing the SPEA2-based multi-objective GPR Surrogate-assisted PSO (SPEA2-MO-GPRS-PSO) to identify a set of non-dominated solutions.

- In Chapter-6, a multi-objective approach is introduced to optimize the placement of SEC and PV-integrated SHCs (PV-SHC) in distribution networks. The approach employs SPEA2-MO-GPRS-PSO to identify optimal locations for these compensators to minimize the overall compensator rating, network power loss, and the number of undervoltage nodes. Additionally, the chapter explores using existing PV systems to provide both active and reactive power compensation by replacing conventional SHCs in PV units.

- In Chapter-7, the overall conclusions of the thesis are presented, along with potential future research directions in this field.

The appendix includes simulation data for the 33-bus and 69-bus radial distribution

networks.

1.6 Contribution of the thesis

The contributions of this thesis are outlined below:

- Development of a planning approach to achieve minimum energy losses in PV-rich distribution networks through optimal multiple SHC placement with different levels of PV penetration.
- Development of a planning strategy aimed at maximizing profit while considering the economic aspects of both PV units and SHCs, including factors, such as load growth, seasonal load variations, and PV generation profiles.
- Development of Parallel-MS-GPRS-PSO approach, specifically designed to address the challenges posed by the optimization problems with many variables.Furthermore, a planning approach is formulated to minimize annual energy loss costs by estimating monthly load curves for residential, commercial, and industrial sectors using Gaussian Probability Distribution, accounting for variations in energy prices based on seasonal changes and load levels.
- Development of an operational optimization approach to determine time-varying VAr compensation set-points for SHCs and charging/discharging set-points for BESS, based on time-varying load demand and PV generation. The converter units are designed to supply reactive power alongside BESS active power injection, enabling the simultaneous maximization of PVHC and reduced energy losses through a multi-objective planning approach.
- Development of a multi-objective planning approach focusing on minimizing power losses, reducing the number of undervoltage nodes, and the overall rating of compensators in the network.

भारतीय प्रौद्योगिकी संस्थान गुवाहाटी
Indian Institute of Technology Guwahati

Chapter 2

Optimal Placement of Multiple Shunt Compensators for Energy Loss Minimization in PV-Integrated Distribution Networks

2.1 Introduction

The integration of renewable energy sources into distribution networks is driven by several factors. These include the depletion of traditional energy supplies, the growing demand for electricity, and the need for cleaner power generation to reduce carbon emissions and pollution. However, the effective integration of DGs within power networks decreases power losses and improves the voltage profile of the network [79, 80]. Additionally, incorporating energy storage systems into power grids enhances power quality, mainly when DG units are present [81]. However, integrating large-scale PV systems into distribution networks presents various challenges, including voltage imbalances, exceeding ampacity limits, and harmonics [82]. References [83] and [84] discuss voltage violations when an excess amount

of PV plants are integrated into distribution networks. In order to improve PVHC, authors in [85] suggests that supplying reactive power to the network can help maintain permissible network losses and voltage profiles. PE-based voltage source compensators inject reactive power into the network [27]. Proper integration of compensators can enhance PVHC in distribution networks [86]. Optimal sizing and placement of PV units and SHCs in the network can improve network parameters such as voltage profiles and reduce power and energy losses [43, 44, 87]. Metaheuristic and mathematical optimization approaches are utilized to determine the optimal locations for PV systems or compensators in the distribution network [88,89]. Table 2.1 presents a qualitative comparison of previous approaches, considering the minimization of network power and energy losses. The table also provides information on the variables and optimization methods used in the respective chapter.

The studies cited in references [22–24, 34, 90, 91] focus on applying metaheuristic techniques to minimize power losses in network systems. The objective function presented in [34] aims to reduce power losses and enhance voltage stability. This study also introduces an improved bacterial foraging search algorithm for determining the size and location of SHCs within the distribution network. The approach discussed in [22] highlights DG and SHC simultaneous installation in radial distribution networks. It optimizes a multi-

Table 2.1: Qualitative comparison of previous approaches for the optimal placement of SHC and DG in distribution networks

Ref. No.	Objective function		Variables		Optimisation approach	
	Power losses	Energy losses	DG location	SHC location	Metaheuristic	Mathematical
[26]	×	✓	✓	×	✓	×
[34]	✓	×	×	✓	✓	×
[22]	✓	×	✓	✓	✓	×
[23]	✓	×	✓	✓	✓	×
[24]	✓	×	✓	✓	✓	×
[90]	✓	×	✓	×	✓	×
[91]	✓	×	×	✓	✓	×
[92]	×	✓	×	✓	×	✓
Proposed work	×	✓	✓	✓	✓	×

objective function that includes minimizing power loss, maximizing the voltage stability index, and minimizing total voltage deviation, employing a lightning search algorithm. The objective function in [23] focuses on enhancing the voltage profile, minimizing power loss, and reducing network operating costs. The optimal location and sizing of DG and SHC are determined using the Bacterial Foraging Optimization Algorithm. Additionally, [24] utilizes the cuckoo search algorithm to minimize power loss by allocating multiple DG and SHCs in the distribution network. In [90] and [93], the allocation of DG units in radial distribution networks is performed considering uncertainties in load demand. Similarly, [91] employs the whale optimization algorithm to determine the optimal allocation of SHCs, aiming to minimize power losses.

However, the mentioned studies [22–24, 34, 90, 91] do not specifically address energy loss minimization. In contrast, reference [26] focuses on DG allocation to determine the minimum energy losses in the network. Furthermore, the authors in [92] determine the optimal location of SHCs to achieve energy loss minimization using a mathematical optimization approach.

These studies primarily concentrate on determining optimal locations of DGs or SHCs and propose various approaches to improve power and energy loss in distribution networks. However, more research must be concentrated on distribution networks with DG integration on all the buses.

Based on the literature presented, the following research gaps emerge:

- Existing studies have primarily focused on integrating larger DGs at specific network locations to minimize power losses. However, this approach becomes challenging when considering larger PV units due to space limitations. Therefore, it is crucial to investigate the impact of distributing PV integration throughout the network and its effect on network performance.

- Previous research has predominantly addressed DG and SHC allocation for power loss

minimization. However, a need remains to explore the optimal allocation of multiple SHCs within DG-integrated distribution networks to minimize energy losses.

These identified research gaps serve as the motivation for the present study. This chapter proposes the objective function of minimizing energy losses in the PV-integrated distribution network. PE-based SHCs reduce harmonic content in the line current by supplying reactive power to the network. Furthermore, the placement of SHCs in the network is optimized for various PV penetration levels. The PSO approach is considered for solving the objective function. The contributions of this chapter are as follows:

- The formulation of the planning approach is developed to obtain the minimum value of energy losses in the PV-integrated distribution network by the optimal placement of SHCs.
- The overall size of the compensator is determined for different penetrations of PVs in the network by considering different numbers of SHC allocations.

The proposed planning approach has been validated using the 33-bus and 69-bus distribution networks.

2.2 Modeling of SHCs in PV-integrated distribution networks for reactive power compensation

SHC is a compensator that utilizes PE-based technology and is connected in parallel (shunt) to the buses in the distribution network. In the present study, SHCs are strategically placed within the PV-integrated distribution network to provide reactive power compensation. The block model representation of SHCs in a PV-integrated distribution network is depicted in Figure 2.1. This illustration visually represents the integration of PV units and multiple SHCs into 33-bus and 69-bus distribution networks. Figures 2.2 and 2.3 illustrate

the internal block diagram and phasor diagram of SHC, respectively. These figures visually depict the configuration and operation of SHC within the distribution network.

The modeling approach employed for SHC in this study is similar to that used for passive distribution networks. Initially, PV units are integrated into the network, and their contribution to active power is determined. Subsequently, before the compensators are installed, adjustments are made to the active power of the network. This adjustment ensures that the PV units supply an appropriate amount of active power to the network while the compensators provide reactive power compensation.

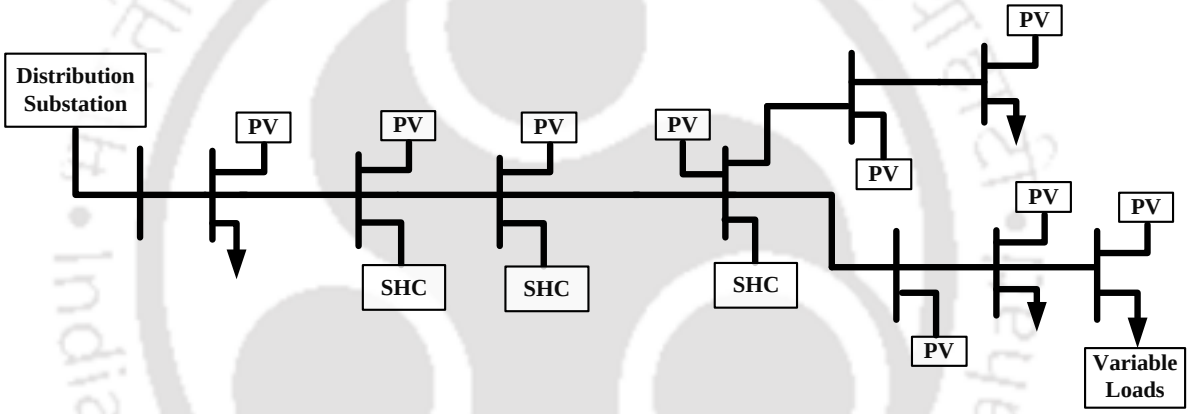

Fig. 2.1: Block model representation of proposed compensator in the PV-integrated distribution network

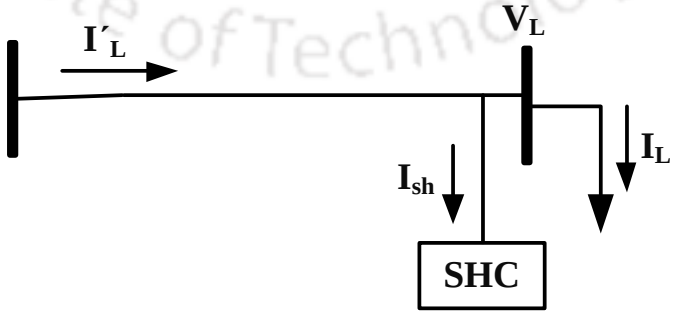

Fig. 2.2: Modelling of SHC - internal block diagram

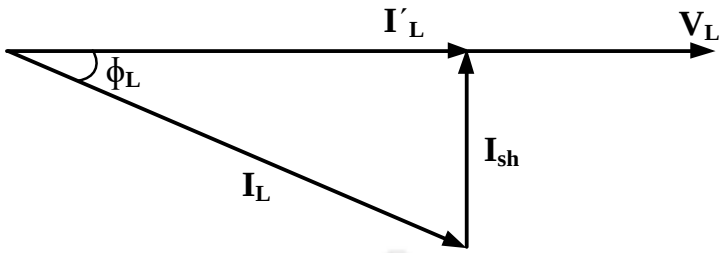

Fig. 2.3: Phasor diagram of SHC

The rating of SHC is determined based on the amount of reactive power it provides, which is a function of the Total Harmonic Distortion (THD) that needs to be compensated. The considered THD to be mitigated is 0.2. From Figure 2.3, the shunt current to be injected into the network can be evaluated using Equation 2.1 [78]:

$$I_{sh} = I_L \sin \Phi_L \tag{2.1}$$

Here, I_{sh} denotes the shunt current provided by the SHC. Φ_L represents the phase angle between the load voltage V_L and the load current I_L at the SHC connection point.

The SHC compensates for the distorted component of the load current, resulting in Equation 2.2:

$$I_L^{dis} = I_{sh}^{dis} \tag{2.2}$$

I_L^{dis} and I_{sh}^{dis} refer to the distorted components of the load current and shunt current, respectively.

The THD is the ratio of the distorted component of the shunt current to the fundamental component, as shown in Equation 2.3. From the definition of THD,

$$THD_{sh} = \frac{I_{sh}^{dis}}{I_{sh}^{fun}} \tag{2.3}$$

$$I_{sh} = I_{sh}^{fun}\sqrt{1 + (THD_{sh})^2} \tag{2.4}$$

$$THD_L \; I_L^{fun} = THD_{sh} \; I_{sh}^{fun} \tag{2.5}$$

THD_L and THD_{sh} denote the THD of the load current and shunt current, respectively. I_L^{fun} and I_{sh}^{fun} represent the fundamental components of the load current and shunt current, respectively.

By using Equations 2.1, 2.4, and 2.5, Equation 2.6 can be derived:

$$I_{sh} = I_L^{fun}\sqrt{(\sin\Phi_L)^2 + (THD_L)^2} \tag{2.6}$$

The Volt-Ampere (VA) rating of SHC (S_{sh}) can be calculated using Equation 2.7:

$$S_{sh} = V_L I_{sh} \tag{2.7}$$

Since no PV unit is connected in parallel to the SHC, it provides only reactive power to the network, as stated in Equation 2.8:

$$Q_{sh} = S_{sh} \tag{2.8}$$

where Q_{sh} represents the reactive power rating of SHC.

If multiple SHCs are placed in the network, they can be installed consecutively, and their ratings can be calculated accordingly. The overall VA rating and reactive power rating of the compensator can be evaluated using Equations 2.9 and 2.10, respectively:

$$(S_{sh})_{total} = \sum_{i=1}^{m} S_{sh_i} \tag{2.9}$$

$$(Q_{sh})_{total} = \sum_{i=1}^{m} Q_{sh_i} \tag{2.10}$$

Here, S_{sh_i} and Q_{sh_i} represent the VA rating and reactive power rating of the i^{th} SHC, respectively, and m denotes the total number of SHCs integrated into the network.

2.3 Incorporation of SHCs for network performance assessment in distribution networks using load flow analysis

Load flow analysis plays a crucial role in assessing the operational parameters of a power network, including bus voltages, line currents, and losses. It is an essential tool for solving power system operation and planning problems. However, conventional load flow methods like Newton-Raphson and Gauss-Seidel face challenges in distribution system power flow analysis. This is primarily due to the radial topology of distribution networks and the high R/X ratio of distribution lines. To overcome these challenges, the Forward-Backward Sweep (FBS) load flow algorithm has emerged as an efficient approach for voltage and current calculations in the distribution network [94]. Unlike the conventional methods, the FBS load flow algorithm proves to be more suitable for distribution systems. It effectively handles the radial nature of distribution networks.

2.3.1 FBS load flow algorithm for distribution network analysis

The FBS load flow algorithm is an iterative technique to determine the voltages and currents at each bus in a distribution network [95]. It involves two steps: forward sweep and backward sweep. In the backward sweep, the algorithm starts from the farthest bus and moves towards the substation, updating the current values at each step. The equations used in the backward sweep are as follows:

$$I_m = \frac{P_m - jQ_m}{V_m^*}, \quad \text{for } m \in [2, \ldots, N] \tag{2.11}$$

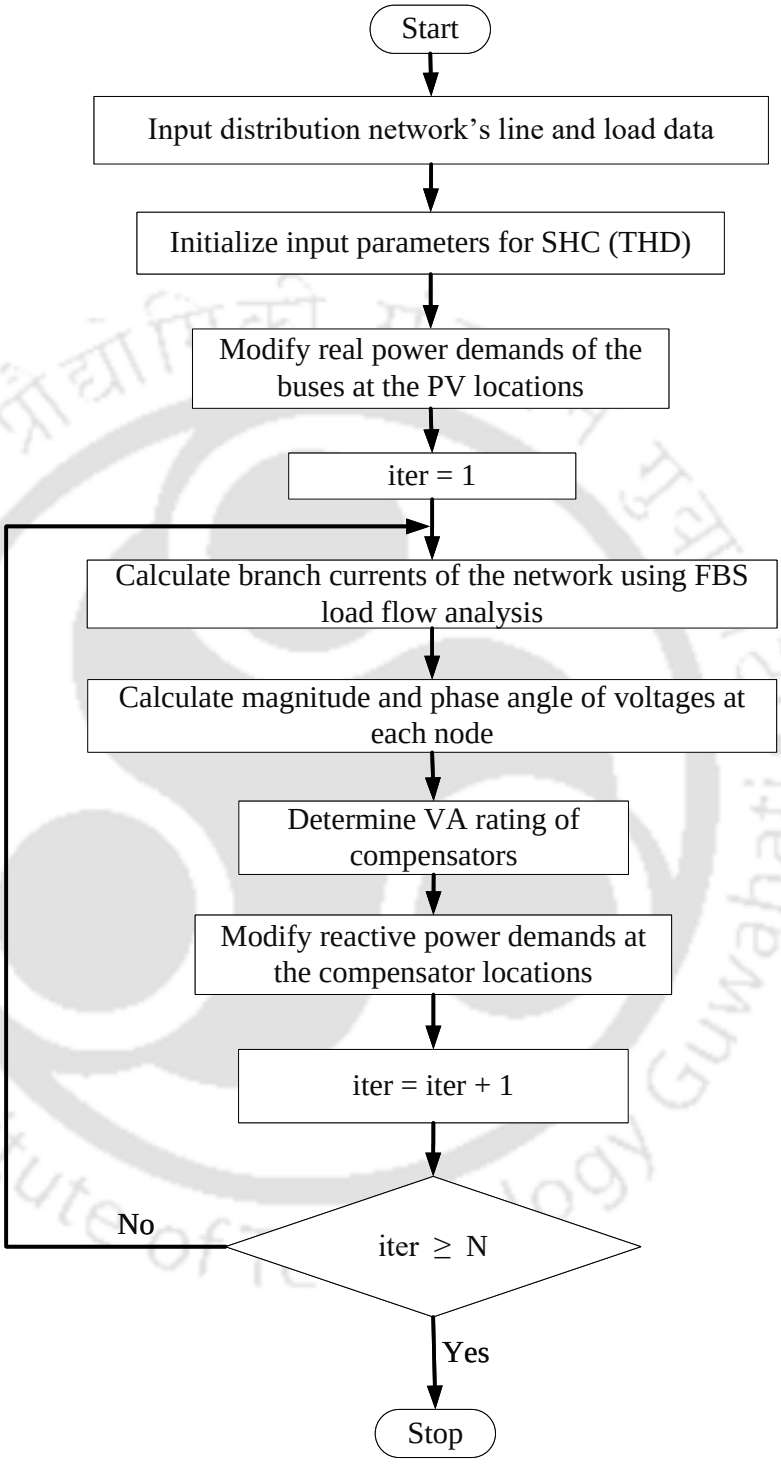

Fig. 2.4: Flowchart of the FBS load-flow algorithm incorporating multiple PE compensators in PV-integrated distribution network (N = total number of iterations)

$$I_{mn} = I_n + \sum_{i \in \aleph} I_i, \quad \text{for } mn \in [1, \ldots, N-1] \tag{2.12}$$

Here, I_m represents the load current at bus m, which is calculated using the active power P_m, reactive power Q_m, and the complex conjugate of the bus voltage V_m^*. I_{mn} represents the line current of line mn, calculated as the sum of the load currents at the receiving end (n) and all downstream buses i in the set $\aleph$.

In the forward sweep, the algorithm updates the bus voltages starting from the substation bus and traverses the network radially. The equation used in the forward sweep is as follows:

$$V_n = V_m - I_{mn} Z_{mn}, \quad \text{for } mn \in [1, \ldots, N-1] \tag{2.13}$$

Here, V_n represents the bus voltage at the receiving end of line mn, calculated as the difference between the bus voltage V_m at the sending end and the product of the line current I_{mn} and the line impedance Z_{mn}.

The FBS load flow algorithm continues iterating between the forward and backward sweeps until convergence is achieved. This ensures accurate results for the network variables, including load currents, line currents, and bus voltages.

2.3.2 Incorporation of SHCs using FBS load flow for network performance assessment in distribution networks

Incorporating SHCs into the network using the FBS load flow approach allows for assessing their impact on network performance. This method considers the presence of PV units in the network and adjusts the active and reactive power demands at each bus accordingly. Initially, PV units are integrated into the network, which modifies the original active power demands of the buses. The modified active power demand at bus i is calculated

as

$$P_i'(t) = P_i(t) - P_{PV(i)}(t) \tag{2.14}$$

where $P_i(t)$ represents the original active power demand and $P_{PV(i)}(t)$ represents the active power supplied by the PV unit at bus i at time t.

Similarly, the modified reactive power demand at the location of SHC is obtained as

$$Q_i'(t) = Q_i(t) - Q_{sh(i)}(t) \tag{2.15}$$

where $Q_i(t)$ represents the original reactive power demand and $Q_{sh(i)}(t)$ represents the reactive power supplied by the SHC at bus i at time t.

The energy losses can be determined by modifying the active and reactive power demands in the network. The flowchart shown in Figure 2.4 illustrates the approach for incorporating SHCs into the network using the FBS Load Flow method.

2.4 Problem formulation for minimizing energy losses in PV-integrated distribution networks

The optimal placement of SHCs in a PV-integrated distribution network is essential for improving network performance. Different numbers of SHCs are strategically placed in the network to determine the minimum energy losses in a day, which are calculated by summing the power losses during each load and PV generation profile scenario.

The objective function is expressed as follows:

$$\text{Minimize Energy Losses} = \sum_{c\in\eta}\sum_{ef\in\mathcal{Z}} PL_{ef(c)}t_c \tag{2.16}$$

where $PL_{ef(c)}$ and t_c correspond to the power losses on branch ef for scenario c and duration of scenario c, respectively. $\mathcal{Z}$ represents the set of all branches in the distribution

network. η represents the load and PV generation profiles set for all scenarios in a day.

When optimizing the objective function, the following constraints are considered:

- **Power balance constraint:** The power generated by the substation and PV units must equal the network's load demand and power losses. This constraint is expressed by Equations 2.17 and 2.18:

$$P_{SS}(t) + P_{PV}(t) = P_L(t) + P_{loss}(t), \quad \forall t \tag{2.17}$$

$$Q_{SS}(t) + Q_{SHC}(t) = Q_L(t) + Q_{loss}(t), \quad \forall t \tag{2.18}$$

where $P_{SS}(t)$ represents the active power generated by the substation at time t, $P_{PV}(t)$ represents the active power generated by the PV units at time t, $P_L(t)$ represents the active power demand of the network load at time t, and $P_{loss}(t)$ represents the active power losses in the distribution network at time t. Similarly, $Q_{SS}(t)$ represents the reactive power generated by the substation at time t, $Q_{SHC}(t)$ represents the reactive power generated by the SHC at time t, $Q_L(t)$ represents the reactive power demand of the network load at time t, and $Q_{loss}(t)$ represents the reactive power losses at time t in the distribution network.

- **Voltage constraint:** The bus voltages in the network must remain within their permissible limits. The minimum and maximum bus voltage limits are denoted by V_{min} and V_{max}, respectively. The voltage at bus i at time t is represented by $V_i(t)$. This constraint is given by Equation 2.19:

$$V_{min} \leq V_i(t) \leq V_{max}, \quad \forall i, t \tag{2.19}$$

- **Thermal constraint:** The current flowing through each line in the distribution

network must not exceed its thermal limit. This constraint is expressed by Equation 2.20:

$$|I_{\text{line}}(ef,t)| \leq I_{\max}(ef,t), \quad \forall t, \forall ef \in \mathcal{Z} \tag{2.20}$$

where, $|I_{\text{line}}(ef,t)|$ denotes the magnitude of the current flowing through line ef at time t. $I_{\max}(ef,t)$ represents the maximum permissible current limit for line ef in the distribution network at time t.

- **SHC location constraint:** To avoid placing multiple SHCs at the same location, a constraint restricts two SHCs from occupying the same location in the distribution network. This constraint is represented by Equation 2.21, where L_{SHC_i} and L_{SHC_j} denote the locations of the i^{th} and j^{th} SHCs, respectively:

$$L_{SHC_i} \neq L_{SHC_j} \tag{2.21}$$

These constraints collectively guide the optimization process to find the optimal placement of SHCs in the PV-integrated distribution network.

2.5 Planning approach for optimal SHC placement in PV-integrated distribution networks using PSO

In this chapter, the focus is on achieving minimum energy losses in the network through the optimal allocation of SHCs. Additionally, the optimization approach is employed to determine the locations of compensators. The PSO, a metaheuristic algorithm, is utilized as a solution strategy to minimize energy losses in the network.

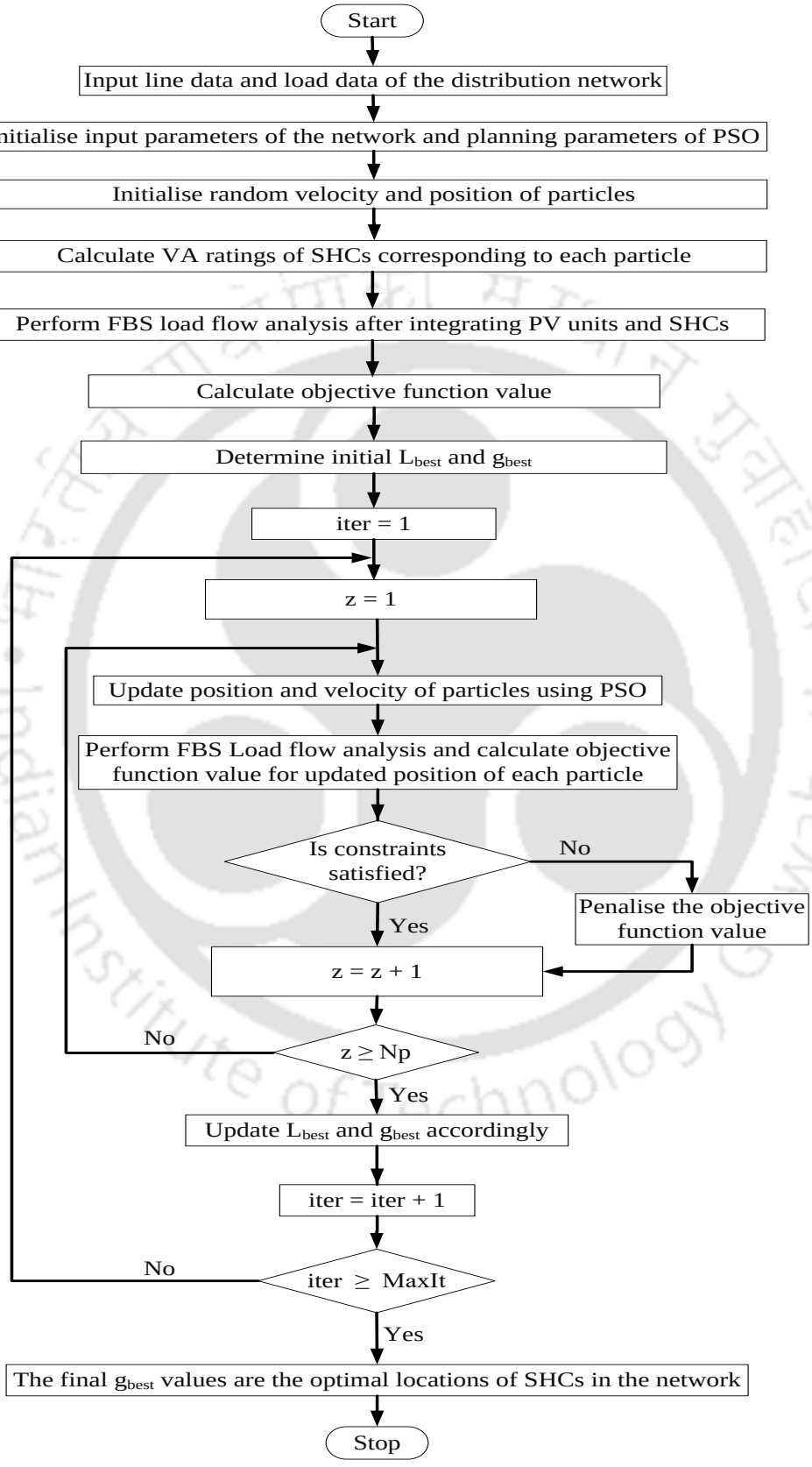

Fig. 2.5 Flowchart illustrating the proposed distribution system planning approach based on PSO

2.5.1 PSO algorithm

The PSO algorithm draws inspiration from the collective behavior of birds flocking or fish schooling [96, 97]. In PSO, the decision variables are particles, each possessing a position and velocity. Each particle keeps track of its best location, known as the local best (L_{best}). Through communication, particles share their local best positions and collectively determine the best solution, represented as global best (g_{best}). The global best solution represents the best outcome achieved collectively by all particles in the swarm through the optimization process after each iteration. This collective achievement is crucial for guiding the algorithm towards convergence and exploration.

The velocity (U_z) and position (X_z) of each particle are updated iteratively using the following equations:

$$U_z^{iter+1} = wU_z^{iter} + c_1 r_1 (L_{best,z}^{iter} - X_z^{iter}) + c_2 r_2 (g_{best}^{iter} - X_z^{iter}) \tag{2.22}$$

$$X_z^{iter+1} = X_z^{iter} + U_z^{iter+1} \tag{2.23}$$

Here, c_1 and c_2 are acceleration coefficients, and r_1 and r_2 are random numbers selected between 0 and 1. The inertia weight, denoted as w, controls the impact of the particle's previous velocity (momentum) in the velocity equation. The cognitive and social parts in the equation represent the influence of a particle's local best position and the global best position, respectively, on its velocity update. By iteratively updating the velocities and positions of particles, the PSO algorithm effectively explores the search space to find the optimal solution for optimization problems.

2.5.2 PSO-based planning approach for SHC placement

In the PSO algorithm, the particles are encoded with the potential locations of SHCs in the network. The objective is to minimize energy losses within the network by finding the

optimal locations of SHC placement. The algorithm iteratively updates the velocities and positions of the particles based on their previous experiences and the collective knowledge of the swarm. After every iteration, the particle values corresponding to the SHC locations are decoded, and the network's energy losses are calculated. The algorithm aims to converge to the best solution, representing the optimal placement of SHCs, resulting in the minimum energy losses. The proposed PSO-based distribution network planning approach is illustrated in Figure 2.5.

Table 2.2: Results obtained from evaluating various PSO parameter sets

Parameters				**Average of optimal values**	**Optimal value**
w	c_1, c_2	***Np***	***MaxIt***		
0.6	1.5, 1.5	200	100	1.5092	1.5016
0.7				1.4994	1.4971
0.8				**1.4975**	**1.4939**
0.9				1.4985	1.4968
0.8	1.5, 0	200	100	1.5015	1.4991
	0, 1.5			1.5032	1.4968
	1.5, 1.5			**1.4975**	**1.4939**
	2.0, 2.0			1.4981	1.4968
	2.5, 2.5			1.5017	1.4973
0.8	1.5, 1.5	50	100	1.5051	1.4999
		100		1.5011	1.4994
		200		1.4975	**1.4939**
		250		**1.4958**	**1.4939**
0.8	1.5, 1.5	200	50	1.5038	1.4968
			75	1.4993	1.4973
			100	1.4975	**1.4939**
			150	**1.4962**	**1.4939**

Table 2.3: PSO parameters

Parameters	**Considered values**
Inertia weight, w	0.8
Acceleration coefficient, c_1	1.5
Acceleration coefficient, c_2	1.5
Population size, N_p	200
Maximum number of iterations, $MaxIt$	100

2.5.3 Selection of PSO parameters

The selection of appropriate PSO parameters is essential for optimizing the performance of the PSO algorithm. The evaluation in Table 4.1 explores various combinations of parameters (w, c_1, c_2, N_p, and $MaxIt$) to assess their impact on minimizing energy losses in a 33-bus distribution network with three SHCs.

The analysis reveals that setting $w = 0.8$ leads to the best overall performance. Keeping c_1 and c_2 at 1.5 yields optimal results across different parameter combinations. Also, maintaining $MaxIt$ at 100 and choosing N_p as 200 or 250 achieves the same optimal outcomes. However, increasing N_p results in longer execution times. Similarly, fixing N_p at 200 and varying $MaxIt$ between 100 and 150 yields optimal results but extends the execution time. Therefore, selecting $N_p = 200$ and $MaxIt = 100$ offers a balanced approach, delivering the better results while minimizing execution time. These insights are valuable for setting effective PSO parameters that enhance convergence. Table 2.3 summarizes the selected parameter values for the optimization process.

2.6 Simulation results and analysis

The proposed approach in this study is validated using the MATLAB/Simulink environment. Two test systems, namely a 33-bus and a 69-bus distribution network, are simulated to evaluate the effectiveness of the approach. The substation bus is identified as the initial bus in both networks, with the other buses categorized as PQ buses. Buses integrated with PV units are classified as PQ buses rather than load buses. PQ buses indicate nodes where both active and reactive power are injected into or extracted from the system. This differentiation is essential for accurately modeling distributed generations and assessing the system's power flow and voltage profiles. The details of these networks are provided below:

- *33-bus radial distribution network [98]*: This is a single feeder radial distribution system with a base VA of 100 MVA and a base voltage of 12.66 kV. During peak

hours, this network experiences a total active power demand of 3.715 MW and a reactive power demand of 2.3 MVAr. Detailed data for this network are available in the Appendix A.

- *69-bus radial distribution network [99]*: This is also a single feeder radial distribution system with a base VA of 10 MVA and a base voltage of 12.66 kV. During peak hours, this network has a total active power demand of 3.8022 MW and a reactive power demand of 2.6946 MVAr. Detailed network data can be found in the Appendix A.

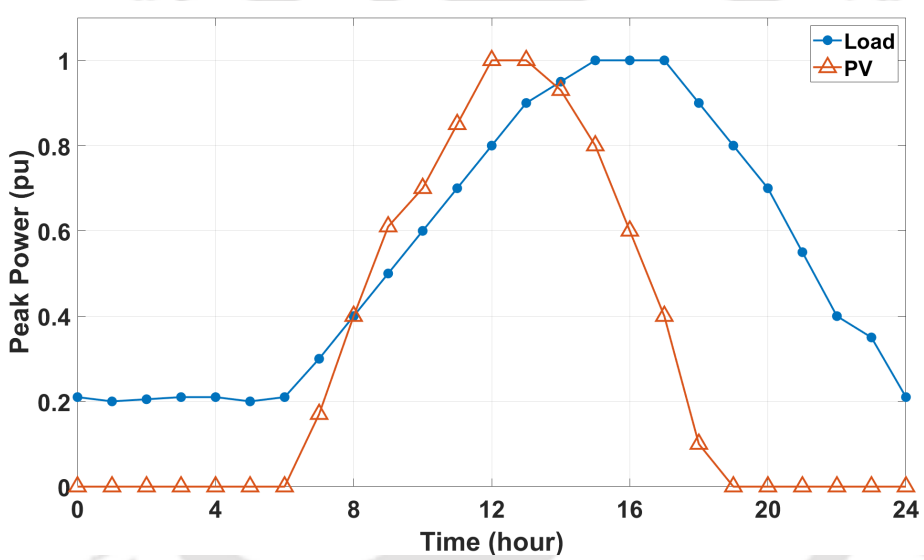

Fig. 2.6: Load and PV generation profile in a day

The daily load curve and PV generation profile are sourced from [100], as shown in Figure 2.6. It is important to note that the energy losses depend on the specific load and PV generation profile considered for each hour. The bus voltage limits are set at 0.9 pu for the minimum and 1.05 pu for the maximum limit, as specified in [101]. The thermal limits for the 33-bus and 69-bus networks are obtained from [102] and [99], respectively. The SHCs are placed at any network bus except the substation bus.

Previous studies on PV system integration in distribution networks have often focused on a limited number of nodes or buses with capacities ranging from approximately 1 MW to 3 MW [23, 24, 26]. However, this approach may not accurately represent real-world

scenarios, especially in urban areas where spatial constraints limit the installation of large-capacity PV systems at specific locations. To address this limitation, this chapter proposes a methodology evenly distributing PV generation capacity across all buses in the distribution network. Each node in the distribution network represents a distinct geographical area, which can be distributed evenly or unevenly. This research focuses on the even distribution of PV systems, assuming each distribution transformer serves an equal area. This approach introduces novelty by exploring the possibilities of PV installation, providing a comprehensive analysis, and enhancing the study's applicability.

To minimize energy losses, three cases are considered for SHC placement in the distribution network:

- **Case-A:** Optimization is performed to determine the optimal location for one SHC.
- **Case-B:** Optimization is performed to determine the optimal locations for two SHCs.
- **Case-C:** Optimization is performed to determine the optimal locations for three SHCs.

The ratings of the SHCs are determined after integrating the desired level of PV units into the distribution network. An equal amount of PV is assumed to be integrated at each distribution network bus, except for the substation bus. The findings of this research highlight the outcomes of integrating PV systems at different capacity levels within the network. This approach facilitates a comprehensive examination of system behaviors across various penetration levels of PV integration.

The MATLAB simulations are conducted on a Ryzen 7-5800 CPU with 16 GB RAM and a 1.9 GHz processor. Table 2.4 presents the optimization times for the 33-bus and 69-bus networks in each case study. It is evident from the table that the 69-bus network requires more time to converge compared to the 33-bus network, primarily due to the higher number of variables involved. Additionally, in Case-C, where three SHCs are integrated, the processing time is longer than in the other cases. This observation highlights that

the convergence time is influenced by both the network's size and the number of SHCs integrated.

Table 2.4: Convergence time of distribution networks in different case studies

Distribution network considered	Planning cases	Execution time (in minutes)
33-bus network	Case-A	10.05
	Case-B	13.39
	Case-C	17.09
69-bus network	Case-A	20.19
	Case-B	32.71
	Case-C	40.09

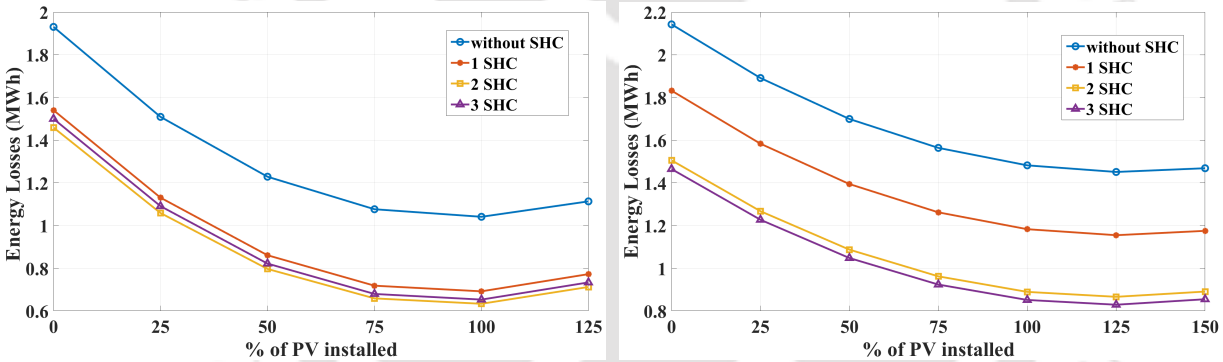

Fig. 2.7: Energy Losses variation when different numbers of SHCs are placed in (a) 33 bus network (b) 69 bus network

2.6.1 Energy losses of the network

Table 2.5 provides the parameter values for the base-case networks. The energy losses of the network after placing the compensators are presented in Tables 2.6 and 2.7 for the 33-bus and 69-bus networks, respectively. Moreover, the tables present the variation in network power losses across all scenarios in 24 hours. In both networks, for all cases and at different levels of PV penetration, the energy losses are lower compared to the base-case scenario. Figure 2.7 depicts the variation of energy losses for the base-case condition and

Table 2.5: Parameters obtained for the base-case networks with PV integration

Distribution network considered	PV generation as % of peak demand	Energy losses (MWh)	Minimum bus voltage (pu)	Maximum bus voltage (pu)	Range of network power losses (kW)
33-bus network	0	1.9307	0.9131	1.0	8.11-202.68
	25	1.5092	0.9226	1.0	7.88-170.20
	50	1.2289	0.9284	1.0	7.67-143.33
	75	1.0768	0.9314	1.0	7.48-134.22
	100	1.0411	0.9338	1.0098	7.30-125.84
	125	1.1133	0.9358	1.0279	6.40-118.12
69-bus network	0	2.1429	0.9092	1.0	8.99-224.95
	25	1.8914	0.9128	1.0002	8.85-205.84
	50	1.6996	0.9163	1.0013	8.71-188.79
	75	1.5642	0.9197	1.0023	8.57-173.72
	100	1.4823	0.9231	1.013	8.45-160.48
	125	1.4513	0.9246	1.0244	8.32-152.50
	150	1.4688	0.9258	1.0356	8.20-147.41

Table 2.6: Solutions obtained for 33-bus distribution network at different PV penetration levels

Planning cases	Location of SHC	PV generation as % of peak demand	Energy losses (MWh)	Minimum bus voltage (pu)	Maximum bus voltage (pu)	Rating of SHC (MVA)	Range of network power losses (kW)
Case-A	30	0	1.5404	0.9211	1.0045	0.8191	17.99-153.46
		25	1.1307	0.9304	1.0046	0.816	16.75-122.57
		50	0.861	0.9362	1.0046	0.8136	9.10-103.99
		75	0.7184	0.9392	1.0047	0.8118	6.44-95.95
		100	0.692	0.942	1.017	0.8106	6.96-88.55
		125	0.7725	0.9438	1.0349	0.81	8.38-84.17
Case-B	30, 6	0	1.459	0.9284	1.0	1.5932	12.57-142.32
		25	1.0588	0.9374	1.0	1.538	12.46-111.97
		50	0.7968	0.9401	1.0	1.4999	11.98-99.03
		75	0.6589	0.9429	1.0	1.4815	8.85-91.24
		100	0.6337	0.9441	1.018	1.4842	8.71-85.26
		125	0.7123	0.9453	1.0361	1.5077	7.83-83.33
Case-C	15, 30, 25	0	1.4939	0.9261	1.006	1.1398	21.11-145.67
		25	1.091	0.935	1.0059	1.1251	17.30-115.29
		50	0.822	0.9406	1.0059	1.1161	8.11-98.25
		75	0.6797	0.9435	1.006	1.1134	5.22-90.31
		100	0.6532	0.9466	1.0213	1.117	7.16-82.86
		125	0.7337	0.9489	1.0395	1.1258	9.87-79.55

Table 2.7: Solutions obtained for 69-bus distribution network at different PV penetration levels

Planning cases	Location of SHC	PV generation as % of peak demand	Energy losses (MWh)	Minimum bus voltage (pu)	Maximum bus voltage (pu)	Rating of SHC (MVA)	Range of network power losses (kW)
Case-A	61	0	1.8323	0.9279	1.0018	1.1563	38.19-157.77
		25	1.5836	0.9313	1.0018	1.1528	35.20-139.84
		50	1.3947	0.9347	1.0018	1.1494	30.27-123.93
		75	1.2621	0.938	1.0052	1.1461	26.01-111.09
		100	1.1831	0.9413	1.0168	1.143	24.89-106.27
		125	1.155	0.943	1.0281	1.1401	24.46-101.69
		150	1.1754	0.9441	1.0393	1.1373	25.28-97.35
Case-B	61, 12	0	1.5059	0.9292	1.0	1.5513	9.41-152.89
		25	1.2675	0.9326	1.0002	1.5371	9.34-135.08
		50	1.0873	0.936	1.0012	1.5291	9.24-119.26
		75	0.9623	0.9393	1.0058	1.5277	9.11-108.65
		100	0.8894	0.9408	1.0174	1.5326	8.95-103.84
		125	0.8663	0.942	1.0288	1.5437	8.77-99.24
		150	0.8909	0.9432	1.0401	1.5602	8.26-94.86
Case-C	17, 11, 61	0	1.465	0.9297	1.0	1.6985	7.69-151.19
		25	1.2273	0.9331	1.0002	1.6744	7.66-133.42
		50	1.0481	0.9364	1.0012	1.6604	7.59-117.63
		75	0.9238	0.9397	1.0078	1.6569	7.49-107.04
		100	0.8516	0.9413	1.0194	1.6643	7.37-102.26
		125	0.8293	0.9425	1.031	1.6826	7.21-97.68
		150	0.8550	0.9437	1.0424	1.7114	6.75-93.34

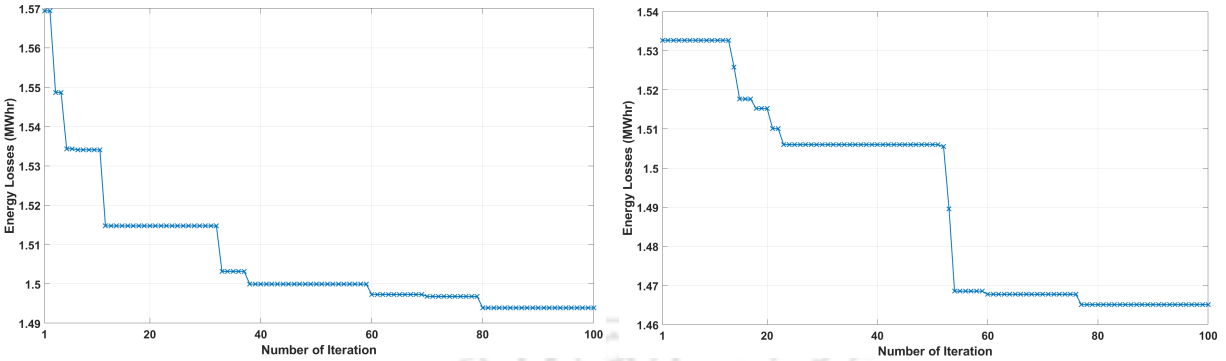

(a) (b)

Fig. 2.8: Convergence curves showing the variation in energy losses for the (a) 33-bus and (b) 69-bus networks with three SHCs installed

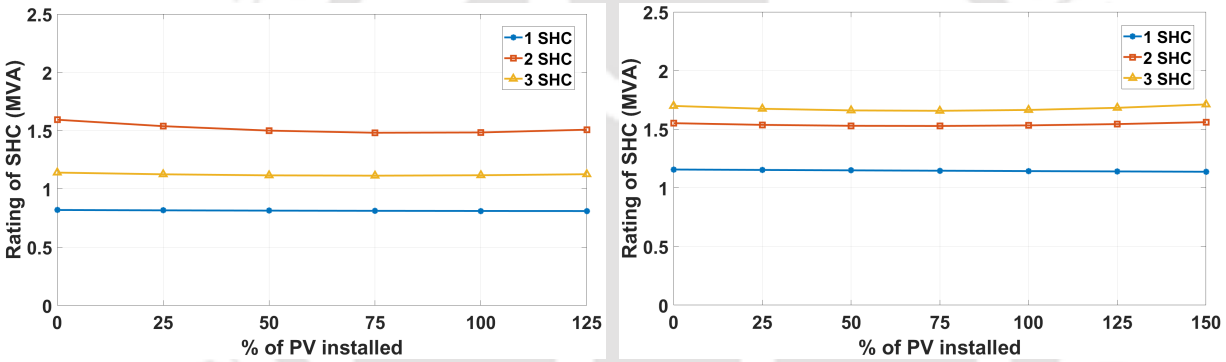

(a) (b)

Fig. 2.9: SHC Rating variation when different numbers of SHCs are placed in (a) 33 bus network (b) 69 bus network

all three cases in both networks. Additionally, Figure 2.9 displays the variations in SHC ratings across all three cases for both networks.

Tables 2.6 and 2.7 show that the energy losses decrease initially as the PV penetration increases. However, after reaching a certain level of PV penetration, the energy losses start to increase again. In the case of the 33-bus network, the minimum energy losses occur when the total PV rating reaches 100% of the peak load, after which the losses increase. On the other hand, for the 69-bus network, the minimum losses are achieved when the total PV rating is 125% of the peak load. It is also noteworthy that Case-B, with 2 SHCs, yields the minimum energy losses for the 33-bus network, while Case-C, with 3 SHCs, results in

the minimum losses for the 69-bus network. These findings indicate that the number of SHCs required for achieving minimum energy losses depends on the network dimensions. This underscores the significance of network size in optimizing the deployment of SHCs to reduce energy losses effectively. Furthermore, the convergence curves presented in Figure 2.8 illustrate the energy loss variations in the 33-bus and 69-bus networks when three SHCs are integrated. These results demonstrate the optimization performance and impact of the proposed compensator placement strategy in minimizing energy losses across both network configurations.

2.6.2 Rating of compensators

The rating of compensators exhibits slight variations with increasing PV penetration. However, Tables 2.6 and 2.7 reveal differences in the compensator ratings among the three cases. In the 33-bus network, compared to Case-A, Case-B requires approximately double the overall rating of compensators, while Case-C necessitates lower ratings than Case-B. Notably, Case-B leads to the minimum energy losses in the 33-bus network.

Similarly, for the 69-bus network, Table 2.7 indicates that Case-C requires the highest overall rating of SHCs, while Case-A and Case-B have lower ratings. It is observed that Case-C yields the minimum energy losses in the 69-bus network. These results suggest that higher ratings of compensators are needed to achieve minimum energy losses. Additionally, the findings suggest that the selection of SHC ratings is more influenced by achieving minimum energy losses rather than solely by the number of SHCs installed. Therefore, optimal network integration with higher-rated compensators minimizes energy losses.

2.6.3 Voltage improvement in the networks

Tables 2.6 and 2.7 show that both the minimum and maximum bus voltages increase with the increase in PV penetration. This indicates that PV integration in the network contributes to voltage improvement. Table 2.8 illustrates the probability of occurrence of

Table 2.8: Probability of occurrence of minimum and maximum bus voltages

Distribution network considered	Planning cases	Probability of occurrence	
		Minimum bus voltage	Maximum bus voltage
33-bus network	Case-A	1/24	1/24
	Case-B	1/24	1/24
	Case-C	1/24	1/24
69-bus network	Case-A	1/24	1/24
	Case-B	1/24	1/24
	Case-C	1/24	1/24

minimum and maximum bus voltages occurring within the analyzed distribution networks. The minimum bus voltage occurs at the 18^{th} hour for the considered load profile, where the peak demand is 0.9 pu and the total PV generation is 0.1 pu. On the other hand, the maximum bus voltage is observed at the 12^{th} hour when the load is at 0.8 pu of the peak load and the entire PV generation is available. It is observed that the bus voltages are influenced by the amount of PV generation in the network.

The presented results for the 33-bus and 69-bus networks consider PV penetration up to 125% and 150% of the peak load, respectively. However, if the PV penetration rating exceeds an additional 25% of the peak load, the maximum bus voltage would surpass the limit of 1.05 pu. Hence, it is essential to note that PV penetration should be carefully managed to avoid violating the voltage constraint.

Table 2.9: Quantitative comparison of the proposed approach with a previous method for the 69-bus distribution network

Parameters	Approach presented in [78]	Proposed approach
Location of SHC	17, 61, 49	61, 12, 17
Location of SEC	2	-
Total SHC rating (MVA)	1.9683	1.726
Overall rating of compensators (MVA)	4.022	1.726
Energy losses (MWh)	1.538	1.4789
Total PV installed (MW)	2.9209	2.9209
Minimum bus voltage (pu)	0.9343	0.9316

Table 2.10: Quantitative comparison of proposed approach with previous approaches for 69-bus distribution network

Parameters	**Approach presented in [103]**	**Approach presented in [104]**	**Approach presented in [105]**	**Proposed approach**
Location of SHC	61	61	12, 61, 64	17, 11, 61
Location of DG	61	61	-	Uniformly distributed among all buses except the substation bus
Total rating of SHC (MVA)	1.301	0.9045	2.457	1.6826
Total rating of DG (MW)	1.828	0.1223	-	4.7525
Energy losses (MWh)	1.022	1.3025	1.8638	0.8293
Minimum bus voltage (pu)	0.9501	0.9259	0.9306	0.9425

2.6.4 Quantitative comparison of the proposed approach with previous approaches

Tables 2.9 and 2.10 provide a quantitative comparison between the proposed approach and previous approaches [78, 103–105]. These results are specifically for the 69-bus distribution network.

Table 2.9 compares the parameter values obtained from the proposed method and the previous method [78]. The proposed approach considers equal PV penetration for all network buses except the substation bus. On the other hand, [78] considers non-uniform PV penetration across the network. Additionally, the proposed approach focuses on optimal SHC placement, while [78] considers both SEC and SHC placement. The results in Table 2.9 demonstrate that the proposed approach achieves lower energy losses compared to [78] for the same level of PV integration. The proposed approach also lowers the total SHC rating and overall compensator rating. However, it should be noted that including SEC in [78] increases the overall compensator rating and helps mitigate voltage sag.

Table 2.10 compares the present approach with [103], [104] and [105]. The minimization of energy losses depends on the ratings and placement of compensators in the network. The compensator and PV locations in [103–105] are determined to minimize network power loss. The energy losses are calculated based on the optimal compensator and PV ratings provided in [103–105] to facilitate comparison. These energy losses consider the current load and PV generation profile depicted in Figure 2.6. Table 2.10 shows that the proposed approach achieves lower energy losses compared to [103–105], despite higher PV integration. The minimum bus voltage remains relatively similar across all approaches.

2.7 Summary

This chapter focuses on achieving energy loss minimization through the optimal allocation of SHCs in PV-integrated distribution networks. The locations of SHCs are determined

using the PSO technique. By supplying reactive power to the network, SHCs effectively mitigate line current harmonics. Simulations are conducted for different levels of PV penetration in the distribution network, and the results are analyzed for various scenarios considering different numbers of SHCs integration. The key findings from the results are as follows:

- The research findings indicate that achieving effective minimization of energy losses requires the integration of 2 SHCs for the 33-bus network and 3 SHCs for the 69-bus network. However, the exact number of SHCs needed depends on the specific dimensions of the network.
- To achieve minimal energy losses, integrating compensators with higher capacities into the network is necessary. This optimization strategy is vital in enhancing network performance and effectively reducing energy losses.
- Bus number 30 is identified as one of the optimal locations for SHC integration in the 33-bus distribution network, while bus number 61 is optimal in the 69-bus network. The high load demand at these specific locations in both networks influences this choice.
- Compared to networks with PV integration without SHCs, the optimal placement of SHCs in PV-integrated distribution networks yields an additional energy loss reduction of approximately 30-35%.

Chapter 3

Economic Evaluation of Multiple Shunt Compensators and PV Units in Distribution Networks for Maximizing Profit

3.1 Introduction

The integration of PV systems into distribution networks is increasingly popular due to the rising demand for renewable energy. This integration offers advantages such as reduced reliance on non-renewable energy, lower greenhouse gas emissions, and enhanced energy security [106]. However, the increase in PV installations presents technical and economic challenges, including network instability due to the fluctuating nature of PV generation and dynamic load demands, as well as power quality issues and voltage fluctuations [107–109]. Distribution system planning is crucial in addressing these challenges by minimizing costs and maximizing benefits, such as reducing energy losses and improving voltage profiles.

Numerous research efforts have focused on enhancing technical features like voltage

stability, power losses, and harmonic distortion through optimal SHC placement [110–112]. Reference [110] devised a method to minimize active and reactive power losses by identifying optimal SHC sizes and locations. In [111], analyzing the effects of SHC allocation on different load models and calculating annual energy savings are investigated. Additionally, in [112], integrating PV systems with SHCs in distribution networks aims to enhance voltage profiles and reduce energy loss, considering 24-hour load variations. Numerous research endeavors have also delved into the optimal sizing and placement of DG units in distribution networks. For instance, [113] formulates a cost function based on total system losses to optimize DG unit sizing and placement across varying load scenarios. Genetic algorithms are employed in [114] to optimize the configuration of a microgrid consisting of various DG sources, aiming to maximize the present net worth. In [115], a multi-objective optimization approach is employed to minimize the total active power losses of the network and reduce the overall DG installation cost. The investigation into optimal placement of DG units to maximize profit, minimize losses, and enhance voltage regulation within distribution networks is explored in [116].

Recent research has begun to address the optimization of SHC placement in distribution networks while concurrently considering both technical and economic considerations. Notably, [92, 117–119] have proposed methodologies that factor in technical and economic elements when identifying optimal SHC locations. In [117], a study evaluated the techno-economic benefits of distribution networks through the simultaneous optimization of PV and SHC placements. Sensitivity analysis methods in [92] are utilized to identify SHC locations within mesh distribution networks, focusing on enhancing voltage profiles and achieving annual cost savings. Alternatively, [118] has introduced an optimization technique that minimizes overall energy loss costs and SHC installation expenses over a predefined planning horizon. A multi-objective optimization framework for SHC allocation in distribution networks is presented in [119], aiming to minimize total annual costs and enhance voltage stability.

Based on the literature discussed above, the following research gaps emerge:

- While the economic benefits of SHC deployment in passive distribution networks have been explored, there is a lack of studies on their potential advantages in active distribution networks. This highlights the need for an economic analysis to determine the benefits of SHC installation in active networks. This significant research gap necessitates a comprehensive assessment of the cost-effectiveness of deploying both PV units and SHCs in distribution networks to determine their collective economic viability.

- Despite the increasing interest in optimizing SHC placement in PV-rich distribution networks, the literature has yet to address the optimal allocation of multiple SHCs to maximize profit from saved energy losses while considering variations in PV generation, load demand, and annual load growth. This gap underscores the need for advanced planning strategies that account for weather conditions and seasonal fluctuations in PV power generation and load demand. Such strategies would enable a more comprehensive placement of both PV units and SHCs to maximize the overall benefits.

This chapter aims to optimize profit by considering installation costs and benefits from energy loss reduction through SHC placement in distribution networks. Addressing research gaps, the chapter undertakes an economic assessment of co-placing PV units and SHCs, accounting for seasonal variations in PV generation and load demand. The PSO method formulates an approach for SHC placement that maximizes overall profit and minimizes energy losses within PV-integrated distribution networks. The contributions of this chapter are as follows:

- Introducing an optimization model that balances installation costs against the benefits of energy loss reduction to determine optimal SHC placements in PV-integrated

distribution networks. This formulation aims to maximize profit while accounting for the economic aspects of both PV units and SHCs.

- Determining optimal SHC allocations across various PV penetration levels to achieve maximum profit within a designated planning horizon while considering load growth, seasonal load variations, and PV generation profiles.

The proposed planning approach has been validated using the 33-bus and 69-bus distribution networks.

3.2 Modelling and placement of compensators in the network

This chapter uses the modeling approach outlined in Section 2.2 for SHC modeling. Based on the methodology described in Section 2.3, this chapter employs the FBS load flow algorithm to calculate SHC ratings, network voltages, and currents. The overall VA and reactive power ratings for multiple integrated SHCs are calculated using Equations 2.9 and 2.10. Furthermore, the variation in active and reactive power demands of the buses due to the placement of PV units and SHCs in the network are calculated through Equations 2.14 and 2.15.

3.3 Economic evaluation of PV and SHC investment costs

3.3.1 Investment cost of PV

The investment in PV contains installation, operational, and maintenance (OM) expenses. Mathematically, it is represented as:

$$\text{Investment of PV}, (IN)_{PV} = (IN)^{PV}_{initial} + (IN)^{PV}_{OM} \tag{3.1}$$

Where $(IN)_{PV}$ denotes the investment cost of PV, $(IN)^{PV}_{initial}$ represents the initial investment, and $(IN)^{PV}_{OM}$ signifies the OM costs associated with the PV system. The initial cost

of the PV system can be determined using:

$$(IN)_{initial}^{PV} = C_{initial}^{PV} \quad P_{PV}^{rating} \tag{3.2}$$

In the equation, $C_{initial}^{PV}$ is the initial cost per unit capacity in \$/kW, and P_{PV}^{rating} denotes the installed capacity of the PV system in kW.

To evaluate the costs and savings due to PV unit and SHC allocation, the Present Worth Factor (PWF) analysis is conducted. Equations (3.3) and (3.4), are employed to determine the present value of future cash flows, which depends on the interest rate (IR) and inflation rate (IF). These equations are essential for conducting a comprehensive cost-benefit analysis over the project's lifespan.

$$\text{PWF for } n^{th} \text{ year, } \beta_n = \left(\frac{1+IF}{1+IR}\right)^n \tag{3.3}$$

$$\text{PWF for planning period, } \beta^{T_p} = \sum_{n=0}^{T_p} \left(\frac{1+IF}{1+IR}\right)^n \tag{3.4}$$

Here, T_p represents the project's duration in years.

Equation (3.3) computes the PWF for the n^{th} year, while equation (3.4) calculates the cumulative PWF over the entire planning period.

The PWF of OM costs over the planning period can be expressed as:

$$(IN)_{OM}^{PV} = C_{OM}^{PV} \quad P_{PV}^{rating} \quad \beta^{T_p} \tag{3.5}$$

In this equation, C_{OM}^{PV} denotes the PV system's OM cost per unit capacity, measured in \$/kW/year.

3.3.2 Investment cost of SHC

The calculation for the investment needed for the installation of an SHC is represented by the equation:

$$(IN)_{SHC} = C_P^{SHC} \quad S_P^{SHC} \quad \beta_n \tag{3.6}$$

In this equation, S_P^{SHC} denotes the SHC's rating in kVA, while C_P^{SHC} signifies the cost of the SHC in \$/kVA.

3.4 Economic evaluation of benefits due to PV and SHC

3.4.1 Cost savings due to energy loss reduction

Reducing energy losses in the distribution network is one of the main goals for the Distribution Network Owner (DNO), as this maximizes profit. The AEL is computed using equation (3.7) based on the seasonal load and PV generation profiles [26]. The seasonal load profile and PV generation curves are depicted in Figures 3.1 (a) and (b), respectively. The four seasonal load and PV profiles are considered to determine the AEL, i.e., Summer, Winter, Spring, and Autumn. It is important to note that in Figure 3.1 (b), the PV generation curves for the spring and autumn seasons are identical.

$$AEL = \sum_{s=1}^{4} \left(\frac{365}{4}\right) \quad (EL_s) \tag{3.7}$$

where EL_s represents the daily energy losses for season 's' (in kWh).

The Saved AEL is then determined using equation (3.8). Here, the Saved AEL represents the reduced energy losses obtained by placing PV units and SHCs in the network compared to the base-case scenario where no PV units or SHCs are installed.

$$Saved\ AEL = (AEL)_{BCS} - (AEL)_{wPS} \tag{3.8}$$

where $(AEL)_{BCS}$ and $(AEL)_{wPS}$ represent the AEL obtained for the base-case network and, after placing PV units along with SHCs, respectively.

The PWF of the cost savings obtained from reducing AEL is calculated using the following equation:

$$CS_{EL} = \sum_{n=0}^{T_p} C_{EL} \;\; (Saved\ AEL)_n \;\; \beta_n \tag{3.9}$$

Here, CS_{EL} represents the cost savings due to AEL reduction in \$. C_{EL} represents the cost of energy loss in \$/kWh. $(Saved\ AEL)_n$ represents the energy loss reduction achieved in the n^{th} year, considering the network's annual load growth.

3.4.2 Financial returns due to the active power produced by PV

Integrating PV units into the distribution network can reduce electricity procurement from the transmission grid, enabling the DNO to sell surplus electricity back to the grid potentially. This analysis assumes that all generated electricity from the PV system is sold to the grid. The PWF for the financial return due to PV-generated power is expressed as:

$$FR_{PV} = \sum_{n=0}^{T_p} EP_{PV} \;\; (RP_{PV})_n \;\; \beta_n \tag{3.10}$$

Here, FR_{PV} signifies the financial returns resulting from the active power produced by the PV system in \$. EP_{PV} represents the price of PV-generated electricity in \$/kWh. $(RP_{PV})_n$ denotes the active power produced by the PV system in the n^{th} year.

3.5 Problem formulation

The proposed methodology focuses on identifying optimal locations for SHCs within a PV-integrated distribution network to maximize profit over a planning period. Various numbers of SHCs are strategically placed at different levels of PV penetration. The optimization approach addresses two scenarios:

- **Scenario-1:** Distribution system companies integrate SHCs into the PV-integrated network, with PVs already positioned in the network. The objective function for Scenario-1 is represented as:

$$\text{Maximize Profit}, Pr_{Sc1} = CS_{EL} - (IN)_{SHC} \tag{3.11}$$

Here, Pr_{Sc1} represents the objective function to maximize profit in Scenario-1.

- **Scenario-2:** Distribution network companies manage customer demand, PV operations, and network distribution. The objective function for Scenario-2 is represented as:

$$\text{Maximize Profit}, Pr_{Sc2} = CS_{EL} + FR_{PV} - (IN)_{SHC} - (IN)_{PV} \tag{3.12}$$

Here, Pr_{Sc2} represents the objective function to maximize profit in Scenario-2.

In Scenario-1, the investment cost is considered as the investment of SHC, while the economic savings reflect the cost savings due to energy loss reduction. However, in Scenario-2, the total investment cost is the investment cost involved in PV units and SHCs within the network. The economic savings represent the overall cost savings from energy loss reduction and the revenue generated by selling PV-generated energy to the electricity market.

When optimizing the objective function to determine the optimal SHC placements within a PV-integrated distribution network, the constraints related to power balance and SHC locations are considered. The power balance constraints are mathematically represented in equations 2.17 and 2.18. The SHC location constraint is mathematically expressed in equation 2.21. This constraint ensures that no two SHCs are placed at the same location within a particular distribution network.

Table 3.1: PSO parameters

Parameters	Considered values
Inertia weight, w	0.8
Acceleration coefficient, c_1	1.5
Acceleration coefficient, c_2	1.5
Population size, N_p	200
Maximum number of iterations, $MaxIt$	100

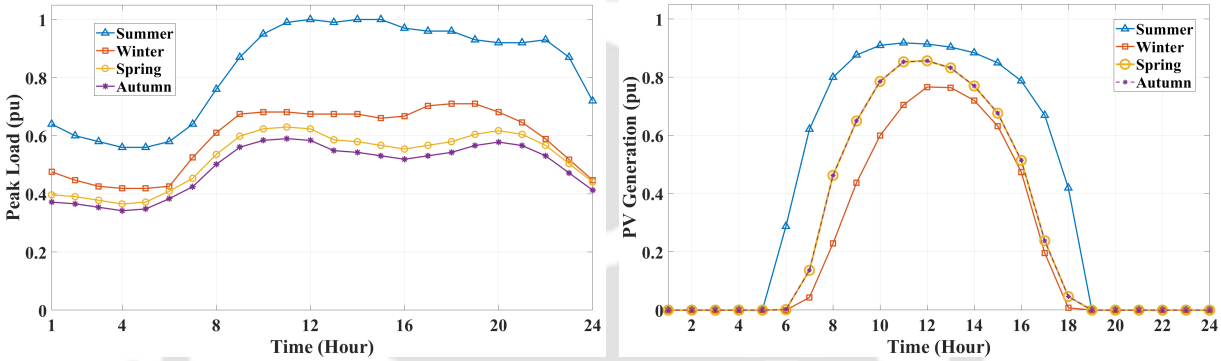

(a) (b)

Fig. 3.1: Seasonal (a) Load profile (b) PV profile

3.6 Solution strategy

The primary objective of this study is to optimize the placement of SHCs within the PV-integrated distribution network. The PSO algorithm is the solution strategy for determining the optimal locations for SHCs in the network. The basics of the PSO algorithm are discussed in subsection 2.5.1. The specific PSO parameters employed for this analysis are elaborated in Table 3.1. The overall planning algorithm uses the FBS load flow algorithm with the SHC model as the support subroutine. The optimization focuses on maximizing the profit obtained due to the optimal placement of SHCs in the network. An illustration of the sequential planning process is provided in the pseudo-code, shown in Figure 3.2.

N_p : Size of population
$MaxIt$: Maximum number of iterations
Begin
Input bus data and line data of the distribution network
Initialise input parameters for PSO
Initialise position and velocity of particles for size N_p
Calculate SHC rating and profit value for corresponding locations
Determine L_{best} and g_{best}
t = 1;
While t <= $MaxIt$
For p = 1:N_p
Update position and velocity of particles using respective equations
Perform FBS load flow algorithm
Calculate objective function value
Update L_{best} and g_{best} accordingly
t = t + 1
End for
End while
The final g_{best} values are the desired locations of the SHCs and the corresponding objective function value is the maximum profit obtained for the considered scenario
End

Fig. 3.2: Pseudo-code for PSO Algorithm to determine optimal SHC locations and maximum profit

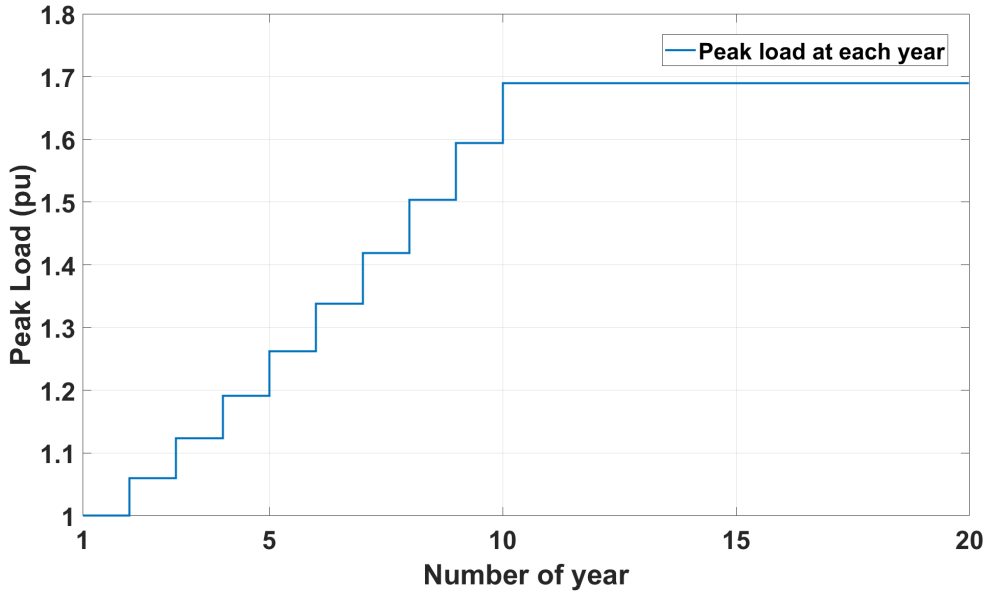

Fig. 3.3: Considered load growth for planning period of 20 years

Table 3.2: Planning and cost parameters

Planning parameters	Cost parameters
T = 20 years [78]	$C^{PV}_{initial}$ = 857 \$/kW [120]
THD = 0.2 [78]	C^{PV}_{OM} = 14.1 \$/kW/year [120]
IF = 9 % [121]	EP_{PV} = 0.048 \$/kWh [120]
IR = 12.5 % [121]	C^{SHC}_{P} = 60 \$/kVA [122]
-	C_{EL} = 0.08 \$/kWh [123]

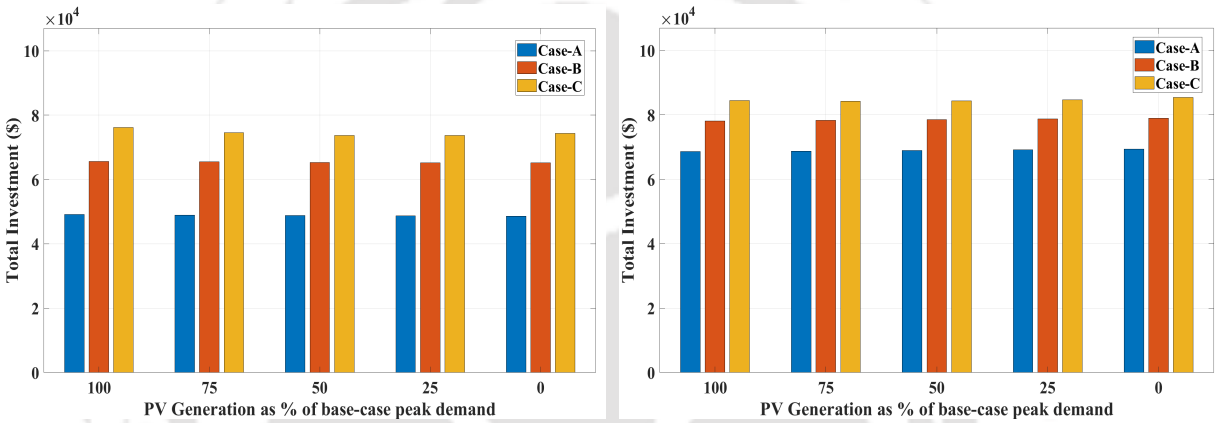

Fig. 3.4: Investment of SHC for (a) 33-bus (b) 69-bus distribution networks

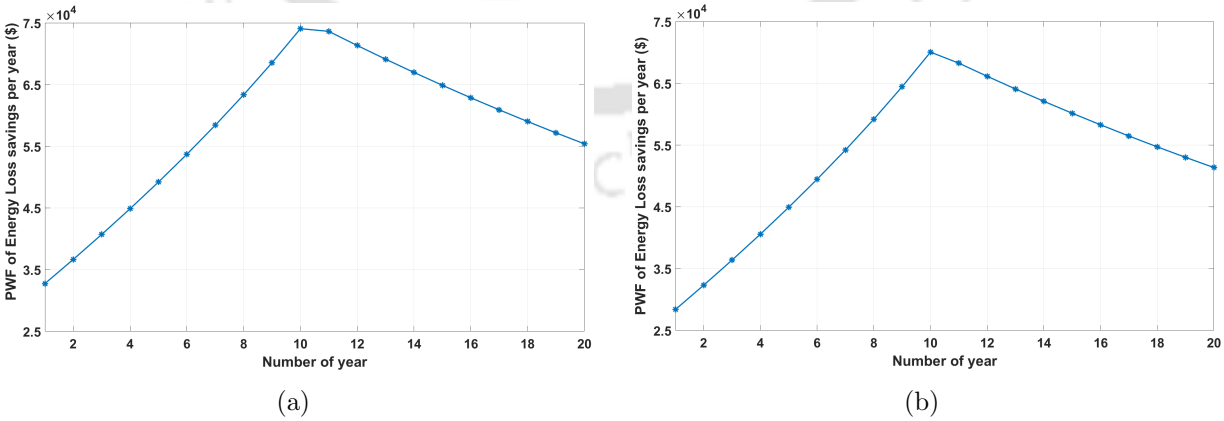

Fig. 3.5: Annual energy loss savings for (a) 33-bus (b) 69-bus distribution networks

Table 3.3: SHC locations and ratings for 33-bus and 69-bus distribution networks at various PV penetration levels

Planning cases	PV generation as % of peak demand	33-bus network			69-bus network		
		Location of SHC		Rating of SHC (MVA)	Location of SHC		Rating of SHC (MVA)
		1st year	11th year		1st year	11th year	
Case-1	0	30	-	0.8191	61	-	1.1563
	25			0.8160			1.1528
	50			0.8136			1.1494
	75			0.8118			1.1461
	100			0.8106			1.1430
Case-2	0	30	13	1.1961	61	21	1.3745
	25			1.1931			1.3709
	50			1.1906			1.3675
	75			1.1888			1.3643
	100			1.1876			1.3612
Case-3	0	30, 10	14	1.3196	61, 16	65	1.4347
	25			1.2908			1.4233
	50			1.2753			1.4169
	75			1.2739			1.4156
	100			1.2866			1.4192

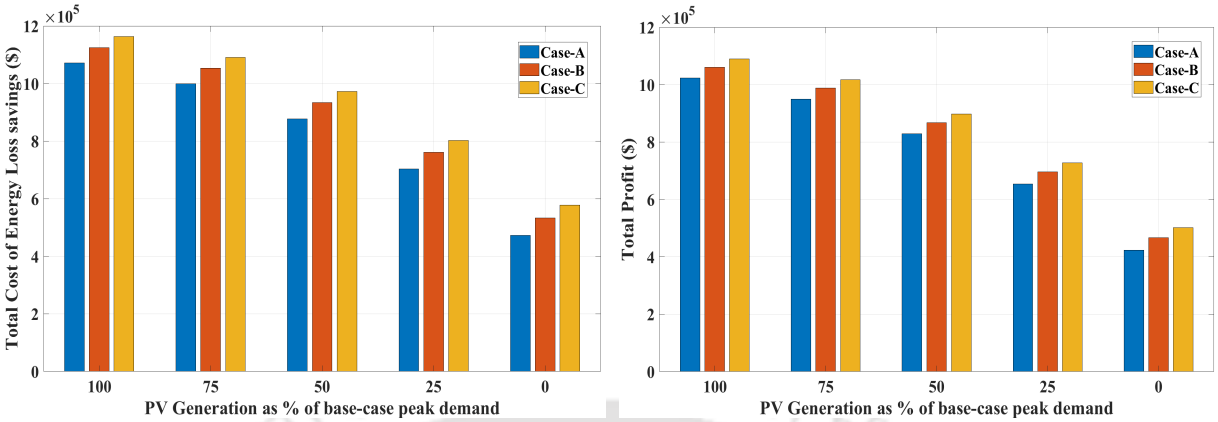

Fig. 3.6: (a) Energy loss savings and (b) Profit for 33-bus distribution network

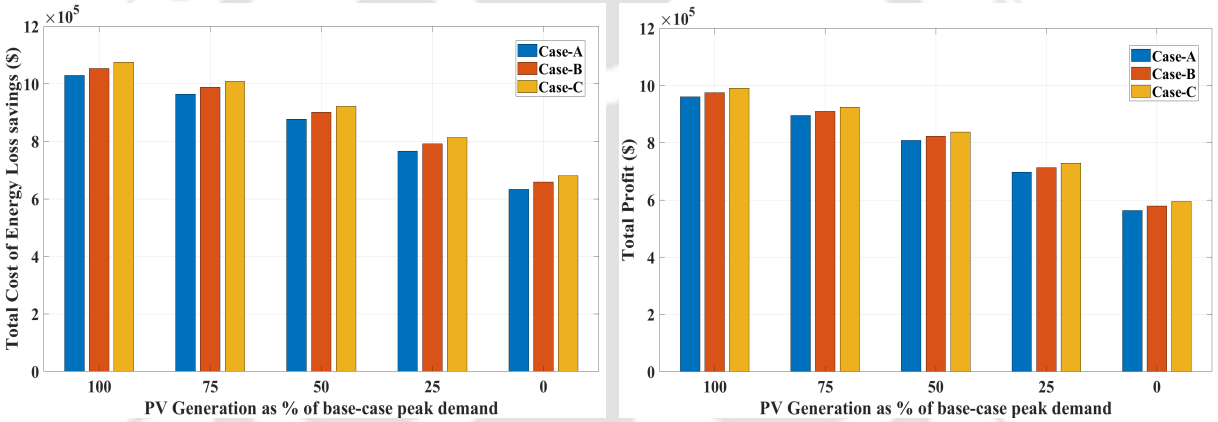

Fig. 3.7: (a) Energy loss savings and (b) Profit for 69-bus distribution network

3.7 Results and discussion : Scenario-1

In order to assess the efficacy of the proposed methodology, the current study employs the MATLAB/Simulink environment to simulate two test systems: the 33-bus and 69-bus distribution networks. The single-line diagrams of the 33-bus and 69-bus distribution networks are provided in Figures A.1 and A.2, respectively. The computation of energy losses depends upon seasonal load and PV profiles, contributing to variable energy loss values influenced by daily load and PV patterns. The analysis relies on seasonal load profiles and PV generation curves shown in Figure 3.1 [26]. Over 20 years, energy loss

calculations consider load growth dynamics, as depicted in Figure 3.3, with a 6% annual growth rate up to the tenth year, followed by a constant load level for the subsequent planning duration [124].

The Ownership of PV installations in distribution networks typically falls into three categories:

- PV owns by the DNO
- PV owns by customers
- PV owns by the third party

Typically, customers or third parties own PV installations in distribution networks rather than the DNO. Customers benefit from receiving PV-generated energy at a lower cost than conventional energy sources, while third parties benefit from utilizing resources made available by customers. The present study assumes that customers or third parties integrate PV units into the network.

This scenario considers three cases targeting optimal SHC placement for profit maximization within the PV-integrated distribution network. The cases are demonstrated based on the number of SHCs integrated into the network. In Case-1, a single SHC is introduced in the first year. Case-2 considers the deployment of two SHCs, with the first SHC positioned in the first year and the second in the eleventh year. Lastly, Case-3 involves the installation of three SHCs, with two integrated in the first year and the third added in the eleventh year. This study also considers various case studies with PV generation potential ranging from 25% to 100% of the total peak load.

The present approach computes the compensator rating after integrating a predetermined level of PV generation into the distribution network. The various planning parameters and related cost components used in the analysis are outlined in Table 3.2. Furthermore, Table 3.3 displays the positions and ratings of SHCs across varying cases and levels of PV integration.

3.7.1 Investment in SHCs

The investment needed to install SHCs in the 33-bus and 69-bus distribution networks is presented in Figure 3.4 for all three cases. It is worth noting that for cases where SHCs are placed in the eleventh year, approximate assessment of investment costs requires consideration of the PWF. This adjustment ensures the desirable comparison of the investment costs associated with SHCs in different years.

The analysis results reveal that Case-1 presents the lowest investment compared to the other cases, given its installation of only one SHC in the first year. Case-2 requires a higher investment than Case-1 but less than Case-3, considering the installation of two SHCs. Case-3 demands the highest investment due to installing three SHCs, two in the first year and one in the eleventh year. Therefore, the investment for SHC installation varies depending on the number of SHCs and their ratings.

3.7.2 Cost savings from energy loss reduction

Figures 3.6 (a) and 3.7 (a) visually display the advantages obtained from energy loss reduction due to the optimal installation of SHCs in various cases for both the 33-bus and 69-bus networks. Additionally, to highlight the effect of the proposed approach, Figures 3.5 (a) and (b) show the changes in AEL savings over 20 years, particularly through Case-3. From Figure 3.5, it is evident that energy loss reduction increases gradually over the years. This is because the base-case network's energy losses rise annually due to growing loads. Consequently, the saved energy losses also increase due to the installation of SHCs. The findings highlight that the cost savings from energy loss reduction hold greater significance in the subsequent ten-year period than its impact in the initial decade, as illustrated in Figure 3.5. This difference is primarily due to the increased load growth during the last ten years. The saved energy losses remain constant during the final ten years due to the constant load conditions. However, the cost savings associated with energy loss reduction experienced a gradual decline throughout the subsequent decade, reflecting the impact of

the PWF.

Furthermore, an important observation is that energy loss reduction remains effective up to PV integration reaching 100% of peak load demand. This implies that the network can accommodate significant PV integration without compromising energy loss reduction. A balanced approach between PV integration and SHC placement is crucial to optimize cost savings. This is because excessive PV integration beyond a certain point could impact the savings obtained due to energy loss reduction.

3.7.3 Overall profit

The profit resulting from the strategic placement of SHCs is illustrated in Figures 3.6 (b) and 3.7 (b) for the 33-bus and 69-bus networks across different cases. Notably, Case-3 has higher profits than other cases. This outcome justifies the increased investment required for its implementation. These findings underscore that reducing energy losses from SHC integration in PV-integrated distribution networks can substantially enhance the cumulative profit yield. Moreover, the outcomes validate the rationale behind investing in installing multiple SHCs within the distribution network.

3.7.4 Comparative analysis of proposed approach and previous approach

A detailed comparison between the outcomes obtained from the present approach and a previous methodology [125] is presented in Table 3.4 for the 69-bus distribution network. Both approaches focus on optimizing the placement of SHCs in a radial distribution network, considering technical and economic aspects. In this assessment, the SHC placement and ratings from the previous approach are adopted for comparison, with simulations conducted using the cost parameters specified in the present study.

The results highlight that the current approach achieves a superior profit outcome compared to the previous methodology. This improvement is due to the strategic SHC placement to optimize savings from energy loss reduction. The present methodology ef-

Table 3.4: Comparison of the proposed approach with previous similar approach for the 69-bus distribution network: Quantitative Analysis

Parameter	Previous work [125]		Present work	
	Only SHC	**Both PV and SHC**	**Only SHC**	**Both PV and SHC**
Location of SHC	64	64	61	61
Rating of SHC (MVA)	0.92	0.92	1.1563	1.143
Location of PV	-	uniformly distributed	-	uniformly distributed
Rating of PV (MW)	0	3.802	0	3.802
Investment of SHC (10^4 \$)	5.52	5.52	6.9379	6.8581
Cost Savings due to energy loss reduction ($\times 10^5$ \$)	5.5491	9.5951	6.63276	10.294
Total profit ($\times 10^5$ \$)	4.9971	9.0431	5.6338	9.6084

fectively identifies SHC locations by incorporating factors such as PV integration, load growth, seasonal load variations, and PV generation profiles. Consequently, it maximizes profit by reducing energy losses within the PV-integrated distribution network.

3.8 Results and discussion : Scenario-2

This scenario explores two distinct cases, each designed to optimize overall profit in the context of PV-integrated distribution networks:

- **Case-A:** This case study involves only the placement of PV units within the distribution network without integrating compensators.
- **Case-B:** In the PV-integrated distribution network, the study places SHC-1 and SHC-2 in the first year, while the integration of SHC-3 is scheduled for the eleventh year. This sequencing is based on the favorable results observed in Scenario-1.

Table 3.5: SHC locations and ratings obtained for 33-bus and 69-bus distribution networks at different PV penetration levels

Planning cases	PV generation as % of peak demand	33-bus network			69-bus network		
		Location of SHC		Rating of SHC (MVA)	Location of SHC		Rating of SHC (MVA)
		1^{st} year	11^{th} year		1^{st} year	11^{th} year	
Case-B	20	30, 10	14	1.2956	61, 16	65	1.4136
	40			1.2798			1.4073
	60			1.2730			1.4043
	80			1.2753			1.4045
	100			1.2866			1.4078
Case-A	No SHC is considered in this planning						

3.8.1 Investment of PV and SHC

Table 3.5 presents the optimal locations and ratings of SHCs in the 33-bus and 69-bus distribution networks at different levels of PV penetration. Figures 3.8 (a) and (b) visually depict the total investment for the 33-bus and 69-bus networks, respectively. While the

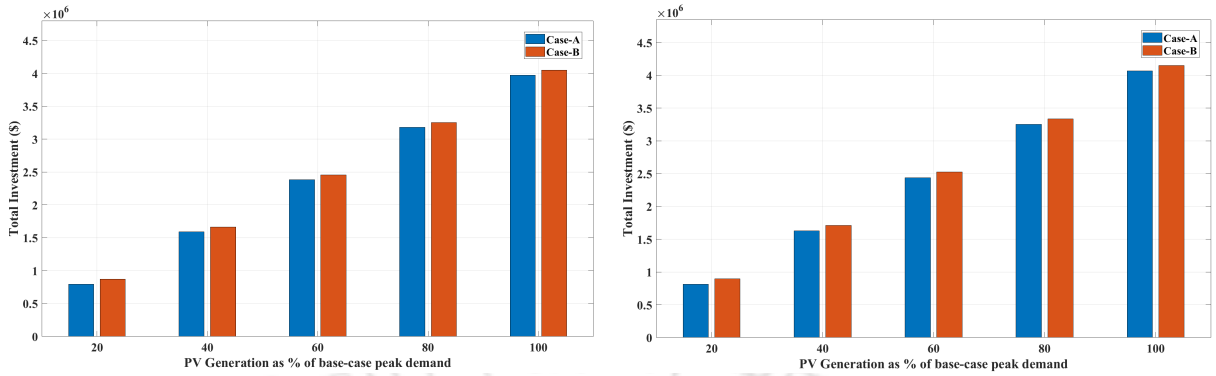

Fig. 3.8: Bar chart presenting the total investment in both the cases for the (a) 33-bus and (b) 69-bus distribution networks

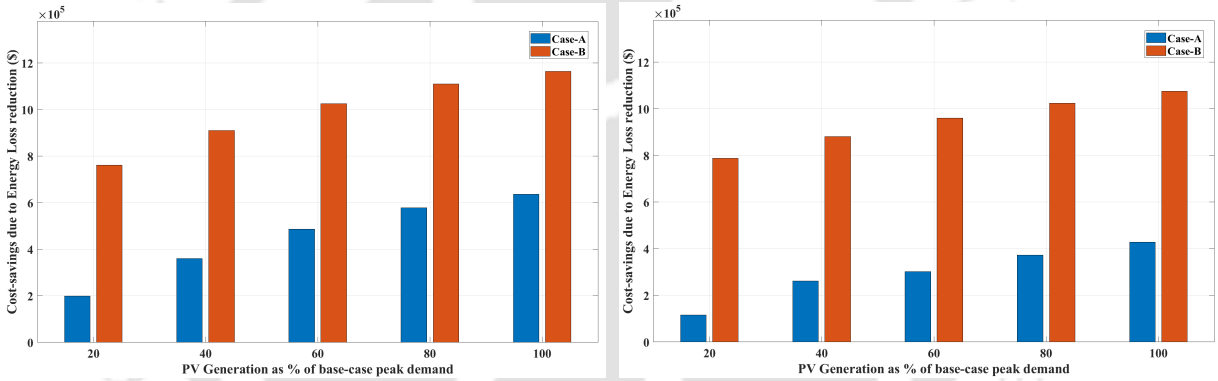

Fig. 3.9: Bar chart presenting the overall cost-saving resulting from Energy Loss reduction in both the cases for the (a) 33-bus and (b) 69-bus distribution networks

investment in PV remains constant across both cases within the distribution network, Case-B incurs slightly higher costs than Case-A due to the addition of compensators. Investment in SHCs varies according to their respective ratings.

3.8.2 Profit obtained due to PV and SHC placement

Figure 3.9 illustrates the cost-savings due to energy loss reduction for both the 33-bus and 69-bus distribution networks. Incorporating SHCs into the network has a noticeable impact on the savings due to energy loss reduction. In Case-A, where only PV units are integrated, the cost saving is relatively modest. Conversely, Case-B, featuring the

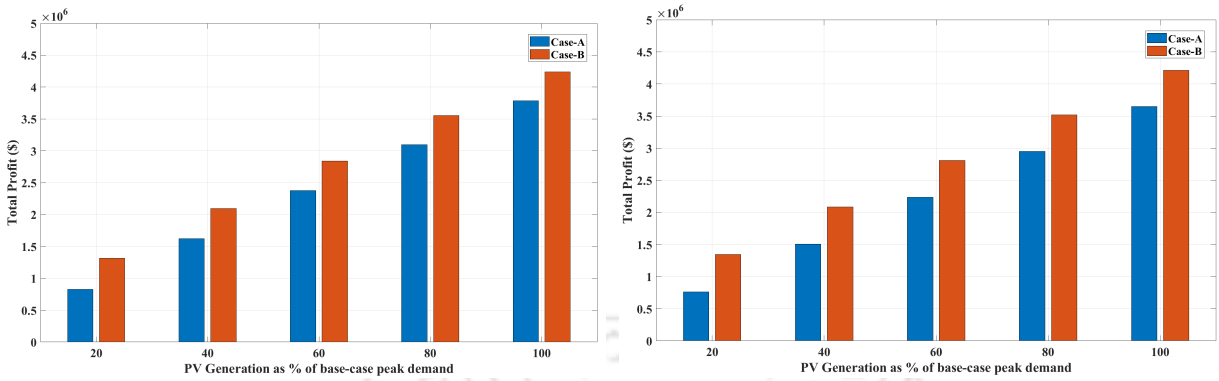

Fig. 3.10: Bar chart presenting the total profit obtained in two cases for the (a) 33-bus and (b) 69-bus distribution networks

integration of three SHCs and PV units, offers more cost savings. Notably, the outcomes signify that networks with higher PV integration exhibit more cost savings due to energy loss reduction.

The bar charts in Figure 3.10 illustrate the overall profit obtained for the 33-bus and 69-bus distribution networks within the two examined cases. It is evident that as the penetration of PV systems increases, the total profit also increases. The primary contributor to profit is obtained from the active power generation derived from the PV installations, a factor that remains constant across all cases. However, the advantageous impact of energy loss reduction is more pronounced in Case-B. Consequently, there is a notable difference in profit between the two cases, with Case-B generating the highest profit. Furthermore, in Figure 3.11, the convergence patterns of the PSO algorithm are shown for both the 33-bus and 69-bus networks. The analyses are performed under the condition where the PV capacity integrated into the network is equal to 100% of the base-case peak load.

3.8.3 Technical aspects in 33-bus and 69-bus distribution networks

The comparison of technical aspects between the 33-bus and 69-bus distribution networks at a load level of $(1.06)^{10}$ of the base-case peak load is summarized in Table 3.6 and visualized in Figure 3.12. The considered PV integration corresponds to 100% of the

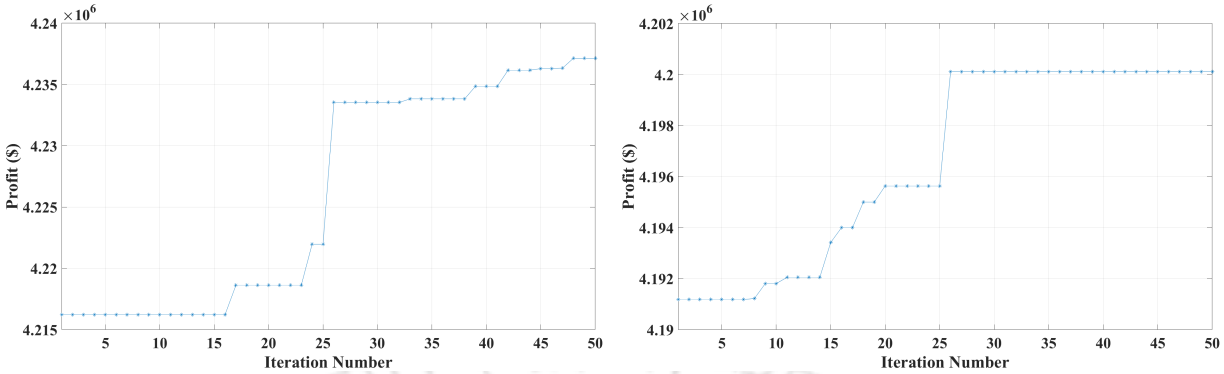

(a) (b)

Fig. 3.11: Convergence plots for the GPRS-PSO Algorithm in the (a) 33-bus and (b) 69-bus networks, under 100% PV Integration

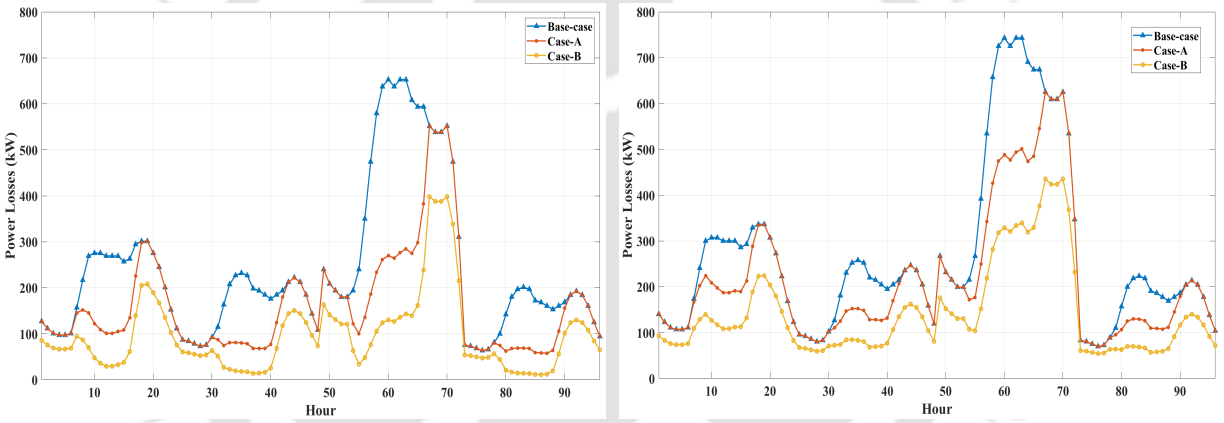

(a) (b)

Fig. 3.12: Comparison of power losses for four seasons (96 hours) with 100% PV integration of initial base-case peak load in the (a) 33-bus and (b) 69-bus distribution network at the 10^{th} year load condition

Table 3.6: Comparison of technical parameters for 100% PV integration of the initial base-case network

Technical Parameter	33-bus network			69-bus network		
	without PV, SHC	Case-A	Case-B	without PV, SHC	Case-A	Case-B
No. of nodes violating voltage constraint	17	16	10	9	9	7
No. of branches violating thermal constraint	5	5	4	17	11	3

peak load of the base case network. Table 3.6 shows that integrating SHCs and PV units in Case-B yields a noteworthy reduction in node and branch count, although some volt-

age and thermal constraints are violated. Conversely, Case-A, comprising only PV units, shows a modest improvement compared to the case without PV or SHC units. Figure 3.12 visually indicates that Case-A significantly reduces power losses. On the other hand, Case-B significantly reduces power losses compared to Case-A. These results suggest that the combination of SHCs and PV units in Case-B leads to a notable improvement in the technical parameters of the distribution network.

3.8.4 Comparative analysis between present and previous approaches

A comprehensive comparison between the outcomes achieved by the present approach and the previous approach [126] is conducted for the 33-bus and 69-bus distribution networks. Table 3.7 compares the results obtained by both methodologies. It is noteworthy that the previous approach involves the installation of PV units on specific buses, whereas the present approach uniformly distributes them among all buses except the substation bus. The PV and compensating device placements, along with their ratings, as per the previous method [126], are used for comparison, employing the cost components from the present work.

It is important to emphasize that while the current approach utilizes SHCs as the compensating devices, the previous method employs capacitors. Although the cost of the SHC is higher than that of the capacitor, it helps mitigate harmonic content in the line current. In contrast, the capacitor only provides reactive power compensation. The comparative analysis shows that the present approach yields higher cost-saving resulting from energy loss reduction in the 33-bus network. The advantage of the previous method is more pronounced in the 69-bus network due to the distinct PV locations. However, it is essential to recognize that the overall profit is more significant in the present method due to the increased penetration of PV in the network. Thus, installing both PV units and SHCs in the present approach increases profitability and results in harmonic reduction.

Table 3.7: Quantitative comparison of proposed approach with previous approach for 33-bus and 69-bus distribution networks

Parameter	33-bus network		69-bus network	
	Previous work [126]	**Present work**	**Previous work [126]**	**Present work**
Location of PV	8	uniformly distributed	61	uniformly distributed
Rating of PV (MW)	1.5	3.715	1.5	3.801
Location of capacitor	30	-	61	-
Rating of capacitor (MVAr)	0.9	-	1.2	-
Location of SHC	-	30, 10, 14	-	61, 16, 65
Rating of SHC (MVA)	-	1.2866	-	1.4078
Cost of capacitor ($/kVAr) [126]	3	-	3	-
Investment of capacitor ($\times 10^3$ $)	2.7	-	3.6	-
Investment of SHC ($\times 10^4$ $)	-	7.4368	-	8.4469
Cost Saving due to energy loss reduction ($\times 10^5$ $)	8.2347	11.635	11.724	10.746
Financial returns due to PV supply ($\times 10^6$ $)	2.8755	7.1216	2.8755	7.2864
Total profit ($\times 10^6$ $)	3.6962	4.2381	4.0443	4.2120

3.9 Summary

This chapter presents a comprehensive planning approach for deploying SHCs in PV-integrated distribution networks. The primary focus is maximizing overall profit through cost-saving from the considered scenarios. The proposed methodology is conducted across various levels of PV penetration. The key findings from the simulation results can be summarized as follows:

- The cost-benefit analysis shows that the savings from reducing energy losses justify the initial investment required for SHC installation. Furthermore, case studies with a higher number of SHCs result in increased overall profits.
- During the planning period of the study, the reduction in energy losses experiences a more significant increase in the latter half, primarily due to more load growth. Notably, incorporating three SHCs delivered superior energy loss reductions compared to the other cases.
- The integration of PV systems shows significant potential for reducing energy losses by approximately 30-40% compared to non-PV conditions. This translated to increased profitability for network operators, highlighting the economic viability of PV integration within distribution networks.
- Across both the 33-bus and 69-bus distribution networks, Case-B consistently shows a 12-15% improvement in profit over Case-A in Scenario-2. This highlights the enhanced profitability achieved by integrating multiple SHCs alongside PV units.

Chapter 4

Multi-Swarm Surrogate Assisted PSO for Operational Optimization of Shunt Compensators to Minimize Annual Energy Loss Cost

4.1 Introduction

Optimization is essential for addressing complex real-world challenges across various domains [127, 128]. As energy demands continue to rise and environmental concerns grow, optimizing power distribution networks, especially those incorporating PV systems, has become essential [129, 130]. Optimizing power distribution networks presents specific challenges [131, 132]. One major challenge involves optimizing the operation of SHCs [133]. This optimization aims to improve network performance and minimize energy losses. The time-varying load and PV generation within distribution networks increase the number of variables, making it crucial to evaluate the real-time performance of the designed objective functions [134]. These challenges directly impact the goal of minimizing operational

expenses, which is essential for maintaining the economic viability of distribution systems. Optimization methods that are capable of handling such complexity are essential to address these high-dimensional objective functions.

Various optimization techniques have historically been employed in power distribution networks, including metaheuristic optimization algorithms [135, 136]. The PSO technique is one of the most extensively studied metaheuristic algorithms in power system optimization [137,138]. However, a key challenge with conventional PSO algorithms is their need for many fitness evaluations to achieve near-optimal solutions, which limits their application in computationally intensive problems. Over the years, researchers have proposed various variants and improvements to enhance the performance and applicability of PSO in different domains. Within the domain of power system optimization, several PSO variants have been employed, including Cooperative PSO [139], Binary PSO [140], Adaptive PSO [141], Quantum-Behaved PSO [142], and Social Learning-based PSO (SL-PSO) [143]. A notable PSO variation is Multi-Swarm PSO, an extension of traditional PSO that introduces multiple swarms, each with its unique set of particles [144, 145]. These adaptations have proven effective in addressing the complexities of power system optimization. Moreover, researchers have developed innovative approaches to enhance PSO techniques further. One such approach is Surrogate-Based PSO, which integrates surrogate models into the optimization process to reduce the computational cost of evaluating objective functions [146, 147]. For instance, [148] introduced surrogate-assisted PSO by incorporating Gaussian process regression as the surrogate model, while [149] adapted a surrogate-based PSO for constrained optimization problems.

Given the increasing complexity of modern power distribution networks and the growing number of variables in objective functions, developing more effective PSO variants remains a significant challenge. The literature reveals several research gaps, including:

- The optimization of power distribution networks becomes more complex due to time-varying loads and PV generation, significantly increasing the number of variables

involved. As the number of variables grows, particularly beyond 150-200, traditional optimization methods struggle to find solutions efficiently. To address this, advanced metaheuristic algorithms must be developed to handle the complexity of high-dimensional optimization problems more effectively.

- Developing PSO variants capable of effectively optimizing high-dimensional objective functions characterized by many variables to address the increasing complexity of power distribution networks.

- Investigating advanced surrogate models is essential for enhancing PSO performance by integrating multiple sub-swarms, which enables more efficient exploration of multi-dimensional optimization problems. Further research should evaluate the potential advantages and effectiveness of combining surrogate-based PSO with a limited number of swarms to achieve improved optimization outcomes.

To address these research gaps, this chapter involves optimizing operational aspects related to compensators in PV-integrated distribution networks, focusing on reducing AEL cost. The optimization process involves determining the VAr set-points for SHCs based on time-varying load and PV generation profiles. Furthermore, a hybrid PSO variant is introduced to optimize objective functions with more variables.

This chapter presents its contributions as follows:

- To ensure an accurate evaluation of the AEL cost, a methodology for estimating monthly load curves in the residential, commercial, and industrial sectors using Gaussian Probability Distribution is employed. This method accounts for variations in energy prices based on seasonal changes and load levels.

- A Parallel-MS-GPRS-PSO variant is designed to address the challenges of large-scale optimization problems.

- A comprehensive statistical analysis compares the proposed Parallel-MS-GPRS-PSO approach with other established PSO variants. This evaluation provides valuable insights into the performance and effectiveness of the proposed methodology, offering a clear understanding of its advantages over existing approaches.

The proposed planning approach undergoes validation on both 33-bus and 69-bus distribution networks. Additionally, it undergoes testing using standard benchmark test functions.

4.2 Optimization problem for minimizing AEL costs

The primary objective of this study is to optimize the operation of SHCs by determining the specific VAr injection for each hour, aiming to minimize AEL costs efficiently. The AEL cost is determined based on energy pricing strategies during peak, off-peak, and intermediate load levels across different seasons within the distribution network. The objective function to minimize AEL cost is formulated as follows:

$$\text{Minimize AEL Cost} = \sum_{s=1}^{4} \sum_{h=1}^{H_s} (PL_{hl} \quad EP_{sl}) \tag{4.1}$$

Here, PL_{hl} represents the power losses at hour h and load level l, H_s denotes the total number of hours in season s, and EP_{sl} denotes the energy price for load level l in season s.

The optimization process integrates various constraints to minimize AEL costs in the network. These constraints include power balance, bus voltage magnitude, and thermal constraints, which are mathematically expressed in Eqs. 2.17-2.20, respectively. Additionally, the SHC reactive power limit constraint is considered and expressed as:

$$|Q_{sh(i)}(t)| \leq Q_{\text{SHC\_max}}, \quad \forall t \tag{4.2}$$

where $Q_{\text{SHC\_max}}$ denotes the maximum allowable reactive power injection limit of the SHC.

4.2.1 Encoding and decoding particle positions for calculating AEL costs

In this method, the positions of particles are encoded to denote solutions within a multi-dimensional search space. These values are then decoded to determine the amount of VAr injections the SHCs provide. The system's voltages and currents are subsequently computed using the forward-backward sweep load flow technique, as discussed in the subsection 2.3.1. The active and reactive power demands at the locations of PV and SHC are adjusted using the equations 2.14 and 2.15 respectively. The AEL in the considered distribution networks is determined based on the estimated load and PV generation curves. These estimates are obtained using the Gaussian Probability Distribution technique explained in Section 4.3. Finally, the objective function value, which represents the AEL costs, is calculated by considering all these factors.

4.3 Modeling load curves with gaussian probability distribution

This section presents the mathematical formulation for estimating load curves using the Gaussian probability density function with varying mean and standard deviation for each hour. This statistical model provides an approach for capturing the variations in the load profile hourly.

4.3.1 Gaussian probability density function for hourly load variations

The Gaussian probability density function for each hour h can be formulated as:

$$f(x_h) = \frac{1}{\sigma_h\sqrt{2\pi}} \exp\left(-\frac{(x_h - \mu_h)^2}{2\sigma_h^2}\right) \tag{4.3}$$

In the given equation, $f(x_h)$ represents the probability density function at hour h, where μ_h signifies the mean and σ_h represents the standard deviation.

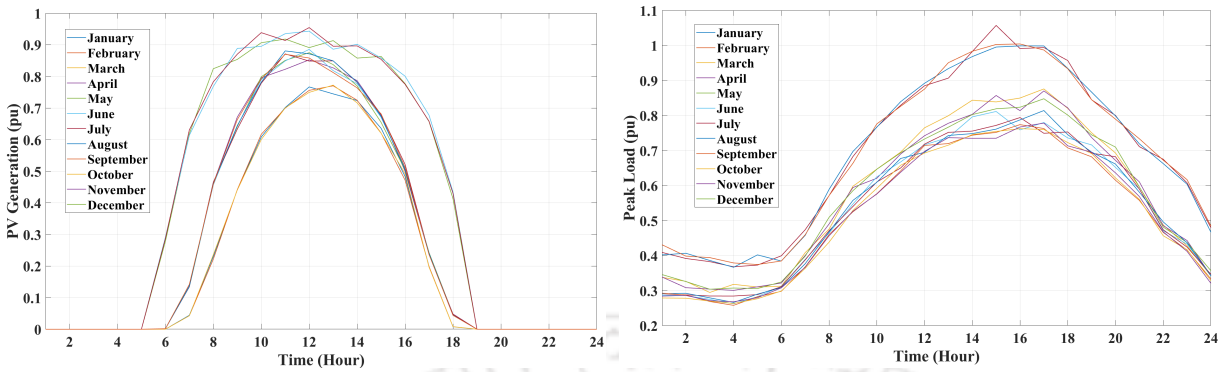

(a) (b)

Fig. 4.1: Monthly estimated average load curves for (a) PV (b) Residential sectors

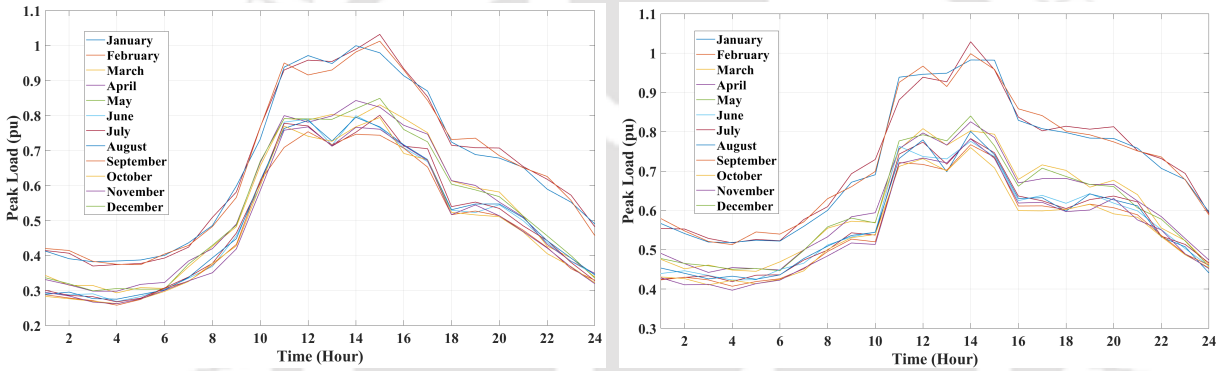

(a) (b)

Fig. 4.2: Monthly estimated average load curves for (a) Commercial (b) Industrial sectors

4.3.2 Estimation of load curves

The Gaussian probability density function is employed to estimate load and PV generation curves. A series of random samples is generated for each hour h within the load curve to represent the essential variability in the load profile. Extending this methodology to estimate load curves for 12 months results in a comprehensive collection of load curves, denoted as:

$$LC = (LC_1, LC_2, LC_3, \ldots, LC_{12}) \tag{4.4}$$

Here, LC_n represents the load curve for the n^{th} month. This study estimates monthly load curves for PV, residential, commercial, and industrial load types. The approach involves

utilizing data sourced from [100], which provides average daily load profiles for each load category. Additionally, seasonal load curves are derived based on four distinct seasons using data specified in [26]. Graphical representations of the resulting load profiles for the PV, residential, commercial, and industrial sectors over 12 months, obtained through the Gaussian probability density function, are shown in Figures 4.1 and 4.2.

4.4 Solution strategy: Parallel-MS-GPRS-PSO

This section presents the Parallel-MS-GPRS-PSO algorithm to determine the optimal VAr set-points for SHCs. The fundamentals of the PSO algorithm are discussed in subsection 2.5.1. A detailed explanation of the MS-GPRS-based PSO is presented below.

4.4.1 GPR Newton's approach for optimization

This subsection introduces the basics of GPR, followed by applying Newton's method for optimization tasks.

4.4.1.1 Modeling data distribution with GPR

GPR is a tool for modeling data distribution and constructing probabilistic models. Given a dataset $\mathcal{D} = (x_i, y_i)_{i=1}^{N}$, where x_i represents input parameters and y_i represents corresponding objective function values, GPR can predict the distribution of an unobserved target output ξ^* at a new input point χ^*. The prediction p is formulated as:

$$p(\xi^*|\chi^*, \mathcal{X}, \mathcal{Y}) = \mathcal{N}(\mu(\chi^*), \sigma^2(\chi^*)) \tag{4.5}$$

In this equation, $\mu(\chi^*)$ denotes the predictive mean, and $\sigma^2(\chi^*)$ denotes the predictive variance, which are parameters of a Gaussian distribution $\mathcal{N}$. The sets $\mathcal{X}$ and $\mathcal{Y}$ represent collections of variables or parameters used in the conditional probability p.

4.4.1.2 Predicting potential optima with Newton's method

Newton's method is employed to optimize the GPR-based surrogate. This iterative method aims to predict the local optima of a function by refining the global solution progressively. In the optimization context, Newton's method predicts potential optimal values for the objective function. The equation governing Newton's method is expressed as:

$$Y^{(k+1)} = Y^{(k)} - \frac{\nabla g(Y^{(k)})}{\nabla^2 h(Y^{(k)})} \tag{4.6}$$

In this equation, $Y^{(k)}$ represents the current estimate of the best solution, $\nabla g(Y^{(k)})$ is the gradient (first derivative), and $\nabla^2 h(Y^{(k)})$ is the Hessian matrix (second derivative) of the objective function. The iterative process continues until the maximum number of functional evaluations is reached.

4.4.1.3 Evaluating predicted optima and updating the global best

The objective function value $f(\chi^*)$ is evaluated at the predicted solution χ^* to assess the predicted optima. This assessment ensures that the predicted optima meets the problem's requirements. If the predicted objective function value $f(\chi^*)$ is better than the previously known best objective function value, an update is made to the global best solution g_{best}:

$$g_{best} = \chi^*, \quad f(g_{best}) = f(\chi^*) \tag{4.7}$$

This iterative process continually improves the optimization performance, leading to the discovery of the best solutions. The GPR Newton's optimization method is outlined in Algorithm 2.

4.4.2 Multi-swarm cooperative mechanism

The Multi-swarm cooperative approach enhances optimization by enabling information exchange among multiple swarms. Each swarm operates independently, exploring different

Algorithm 1 Overview of parallel-MS-GPRS-PSO approach

Input Parameters

- $w_{\max}$: Maximum inertia weight
- $w_{\min}$: Minimum inertia weight
- num_swarm: Number of swarms
- s_iter: Surrogate data storage iteration threshold
- dim: Dimensionality of the problem

Initialization

- Initialize a Parallel-environment with num_swarm worker processes
- parfor $swarm = 1$ to num_swarm:
  - Initialize position and velocity of particles for size N_p
  - Calculate the objective function value for corresponding particles
  - Determine p_{best} and $g_{best(m)}$ in each swarm
  - Find the global best solution among all the swarms

Optimization loop

- $iteration = 1$
- While $iteration \leq MaxIt$:
  - parfor $swarm = 1$ to num_swarm:
    - For $p = 1$ to N_p:
      - Update position and velocity of particles using Equations 2.22 and 2.23
      - Calculate objective function value
      - If $iteration \leq s\_iter$, the particle data is utilized to construct the surrogate model
      - Otherwise, if $iteration > s\_iter$, Perform GPR Newton's optimization (see Algorithm 2)
      - Update p_{best} and $g_{best(m)}$ accordingly
      - Update swarm
  - Find the global best fitness value by sharing the best solutions among swarms (Equation 4.8)
  - $iteration = iteration + 1$

Finalization

- Close the Parallel-pool
- Display the final best objective function value and corresponding particle positions

Algorithm 2 GPR newton optimization approach

Input parameters:

- f_eval: Maximum number of function evaluations
- $maxLocalIter$: Maximum local iterations for GPR Newton optimization

GPR Newton's optimization

- parfor $swarm = 1$ to num_swarm:
  - Train the GPR model using the stored surrogate data set
  - For $local\_iterations = 1$ to $maxLocalIter$:
    - Predict potential optima using Newton's method with f_eval function evaluations based on Equations 4.5 and 4.6
    - Calculate the real objective function value of the predicted optimal particle
    - Update $g_{best(m)}$ if the predicted optimal objective function value is lower than the previous value using Equation 4.7

regions of the search space. A cooperative mechanism is employed to enhance collaboration and knowledge-sharing where each swarm's best solutions are periodically shared among all swarms. During each iteration, the global best solutions ($g_{\text{best(m)}}$) obtained by each swarm m are compared to identify the most promising solutions. The overall global best value (g_{best}) for that iteration is determined as the minimum among these global best values:

$$g_{\text{best}} = \min(g_{\text{best}(1)}, g_{\text{best}(2)}, \ldots, g_{\text{best}(m)}) \tag{4.8}$$

Information exchange occurs after every iteration until the final iteration, providing continuous collaboration among swarms throughout the optimization process. This cooperative approach contributes to the overall convergence of the algorithm toward high-quality solutions.

4.4.3 Parallel-MS-GPRS-PSO approach

The Parallel-MS-GPRS-PSO Approach integrates GPR and PSO within a multi-swarm framework, employing parallel computing for efficient computation. In this approach, mul-

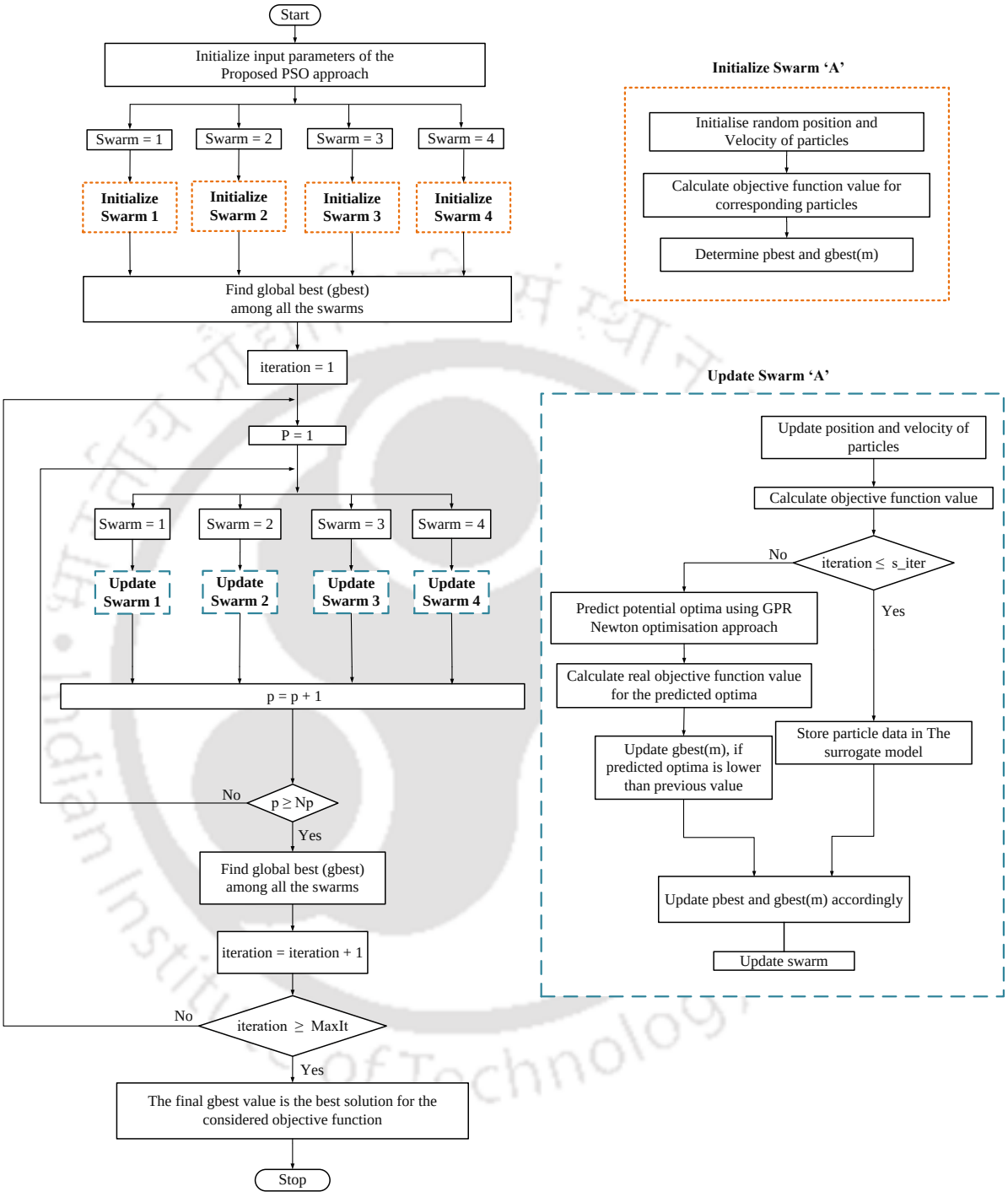

Fig. 4.3: Flowchart for the proposed Parallel-MS-GPRS-PSO approach

tiple swarms of particles operate concurrently, each swarm executing its PSO algorithm independently. This concurrent operation of sub-swarms significantly reduces the time required to converge to the optimal solutions. Knowledge-sharing mechanisms are employed

among swarms to enhance the optimization process. The best solutions identified in one swarm are periodically shared with others, facilitating a collaborative search for the best solutions throughout the optimization process. Additionally, the approach incorporates GPR Newton's optimization after a predefined number of surrogate iteration thresholds (s_iter) to refine the search process. The optimization operates within a predefined maximum number of iterations. The final global best solution obtained at the end of iterations represents the optimal solution for the objective function. To provide a comprehensive understanding of the Parallel-MS-GPRS-PSO approach, the detailed algorithm is outlined in Algorithm 1, and its corresponding flowchart is illustrated in Figure 4.3.

Table 4.1: Results obtained from evaluating various PSO parameter sets

Parameters			**Best value among 10 runs**
s_iter	**f_eval**	**num_swarm**	
25	1000	4	4.74E+01
50			**3.52E+01**
75			3.76E+01
100			8.98E+01
50	500	4	4.38E+01
	750		4.17E+01
	1000		**3.52E+01**
50	1000	2	1.08E+02
		3	4.11E+01
		4	**3.52E+01**

4.4.4 Parameter selection for the proposed approach

Selecting the best parameters is crucial for optimizing the performance of the proposed algorithm. The outcomes of evaluating different parameter combinations, including s_iter, f_eval, and num_swarm, are summarized in Table 4.1, focusing on minimizing the 50-dimensional Rosenbrock test function. The Rosenbrock test function details can be found in [150].

From Table 4.1, the analysis reveals that setting s_iter to 50 provides the best results.

Maintaining f_eval at 1000 yields the best results across different parameter configurations, and additionally, setting num_swarm to 4 yields the most favorable performance. These insights are crucial for selecting parameters that improve convergence.

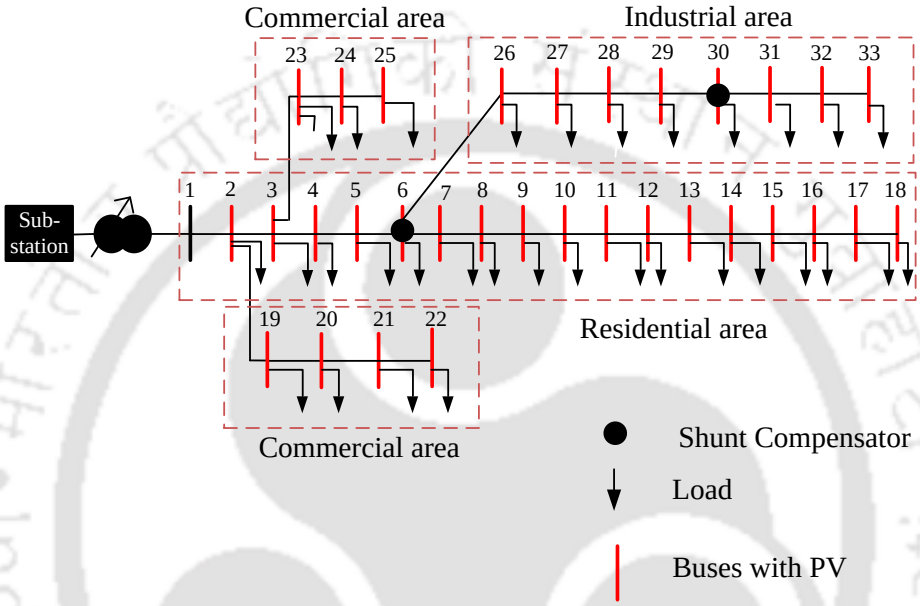

Fig. 4.4: 33-bus distribution network with PV and SHC

4.5 Simulation results and discussion

The validation of this study is performed using the MATLAB/Simulink environment, focusing on 33-bus and 69-bus radial distribution networks. The single-line diagrams of these networks are provided in Fig. 4.4 and Fig. 4.5, respectively. The geographical layout of the network's residential, commercial, and industrial zones is based on data from [100], which provides detailed descriptions of these areas. PV units are uniformly distributed across all buses except the substation bus. Each distribution network has strategically positioned SHCs—two SHCs at buses 30 and 6 for the 33-bus network and three SHCs at buses 17, 11, and 61 for the 69-bus network. The SHC placements are derived from chapter

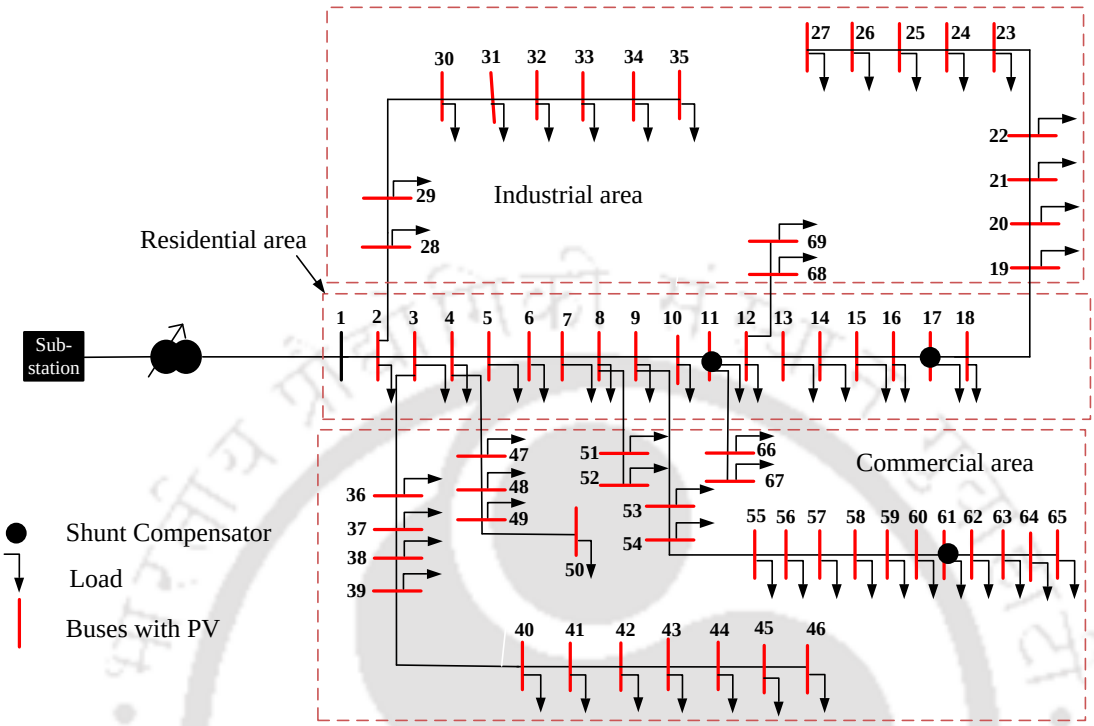

Fig. 4.5: 69-bus distribution network with PV and SHC

2 based on optimal results obtained by supplying constant reactive power from the SHCs to minimize energy losses.

The present analysis considers variations in average load demand and PV generation over 12 months to calculate the AEL cost. Monthly average load profiles are estimated using the Gaussian probability density function, as illustrated in Figures 4.1 and 4.2. Seasonal energy prices, corresponding to load conditions, are detailed in Table 4.3. Additionally, Table 4.4 categorizes load levels by the percentage of load consumption [151]. The total reactive power demand allocated to SHCs at specific load levels is distributed among individual SHCs based on their MVA ratings during the operational optimization.

The objective function for minimizing AEL costs incorporates the 24-hour time-varying nature of load and PV generation profiles over 12 months, resulting in a high-dimensional 288-variable problem. A novel PSO variant named Parallel-MS-GPRS-PSO has been pro-

posed to address the challenges of optimizing this high-dimensional objective function. Furthermore, the proposed approach is compared with other PSO variants to assess its effectiveness, including PSO with linearly decreasing inertia weight (PSO-LDIW) [152], Multi-Swarm Self-Adaptive and Cooperative PSO (MSCPSO) [153], and PSO with GPR surrogate model (PSO-GPR) [148]. The experiments are conducted in the MATLAB/Simulink environment, using a population size of 50 for 30-dimensional and 50-dimensional problems and 100 for 100-dimensional problems; for PSO-GPR and Parallel-MS-GPRS-PSO, a threshold of 50 surrogate iterations is set for 30, 50, and 100-dimensional problems. Both MSCPSO and Parallel-MS-GPRS-PSO use a total of 4 swarms during the optimization process. Detailed parameter values for each optimization technique are provided in Table 4.2.

Table 4.2: Parameter values considered for different PSO variants

Type of PSO variant	**Parameter values**
PSO-LDIW	$c_1 = 1.5$; $c_2 = 1.5$; $w_{\max} = 0.9$; $w_{\min} = 0.5$; $MaxIt = 200$
MSCPSO	$c_1 = 1.5$; $c_2 = 1.5$; $w_{\max} = 0.9$; $w_{\min} = 0.5$; $num\_swarm = 4$; $MaxIt = 200$
PSO-GPR	$c_1 = 1.5$; $c_2 = 1.5$; $w_{\max} = 0.9$; $w_{\min} = 0.5$; $s\_iter = 50$; $f\_eval = 1000$; $MaxIt = 200$; $maxLocalIter = 3$;
Parallel-MS-GPRS-PSO	$c_1 = 1.5$; $c_2 = 1.5$; $w_{\max} = 0.9$; $w_{\min} = 0.5$; $s\_iter = 50$; $f\_eval = 1000$; $maxLocalIter = 3$; $num\_swarm = 4$; $MaxIt = 200$

Table 4.3: Energy prices for different seasons at different load conditions

Seasons	**Energy price ($/kWh) [151]**		
	Off-peak	**Intermediate**	**Peak**
Summer	0.07	0.13	0.16
Winter	0.08	0.12	0.13
Spring/Autumn	0.07	0.09	-

Table 4.4: Load levels

Load levels		
Off-peak	**Intermediate**	**Peak**
< 50 %	50 - 80 %	> 80 %

4.5.1 Comparative analysis of AEL cost reduction strategies with SHCs

The comparative analysis of two distinct approaches is presented for minimizing AEL costs with SHCs: (i) SHCs with variable VAr injection set points and (ii) SHCs with constant or rated VAr injection. Table 4.5 provides an overview of the AEL costs obtained using these approaches across different levels of PV integration. The results highlight that employing SHCs with variable VAr injection set points leads to significantly lower AEL costs than using SHCs with constant or rated VAr injection. Additionally, there is a noticeable decrease in AEL costs with increasing levels of PV integration, suggesting that increased PV integration contributes to reduced energy losses within the distribution network.

Furthermore, the comparison extends to other PSO variants, demonstrating the superior performance of the proposed Parallel-MS-GPRS-PSO approach in minimizing AEL costs. The adaptive nature of the proposed approach is particularly beneficial in scenarios with frequent load fluctuations. It determines the optimal reactive power SHCs provide based on specific load demands. This strategy proves to be effective in addressing high-dimensional optimization problems.

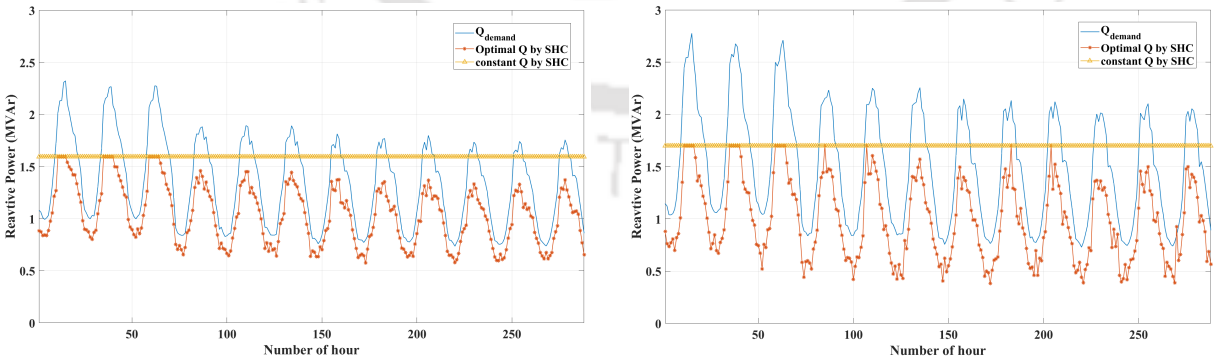

Fig. 4.6: Q_{demand}, constant Q and optimal Q provided by SHC in the (a) 33-bus (b) 69-bus distribution networks

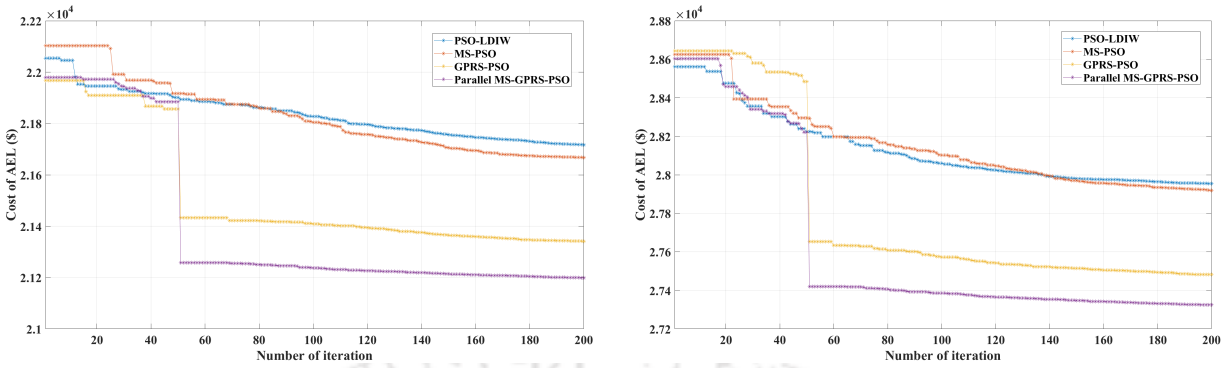

Fig. 4.7: Convergence plots of PSO variants for the cost of AEL when 100% PV is integrated into the (a) 33-bus (b) 69-bus distribution networks

4.5.2 Optimal VAr injection strategies for SHCs in response to load variations

Figure 4.6 displays the optimal reactive power injection settings for SHCs in both the 33-bus and 69-bus networks across a 288-hour load variation, utilizing the proposed Parallel-MS-GPRS-PSO approach. These visuals illustrate the total reactive power demand profile over this period, including the baseline constant reactive power supplied by the SHCs. An important observation from these figures is the variation of the optimal VAr injection set points for the SHCs in response to load fluctuations. These set points adjust dynamically based on load demands, highlighting the necessity of variable VAr injection levels to minimize overall AEL cost under varying load conditions. Specifically, the results demonstrate an increased demand for VAr injection during periods of higher load. This highlights the importance of operating SHCs to their rated VAr capacity during high-load scenarios.

Additionally, Figure 4.7 illustrates the convergence patterns of four PSO variants for the 33-bus and 69-bus distribution networks, respectively. Both PSO-GPR and Parallel-MS-GPRS-PSO exhibit the PSO approach for the initial 50 iterations. Beyond this stage, the optimization procedure continues, incorporating best value estimation through GPR Newton's optimization method. The convergence plots visually demonstrate a significant drop in achieved values after the 50th iteration. Notably, the Parallel-MS-GPRS-PSO approach demonstrates superiority by achieving the optimal values compared to other PSO

variants, highlighting its effectiveness in optimizing the AEL cost.

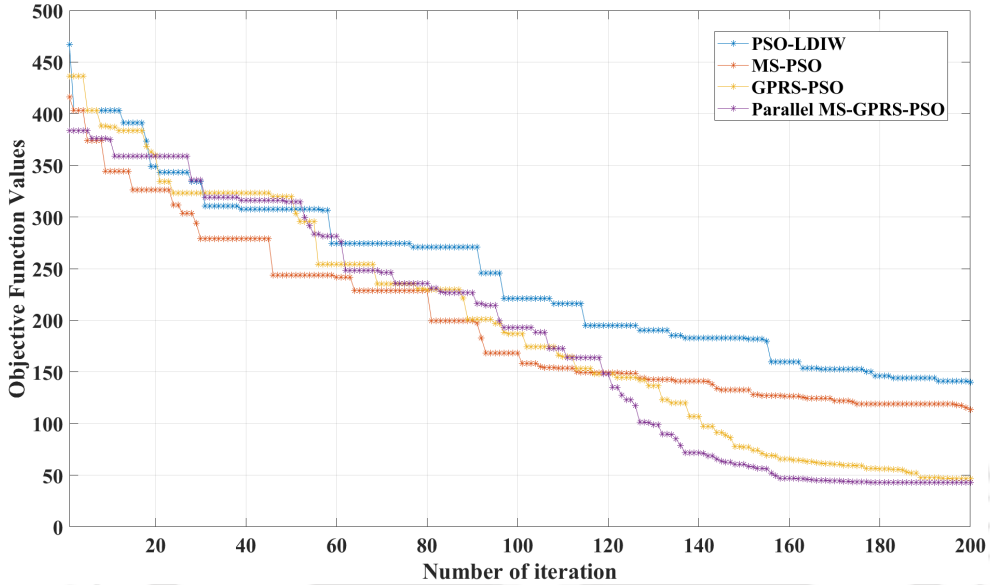

Fig. 4.8: Convergence plots illustrating the performance of different PSO variants on the 30-dimensional Rastrigin test function (F1)

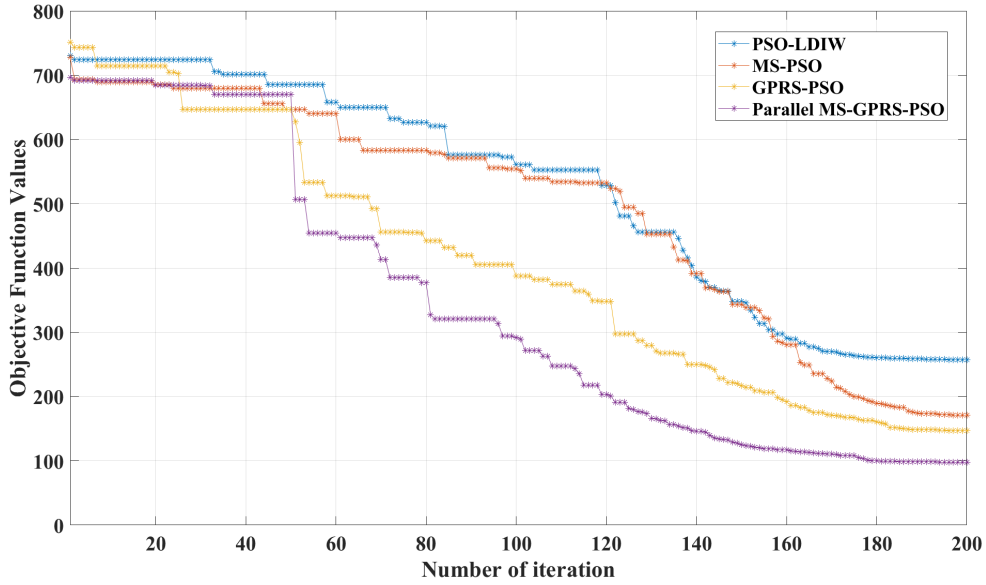

Fig. 4.9: Convergence plots illustrating the performance of different PSO variants on the 50-dimensional Rastrigin test function (F1)

Table 4.5: Comparison of operational optimization outcomes in distribution networks

Parameter		33-bus network			69-bus network		
PV generation as % of peak demand		0	50	100	0	50	100
Location of SHC		30, 6	30, 6	30, 6	17, 11, 61	17, 11, 61	17, 11, 61
Rating of SHC (MVA)		1.5932	1.4999	1.4842	1.6986	1.6604	1.6643
Cost of AEL ($\times 10^4$ \$)	Rated VAr injection by SHC	5.4709	3.1017	2.5231	5.6477	4.2279	3.5737
	PSO-LDIW	5.0043	2.7330	2.1717	4.8275	3.4663	2.7954
	MSCPSO	4.9975	2.7317	2.1667	4.8231	3.4556	2.7918
	PSO-GPR	4.9567	2.6835	2.1342	4.7615	3.3871	2.7482
	Parallel-MS-GPRS-PSO	4.9506	2.6797	2.1198	4.7602	3.3828	2.7324

Table 4.6: Description of benchmark test functions

Function No.	Test Function [150]	Search Space	No. of dimensions (D)	Global optimum	Characteristic
F1	Rastringin	[-5.12, 5.12]	30/50/100	0	Complex Multi-modal
F2	Rosenbrock	[-5 5]	30/50/100	0	Uni-modal with narrow valley
F3	Powell	[-4 5]	30/50/100	0	Multi-modal
F4	Ackley	[-32.768, 32.768]	30/50/100	0	Complex Multi-modal
F5	Griewank	[-600 600]	30/50/100	0	Complex Multi-modal
F6	Schwefel	[-500 500]	30/50/100	0	Complex Multi-modal
F7	Styblinski-Tang	[-5 5]	30/50/100	-39.166*D	Complex Multi-modal

Table 4.7: Comparative Results on 30-dimension benchmark test functions with other PSO variants

Function No.	Analytics	PSO-LDIW	MSCPSO	PSO-GPR	Parallel-MS-GPRS-PSO
F1	Best	1.40E+02	1.13E+02	4.65E+01	**4.28E+01**
	Worst	2.84E+02	2.26E+02	1.43E+02	**1.35E+01**
	Mean	2.08E+02	1.68E+02	1.05E+02	**8.04E+01**
	Std.	4.16E+01	3.49E+01	**3.21E+01**	3.28E+01
F2	Best	2.21E+02	7.62E+01	9.38E+01	**1.94E+01**
	Worst	3.04E+03	6.12E+02	2.78E+03	**2.80E+01**
	Mean	6.77E+02	1.99E+02	1.29E+03	**2.42E+01**
	Std.	8.49E+02	1.53E+02	1.22E+03	**2.18E+00**
F3	Best	3.19E+02	1.09E+02	1.68E+02	**1.24E-03**
	Worst	3.42E+03	1.84E+03	5.43E+02	**4.42E+02**
	Mean	1.15E+03	4.57E+02	3.91E+02	**3.26E+02**
	Std.	1.08E+03	5.03E+02	**1.11E+02**	1.38E+02
F4	Best	5.13E+00	2.48E+00	3.26E-03	**4.49E-04**
	Worst	8.59E+00	5.01E+00	1.34E+00	**9.33E-04**
	Mean	6.43E+00	3.29E+00	3.48E-01	**6.37E-04**
	Std.	1.03E+00	7.02E-01	5.57E-01	**1.61E-04**
F5	Best	2.61E+00	1.14E+00	1.09E-04	**9.75E-06**
	Worst	9.74E+01	9.14E+01	6.66E-02	**4.42E-02**
	Mean	3.99E+01	1.06E+01	**1.38E-02**	1.40E-02
	Std.	4.65E+01	2.84E+01	2.08E-02	**1.63E-02**
F6	Best	2.56E+03	2.50E+03	2.85E+03	**2.38E+03**
	Worst	5.49E+03	4.42E+03	5.61E+03	**4.41E+03**
	Mean	3.78E+03	**3.35E+03**	3.97E+03	3.39E+03
	Std.	8.44E+02	6.74E+02	8.22E+03	**5.54E+02**
F7	Best	-1.12E+03	-1.12E+03	-1.09E+03	**-1.13E+03**
	Worst	-9.87E+02	-9.60E+02	-1.02E+03	**-1.03E+03**
	Mean	-1.04E+03	-1.04E+03	-1.06E+03	**-1.08E+03**
	Std.	3.87E+01	4.43E+01	**1.89E+01**	2.97E+01

4.6 Empirical study on benchmark test functions

Extensive tests are conducted using seven common benchmark functions to evaluate the proposed algorithm as described in Table 4.6 [150]. The mathematical equations for the considered benchmark test functions are as follows:

$$\text{Rastrigin Function, F1}(\mathbf{x}) = 10n + \sum_{i=1}^{n} \left[x_i^2 - 10\cos(2\pi x_i)\right] \tag{4.9}$$

Table 4.8: Comparative results on 50-dimension benchmark test functions with other PSO variants

Function No.	Analytics	PSO-LDIW	MSCPSO	PSO-GPR	Parallel-MS-GPRS-PSO
F1	Best	2.56E+02	1.71E+02	1.46E+02	**9.78E+01**
	Worst	4.22E+02	3.92E+02	4.54E+02	**3.19E+02**
	Mean	3.38E+02	2.89E+02	2.54E+02	**1.88E+02**
	Std.	**4.89E+01**	6.02E+01	9.35E+01	7.86E+01
F2	Best	1.29E+02	1.13E+02	5.51E+01	**3.52E+01**
	Worst	1.03E+04	8.20E+05	2.61E+03	**2.55E+03**
	Mean	2.45E+03	5.74E+04	1.13E+03	**3.54E+02**
	Std.	3.97E+03	2.07E+05	1.26E+03	**7.75E+02**
F3	Best	5.56E+02	4.13E+02	2.26E+02	**4.37E+01**
	Worst	1.08E+04	7.57E+03	**2.96E+03**	3.31E+03
	Mean	5.37E+03	3.59E+03	1.36E+03	**5.68E+02**
	Std.	2.47E+03	1.87E+03	1.12E+03	**9.92E+02**
F4	Best	1.26E+01	6.42E+00	5.83E-01	**2.51E-02**
	Worst	1.94E+01	1.72E+01	1.53E+01	**1.52E+01**
	Mean	1.66E+01	1.29E+01	**6.30E+00**	7.01E+00
	Std.	**1.71E+00**	3.21E+00	5.30E+00	7.16E+00
F5	Best	2.57E+01	1.03E+01	6.02E-01	**1.70E-02**
	Worst	3.01E+02	2.80E+02	2.71E+02	**9.09E+01**
	Mean	1.59E+02	7.84E+01	1.36E+02	**6.33E+01**
	Std.	7.81E+01	7.30E+01	8.75E+01	**4.36E+01**
F6	Best	5.58E+03	5.65E+03	6.73E+03	**5.45E+03**
	Worst	1.09E+04	8.65E+03	8.53E+03	**8.47E+03**
	Mean	8.12E+03	**7.18E+03**	7.87E+03	7.33E+03
	Std.	1.42E+03	9.66E+02	**7.13E+02**	9.60E+02
F7	Best	-1.69E+03	-1.76E+03	**-1.80E+03**	-1.77E+03
	Worst	-1.46E+03	-1.58E+03	-1.58E+03	**-1.65E+03**
	Mean	-1.59E+03	-1.69E+03	-1.72E+03	**-1.73E+03**
	Std.	6.44E+01	4.70E+01	6.10E+01	**4.28E+01**

$$\text{Rosenbrock Function, F2}(\mathbf{x}) = \sum_{i=1}^{n-1} \left[100(x_{i+1} - x_i^2)^2 + (x_i - 1)^2\right] \tag{4.10}$$

$$\begin{aligned}\text{Powell Function, F3}(\mathbf{x}) = \sum_{i=1}^{n/4} \Big[&(x_{4i-3} + 10x_{4i-2})^2 + 5(x_{4i-1} - x_{4i})^2 \\ &+ (x_{4i-2} - 2x_{4i-1})^4 + 10(x_{4i-3} - x_{4i})^4\Big]\end{aligned} \tag{4.11}$$

Table 4.9: Comparative results on 100-dimension benchmark test functions with other PSO variants

Function No.	Analytics	PSO-LDIW	MSCPSO	PSO-GPR	Parallel-MS-GPRS-PSO
F1	Best	1.14E+03	9.34E+02	3.29E+02	**2.91E+02**
	Worst	1.45E+03	1.35E+03	9.15E+02	**8.38E+02**
	Mean	1.27E+03	1.16E+03	6.86E+02	**5.66E+02**
	Std.	**1.06E+03**	1.11E+03	2.05E+02	2.01E+02
F2	Best	1.53E+05	3.93E+04	1.95E+03	**9.87E+02**
	Worst	3.19E+05	2.91E+05	1.68E+05	**1.12E+05**
	Mean	2.31E+05	1.68E+05	5.70E+04	**5.41E+04**
	Std.	5.64E+04	6.60E+04	5.77E+04	**3.43E+04**
F3	Best	1.20E+04	1.15E+04	3.09E+02	**2.91E+02**
	Worst	3.12E+04	2.96E+04	2.73E+04	**7.02E+03**
	Mean	2.03E+04	1.95E+04	6.70E+03	**1.88E+03**
	Std.	5.63E+03	4.43E+03	8.79E+03	**2.26E+03**
F4	Best	2.03E+01	1.91E+01	1.64E+01	**5.27E+00**
	Worst	2.08E+01	2.07E+01	1.90E+01	**1.71E+01**
	Mean	2.05E+01	2.01E+01	1.77E+01	**1.23E+01**
	Std.	**1.59E-01**	3.28E-01	1.01E+00	3.83E+00
F5	Best	7.42E+02	5.51E+02	2.87E+02	**9.72E+01**
	Worst	1.38E+03	1.02E+03	9.11E+02	**6.31E+02**
	Mean	1.11E+03	7.58E+02	5.14E+02	**3.81E+02**
	Std.	1.83E+02	**1.38E+02**	1.89E+02	1.73E+02
F6	Best	2.04E+04	1.68E+04	1.66E+04	**1.44E+04**
	Worst	2.35E+04	2.18E+04	2.31E+04	**2.17E+04**
	Mean	2.19E+04	1.94E+04	1.93E+04	**1.86E+04**
	Std.	**1.07E+03**	1.46E+03	2.02E+03	2.39E+03
F7	Best	-2.70E+03	-2.81E+03	-3.42E+03	**-3.47E+03**
	Worst	-2.24E+03	-2.45E+03	-3.17E+03	**-3.18E+03**
	Mean	-2.51E+03	-2.66E+03	-3.30E+03	**-3.31E+03**
	Std.	1.43E+02	1.29E+02	8.55E+01	**7.29E+01**

$$\text{Ackley Function, F4}(\mathbf{x}) = -20\exp\left(-0.2\sqrt{\frac{1}{n}\sum_{i=1}^{n}x_i^2}\right) - \exp\left(\frac{1}{n}\sum_{i=1}^{n}\cos(2\pi x_i)\right) + 20 + e \tag{4.12}$$

$$\text{Griewank Function, F5}(\mathbf{x}) = 1 + \frac{1}{4000}\sum_{i=1}^{n}x_i^2 - \prod_{i=1}^{n}\cos\left(\frac{x_i}{\sqrt{i}}\right) \tag{4.13}$$

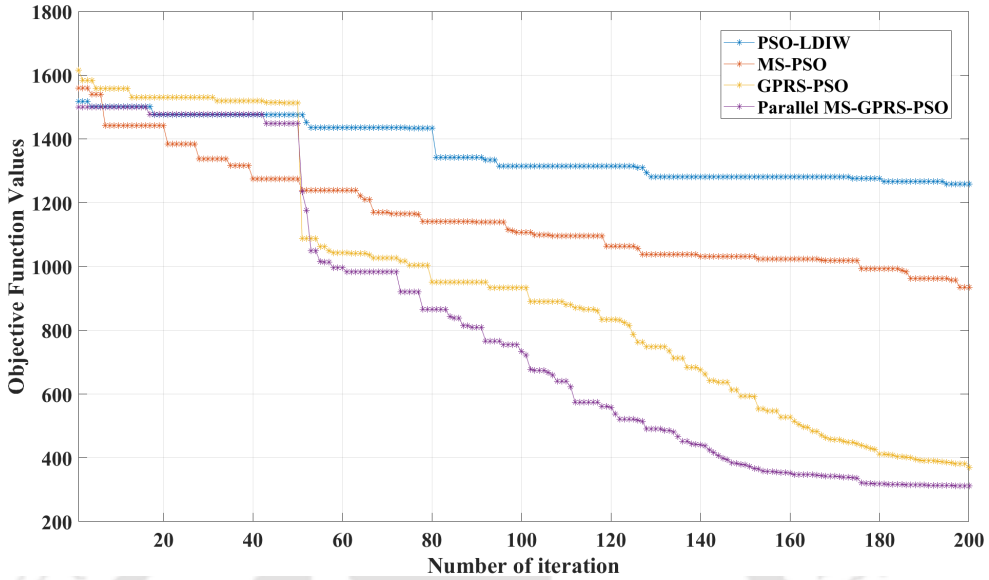

Fig. 4.10: Convergence plots illustrating the performance of different PSO variants on the 100-dimensional Rastrigin test function (F1)

$$\text{Schwefel Function, F6}(\mathbf{x}) = 418.9829n - \sum_{i=1}^{n} x_i \sin(\sqrt{|x_i|}) \tag{4.14}$$

$$\text{Styblinski-Tang Function, F7}(\mathbf{x}) = \frac{1}{2}\sum_{i=1}^{n} \left[x_i^4 - 16x_i^2 + 5x_i\right] \tag{4.15}$$

4.6.1 Comparison results on benchmark problems with other PSO variants

The results of the comparative tests on benchmark functions are presented in Tables 4.7, 4.8, and 4.9 for 30-dimensional, 50-dimensional, and 100-dimensional problems, respectively. Various variants of the PSO algorithm are considered during the evaluation, including PSO-LDIW, MSCPSO, and PSO-GPR. The data includes the best, worst, mean, and standard deviation values derived from 10 independent runs, providing valuable insights into the performance of these PSO variants.

Analysis of the data in Tables 4.7, 4.8, and 4.9 reveals significant differences in the best, worst, mean, and standard deviation values across the various optimization algorithms. The disparities in the best fitness values underscore the impact of algorithm choice

on optimization quality. Additionally, the standard deviations highlight varying levels of spread in fitness values. Different algorithms exhibit strengths in optimizing specific benchmark functions. For instance, Parallel-MS-GPRS-PSO achieves the best fitness in Function F1, indicating its effectiveness in solving that problem. Conversely, PSO-GPR excels in Function F7 within a 50-dimensional analysis. The worst and mean values also vary and do not consistently favor a single technique. These findings emphasize the importance of selecting an algorithm corresponding to the characteristics of the optimization problem, as no single algorithm consistently excels across all benchmark functions. However, it is notable that the Parallel-MS-GPRS-PSO algorithm outperforms the others across different test functions, achieving significantly lower objective function values and providing the best solutions. Although Parallel-MS-GPRS-PSO often yields the best solutions, other algorithms sometimes show lower standard deviation values for certain test functions. This discrepancy may result from the closeness of the best values provided by specific algorithms in individual runs. The proposed algorithm sometimes exhibits a wide range of solutions across different runs, which can be attributed to the stochastic nature of optimization problems. These variations can be valuable, as they may help identify diverse solutions that are useful in practice, especially for multi-modal objective functions.

The 100-dimensional test functions in Table 4.9 show that the Parallel-MS-GPRS-PSO consistently outperforms conventional PSO variants by achieving lower best values. This superiority is particularly evident for complex multi-modal test functions such as Rastrigin and Griewank. Additionally, there is a more significant variation in the best values obtained by the proposed approach compared to other PSO variants in the 100-dimensional analysis. Conversely, for the 50-dimensional analysis, the best values provided by Parallel-MS-GPRS-PSO show less variation than other techniques. These findings support using the proposed approach for high-dimensional optimization problems to obtain more approximate optimal values.

The Parallel-MS-GPRS-PSO algorithm demonstrates superior performance in terms of

convergence compared to other PSO variants. Both PSO-GPR and Parallel-MS-GPRS-PSO exhibit enhanced convergence after 50 iterations. This improvement is attributed to the introduction of GPR-based Newton's optimization at the 50^{th} iteration, which significantly helps predict the best value around the global best solution and facilitates faster convergence. Figures 4.8, 4.9, and 4.10 illustrate the convergence profiles for the Rastrigin test function when applied to 30-dimensional, 50-dimensional, and 100-dimensional problems.

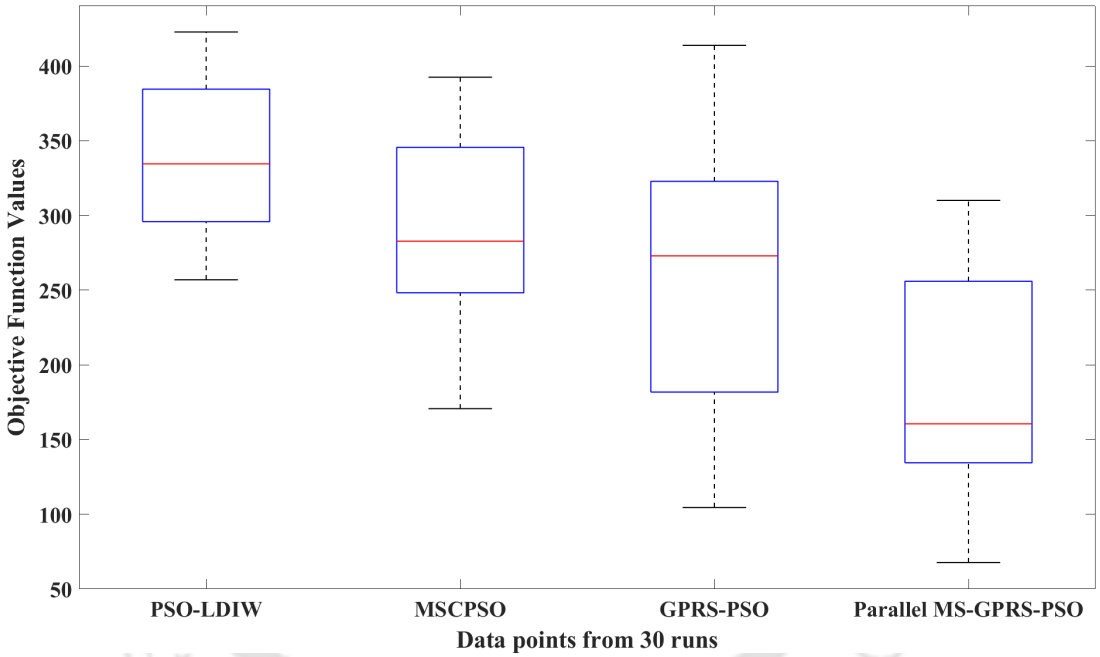

Fig. 4.11: Box-Plots illustrating optimal values obtained across 30 Runs for 50-Dimensional Rastrigin function (F1) using four PSO Variants

4.6.2 Statistical analysis of various PSO variants

A comparative analysis of four different PSO variants is conducted for the 50-dimensional Rastrigin test function to identify the best approach. The details of the Rastrigin test function are provided in [150]. Figure 4.11 displays a box plot illustrating the results of running each PSO variant 30 times independently.

The Kruskal-Wallis test is employed to assess the performance differences among the

PSO variants. This is a non-parametric statistical test suitable for non-normally distributed data. The test yields a highly significant p-value of 4.4474×10^{-10}, indicating that at least one PSO variant outperforms the others. Subsequent post-hoc comparisons using Bonferroni-corrected p-values reveal specific pairs of PSO variants with statistically significant performance distinctions. The adjusted p-values below 0.05 indicate these significant differences. Table 4.10 summarizes the results of these comparisons, highlighting that the Parallel-MS-GPRS-PSO variant exhibits notably superior performance compared to the other three PSO variants. Additionally, Figure 4.11 highlights that the proposed PSO variant achieves the lowest objective function values, indicating its superior performance compared to the other variants. These results suggest that Parallel-MS-GPRS-PSO offers a highly effective alternative to conventional PSO variants for optimizing objective functions. Parallel-MS-GPRS-PSO demonstrates significant potential for high-dimensional optimization challenges by consistently outperforming other PSO approaches.

Table 4.10: Results of post-hoc comparisons between PSO variants when Rastrigin function executed for 30 runs

PSO variant 1 (Group 1)	**PSO variant 2 (Group 2)**	**Adjusted p-value (Bonferroni)**	**Interpretation**
PSO-LDIW	MSCPSO	0.0734	No significant difference
PSO-LDIW	PSO-GPR	0.0023	Significant difference
PSO-LDIW	Parallel-MS-GPRS-PSO	0.0000	Significant difference
MSCPSO	PSO-GPR	1.0000	No significant difference
MSCPSO	Parallel-MS-GPRS-PSO	0.0001	Significant difference
PSO-GPR	Parallel-MS-GPRS-PSO	0.0093	Significant difference

Table 4.11: Computational times (in seconds) for various PSO variants

PSO variant	**Average computation time (in seconds)**
PSO-LDIW	1.21E+00
MSCPSO	2.41E+01
PSO-GPR	1.89E+02
Parallel-MS-GPRS-PSO	2.67E+02

4.6.3 Performance comparison of PSO variants in computational efficiency

The MATLAB simulation is performed on a Ryzen 7-5800 CPU @ 16 GB RAM, 1.9 GHz processor. Table 4.11 presents a detailed analysis of the average computational times associated with different PSO variants when applied to Rastrigin test functions. The table displays the average computation times in seconds for each PSO variant. As shown in Table 4.11, significant differences exist in computational performance among the PSO variants. PSO-LDIW is the most time-efficient option, while Parallel-MS-GPRS-PSO exhibits longer computation times. Despite this, the optimization results demonstrate that the suggested Parallel-MS-GPRS-PSO outperforms other PSO variations in terms of achieving superior optimization outcomes. It is crucial to consider a balance between computational time and optimization quality when selecting the most appropriate PSO variant, depending on the problem's dimensionality. These research findings highlight the effectiveness and adaptability of various PSO variants. This provides valuable insights for making decisions when customizing optimization algorithms to meet specific task requirements.

4.6.4 Comparison of the proposed approach with other surrogate-based PSO and metaheuristic algorithms

A comprehensive analysis of results from various surrogate-based algorithms applied to 30-dimensional and 50-dimensional benchmark test functions is presented in Tables 4.12 and 4.13, respectively. These tables include performance metrics for algorithms such as Surrogate-Assisted Cooperative Swarm Optimization (SACOSO) [154], Multiobjective Infill Criterion Driven Gaussian Process-Assisted SL-PSO (MGP-SLPSO) [155], Variable Surrogate Model-Based PSO (VSM-PSO) [156], and Parallel-MS-GPRS-PSO on functions F1, F2, F4, and F5. The data in these tables demonstrate that the Parallel-MS-GPRS-PSO algorithm performs better than other surrogate algorithms across diverse test functions by achieving the best objective function values. This indicates the effectiveness of the proposed Parallel-MS-GPRS-PSO algorithm in optimizing high-dimensional objective functions. Al-

Table 4.12: Comparative results on 30-dimension benchmark test functions with other surrogate-based algorithms

Function No.	Analytics	SACOSO [154]	MGP-SLPSO [155]	VSM-PSO [156]	Parallel-MS-GPRS-PSO
F1	Best	2.35E+02	**2.90E+01**	2.01E+02	4.28E+01
	Worst	3.34E+02	1.46E+02	2.94E+02	**1.35E+02**
	Mean	2.90E+02	**8.02E+01**	2.51E+02	8.04E+01
	Std.	**2.21E+01**	2.82E+01	2.42E+01	3.28E+01
F2	Best	2.71E+02	7.28E+01	1.03E+02	**1.94E+01**
	Worst	1.09E+03	2.87E+02	2.13E+02	**2.80E+01**
	Mean	5.80E+02	1.20E+02	1.52E+02	**2.42E+01**
	Std.	2.00E+02	3.91E+01	3.91E+01	**2.18E+00**
F4	Best	1.09E+01	5.53E+00	3.43E+00	**4.49E-04**
	Worst	1.65E+01	1.77E+01	5.15E+00	**9.33E-04**
	Mean	1.30E+01	1.02E+01	4.03E+00	**6.37E-04**
	Std.	1.36E+00	3.10E+00	4.68E-01	**1.61E-04**
F5	Best	3.74E+01	6.70E-03	2.15E-03	**9.75E-06**
	Worst	8.99E+01	1.00E+00	**3.35E-03**	4.42E-02
	Mean	5.83E+01	8.54E-01	**2.39E-03**	1.40E-02
	Std.	1.37E+01	8.07E-01	**4.99E-04**	1.63E-02

Table 4.13: Comparative results on 50-dimension benchmark test functions with other surrogate-based PSO algorithms

Function No.	Analytics	SACOSO [154]	MGP-SLPSO [155]	VSM-PSO [156]	Parallel-MS-GPRS-PSO
F1	Best	3.58E+02	2.05E+02	2.50E+02	**9.78E+01**
	Worst	4.74E+02	4.29E+02	4.81E+02	**3.19E+02**
	Mean	4.24E+02	2.95E+02	4.04E+02	**1.88E+02**
	Std.	2.99E+01	**5.78E+01**	5.97E+01	7.86E+01
F2	Best	1,54E+02	8.84E+02	1.14E+02	**3.52E+01**
	Worst	3.64E+02	**1.65E+02**	2.75E+02	2.55E+03
	Mean	2.49E+02	**1.20E+02**	1.88E+02	3.54E+02
	Std.	5.43E+01	**1.87E+01**	3.04E+01	7.75E+02
F4	Best	1.06E+00	7.77E+00	4.09E+00	**2.51E-02**
	Worst	**1.46E+01**	1.21E+01	2.00E+01	1.52E+01
	Mean	1.30E+01	9.31E+00	8.68E+00	**7.01E+00**
	Std.	**1.00E+00**	1.13E+00	6.36E+00	7.16E+00
F5	Best	3.69E+00	3.74E-02	6.42E-01	**1.70E-02**
	Worst	7.61E+00	**6.14E-01**	9.84E-01	9.09E+01
	Mean	5.54E+00	**1.54E-01**	8.34E-01	6.33E+01
	Std.	1.04E+00	**1.30E-01**	7.38E-02	4.36E+01

Table 4.14: Comparative results on 50-dimension benchmark test functions with other metaheuristic algorithms

Function No.	Analytics	aRBF-NFO [157]	SAEA-HAS [158]	LSADE [159]	Parallel-MS-GPRS-PSO
F1	Mean	4.33E+02	3.29E+02	4.28E+02	**1.88E+02**
	Std.	3.37E+01	**3.32E+01**	6.35E+01	7.86E+01
F2	Mean	3.79E+05	3.57E+04	6.28E+04	**3.54E+02**
	Std.	2.43E+05	1.08E+04	1.20E+03	**7.75E+02**
F4	Mean	1.93E+01	1.65E+01	1.60E+01	**7.01E+00**
	Std.	3.43E-01	**2.14E-01**	4.04E-01	7.16E+00
F5	Mean	4.49E+02	1.81E+02	1.69E+02	**6.33E+01**
	Std.	5.54E+01	**1.47E+01**	1.61E+01	4.36E+01

though other surrogate methods may exhibit lower mean and standard deviation values for certain test functions, the overall superiority of the Parallel-MS-GPRS-PSO algorithm is evident in providing the optimal objective function values across various test functions.

The outcomes of various metaheuristic algorithms applied to 50-dimensional benchmark test functions are summarized in Table 4.14. The algorithms evaluated include Radial Basis Functions Neighborhood Field Optimizer (aRBF-NFO) [157], Surrogate-Assisted Evolutionary Algorithm with Hierarchical Surrogate Technique and Adaptive Infill Strategy (SAEA-HAS) [158], Lipschitz Surrogate-Assisted Differential Evolution (LSADE) [159], and Parallel-MS-GPRS-PSO, with functions F1, F2, F4, and F5 being analyzed. The results reveal that the Parallel-MS-GPRS-PSO algorithm consistently achieves the best mean objective function values. However, the SAEA-HAS method is noted for having lower standard deviation values for certain test functions.

4.7 Summary

This chapter introduces Parallel-MS-GPRS-PSO, an advanced optimization technique for addressing high-dimensional, constrained engineering problems. The methodology focuses on the operational optimization of SHCs to reduce AEL costs in PV-integrated distribution networks. The key outcomes from the simulations are as follows:

- The operational optimization of SHCs using the Parallel-MS-GPRS-PSO in the 33-bus and 69-bus distribution networks results in significant reductions in AEL costs. Specifically, the approach achieves a 9-15% reduction in AEL costs for the 33-bus network and a 15-23% reduction for the 69-bus network, demonstrating its effectiveness in optimizing operational costs in distribution networks.

- In the analysis of 100-dimensional benchmark functions, the Parallel-MS-GPRS-PSO exhibits more significant variability in the best values achieved compared to other PSO variants. Conversely, for 50-dimensional problems, this method shows reduced

variability in the optimal values compared to other approaches. These findings validate the Parallel-MS-GPRS-PSO's capability to handle high-dimensional optimization tasks effectively.

- Comprehensive testing and statistical analysis highlight the superior performance of Parallel-MS-GPRS-PSO. It consistently outperforms conventional PSO variants across various benchmark test functions and independent runs, validating its efficacy in achieving the optimal objective function values.

Chapter 5

Simultaneous Optimization of PV Hosting Capacity and Energy Losses in Distribution Networks through Operational Optimization of BESS and SHCs

5.1 Introduction

The depletion of traditional energy sources and the rising electricity demand have driven a global shift towards renewable energy alternatives. Integrating PV systems into distribution networks has emerged as a strategy for achieving sustainability goals and reducing carbon emissions. However, the rapid integration of PV systems into distribution networks poses operational challenges such as over-voltage, line losses, and thermal constraints, particularly in high PV penetration areas. Additionally, the intermittent nature of solar power complicates grid stability and reliability [160, 161]. Researchers and industry experts are

exploring innovative solutions to address these challenges to enhance DG Hosting Capacity (DGHC) [162, 163]. Active network management technologies, including network reconfiguration, reactive power compensation, and voltage control, have shown potential in increasing DGHC and improving network performance [164, 165]. Numerous studies have investigated how to boost PVHC in distribution networks. These approaches include the optimal placement of SHCs [166], and BESS [167] to address voltage issues and maximize PV integration. Additionally, advanced control strategies for PV inverters have been proposed to mitigate voltage fluctuations and enhance network stability [168, 169].

Researchers have proposed various strategies to enhance hosting capacity and minimize energy losses. In [170, 171], a multi-objective, multi-period non-linear programming model utilizes demand response to achieve these goals. In [172, 173], a multi-objective optimization approach optimally allocates voltage source converters to improve PVHC and reduce energy losses. The focus in [174] is on maximizing the hosting capacity for wind power networks to benefit both wind farm owners and distribution network operators. A stochastic multi-objective optimization model in [175] enhances hosting capacity in wind plants by considering purchased energy costs and operation and maintenance costs. Active distribution network management through optimal capacitor switching, voltage regulator tap adjustments, and smart PV inverter control are proposed in [176], formulated as a mixed-integer non-linear programming model. The integration of smart inverters, particularly during high solar radiation periods, is extensively explored in [177]. Furthermore, [178] suggests a two-stage method to maximize hosting capacity amidst renewable energy uncertainties, involving voltage profile adjustments and optimal PV and wind turbine plant allocation.

Existing studies primarily focus on maximizing DGHC through various active network management technologies and optimal allocation of compensating devices. However, several research gaps exist, as follows:

- Integrating PV up to a certain threshold can enhance network performance by im-

proving bus voltage magnitude, reducing energy loss, and minimizing line current flow. Beyond this limit, network performance degrades, and energy loss increases. Thus, there is a need for a simultaneous optimization approach to maximize PVHC while minimizing energy loss.

- BESS and its converter can be a dispatchable source of active and reactive power. Strategies for charging/discharging the BESS and managing reactive power based on time-varying load and PV generation are essential to optimize this unit. Additionally, the operational optimization of BESS to maximize PVHC while minimizing energy losses still needs to be explored in the literature.

This chapter presents a multi-objective optimization approach to optimize PVHC and energy losses in distribution networks simultaneously. An operational optimization strategy is proposed to determine the VAr compensation/injection set-points for SHCs and BESS charging/discharging set-points in response to time-varying load demand and PV generation. The selected solution approach is the multi-objective GPR Surrogate-Assisted PSO (MO-GPRS-PSO) algorithm, which applies the Pareto dominance principle to identify a set of non-dominated solutions, referred to as the Pareto-approximation set. The SPEA2 is incorporated within MO-GPRS-PSO for fitness assignment and solution archiving. The key contributions of this work include:

- Developing a multi-objective planning approach for optimizing PVHC and energy losses simultaneously in distribution networks.

- Modeling converter approaches to provide reactive power alongside BESS active power injection, thereby maximizing PVHC and minimizing energy losses.

- Formulating an operational optimization approach to determine time-varying VAr compensation set-points for SHCs and charging/discharging set-points for BESS. This involves optimizing active and reactive power through a 24-hour period in response to varying load demand and PV generation.

Two distribution networks, the 33-bus network and the 69-bus network, are utilized for analysis to validate the proposed approach.

5.2 Multi-objective optimization planning for PVHC and energy loss in the distribution network

This section addresses the multi-objective optimization problem designed to optimize both PVHC and energy loss in distribution networks simultaneously. It details the formulation of this multi-objective optimization problem.

5.2.1 Multi-objective optimization problem

In a distribution network that includes PV units and BESS-integrated SHC (BESS-SHC), SHCs provide reactive power compensation. This study focuses on optimizing the operations of SHCs, BESS, and PVHC within the network. This optimization process, called operational optimization, determines the optimal VAr injections by SHCs and the hourly charging or discharging of the BESS. In this approach, the encoded particle positions are decoded to determine the total integration of PV systems, the reactive power contributions by SHCs, and the charge or discharge operations of the BESS.

The optimization considers the following objective functions:

$$F_1\text{: } \textit{Maximize PVHC (in \%)} = \frac{\sum_{i=2}^{\mathcal{A}} PV_i}{P_{\text{BCPL}}} \tag{5.1}$$

$$F_2\text{: } \textit{Minimize Energy Losses} = \sum_{c\in\eta} \sum_{ef\in\mathcal{Z}} PL_{ef(c)} \;\; t_c \tag{5.2}$$

Here, PV_i denotes the total capacity of PV systems installed at bus i within the distribution network. The symbol $\mathcal{A}$ indicates the total number of buses present in the network. P_{BCPL} refers to the peak load of the distribution network in the base-case scenario prior to any PV integration.

5.2.2 Integration of PV, BESS, and SHC in the distribution network

The planning strategy is designed to minimize energy losses and maximize PVHC simultaneously within the distribution network. The FBS load flow algorithm is applied to compute network voltages and currents, as outlined in Section 2.3. Following PV integration, the active power demands at the buses are adjusted hourly using Equation 2.14. The revised reactive power demand for a bus equipped with a BESS-SHC is represented by Equation 2.15.

The adjusted active power demand of a bus equipped with a BESS-SHC is calculated based on whether the BESS is charging or discharging, as indicated by Equations 5.3 and 5.4.

$$P'_i(t) = P_i(t) - P_{BESS(i)}(t), \quad \text{if the BESS is in discharging mode} \tag{5.3}$$

$$P'_i(t) = P_i(t) + P_{BESS(i)}(t), \quad \text{if the BESS is in charging mode} \tag{5.4}$$

$P'_i(t)$ denotes the modified active power demand at bus i for hour t, accounting for the BESS's charging or discharging state. $P_{BESS(i)}(t)$ represents the active power, either charging or discharging, of the BESS unit connected to bus i at hour t.

The BESS is considered to be in charging mode during periods of PV generation and in discharging mode when there is no PV generation. The network's energy losses can be calculated after adjusting the reactive and active power demands for each hour.

5.2.3 Optimization constraints

The optimization process takes into account several constraints while optimizing the network's objective functions:

1. **Power balance constraint:** Refer to Equations 2.17 and 2.18.

2. **Voltage constraint:** Refer to Equation 2.19.

3. **Thermal limit constraint:** Refer to Equation 2.20.

4. **BESS State of Charge (SOC) constraint:**

$$SOC_{\min} \leq SOC(t) \leq SOC_{\max}, \quad \forall t \tag{5.5}$$

where $SOC(t)$ represents the SOC of the BESS at time t. $SOC_{\min}$ and $SOC_{\max}$ are the minimum and maximum allowable SOC of the BESS.

5. **BESS SOC balance constraint:** This constraint ensures that the BESS starts and ends the day with the same SOC, maintaining a balanced charge and discharge cycle over 24 hours.

$$SOC_b(t_{sd}) = SOC_b(t_{ed}) \quad \forall b \in \mathcal{I} \tag{5.6}$$

where $SOC_b(t_{sd})$ and $SOC_b(t_{ed})$ represent the SOC of BESS b at the beginning of the day and the end of the day. $\mathcal{I}$ denotes the set of all BESS units under consideration.

6. **SHC reactive power limit constraint:** Refer to Equation 4.2.

Integrating PV systems beyond a certain threshold can lead to increased power losses. As a result, efforts to maximize PVHC often lead to higher power and energy losses [179]. This creates a conflict between maximizing PVHC and minimizing energy losses, making it necessary to employ a multi-objective optimization approach to balance both objectives effectively. This multi-objective approach produces a set of non-dominated solutions, where no individual solution is superior to the others [180]. Utilities can choose the most suitable solution from this set based on their specific needs. For instance, if minimizing energy losses is the priority, the solution with the lowest PVHC may be preferred, and vice versa. Various multi-objective optimization techniques are available [181], such as weighted aggregation, Pareto-based methods, and lexicographic ordering. In this study, the Pareto-based

approach is employed.

5.2.4 Pareto-dominance principle

The Pareto-dominance principle [182] states that in an optimization problem with M objectives, a solution 'a' is said to dominate another solution 'b' if the following two conditions are satisfied:

1. Solution 'a' is not worse than solution 'b' across all objectives:
   - For minimization objectives: $\forall e,\ f_e(a) \leq f_e(b)$
   - For maximization objectives: $\forall e,\ f_e(a) \geq f_e(b)$, where $e = 1, 2, \ldots, M$.
2. Solution 'a' is strictly better than solution 'b' in at least one objective:
   - For minimization objectives: $f_h(a) < f_h(b)$ for at least one $h \in \{1, 2, \ldots, M\}$
   - For maximization objectives: $f_h(a) > f_h(b)$ for at least one $h \in \{1, 2, \ldots, M\}$.

The set of all optimal non-dominated solutions is called the Pareto-optimal set.

5.3 Solution strategy: SPEA2-MO-GPRS-PSO

Multi-objective optimization is essential for managing multiple conflicting objectives and identifying optimal trade-off solutions. This research employs the SPEA2-MO-GPRS-PSO method to address these multi-objective challenges.

The MO-GPRS-PSO algorithm is an extension of the GPRS-PSO, adapted explicitly for multi-objective optimization. Each particle in this approach is evaluated using multiple fitness values corresponding to various objectives. Most multi-objective optimization techniques use the Pareto-dominance principle to identify non-dominated solutions. These solutions are graphically represented as the Pareto Approximation Front (PAF).

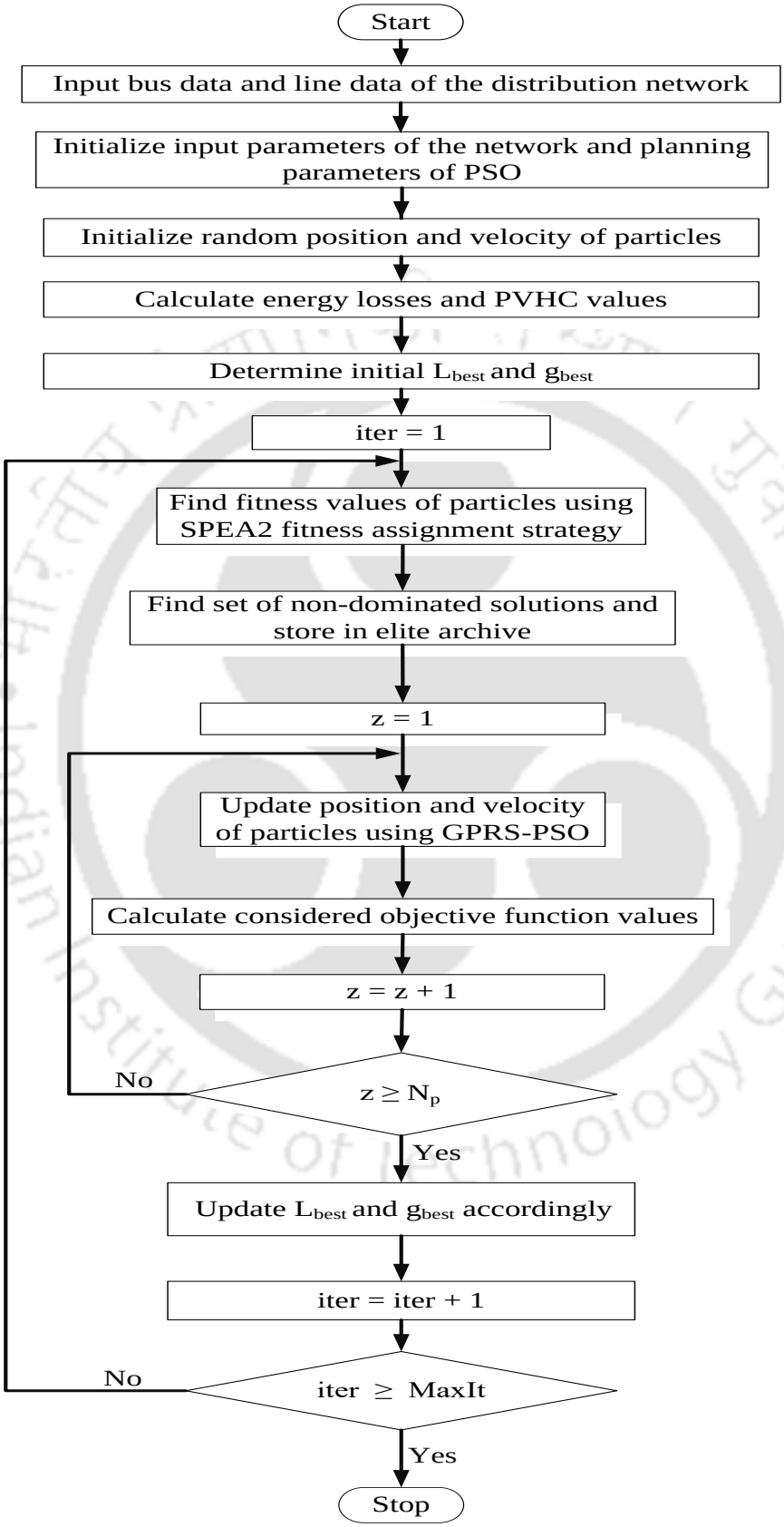

Fig. 5.1: Flow-chart for the proposed SPEA2-MO-GPRS-PSO approach

In the SPEA2-MO-GPRS-PSO method, the process involves generating a new population using the GPRS-PSO technique (refer to Sections 2.5.1 and 4.4.1). The non-dominated solutions obtained from the MO-GPRS-PSO algorithm are stored in an elite archive. This archive is crucial for assigning fitness values to the archive members and the current population, following the SPEA2 fitness assignment strategy [183]. Fitness values are computed based on each particle's non-domination rank and the density of solutions in its neighborhood [182]. The archive is updated iteratively with newly identified non-dominated solutions, and the PAF is gradually being constructed. The SPEA2-MO-GPRS-PSO approach is illustrated in Figure 5.1, and the optimization parameters are detailed in Table 5.1.

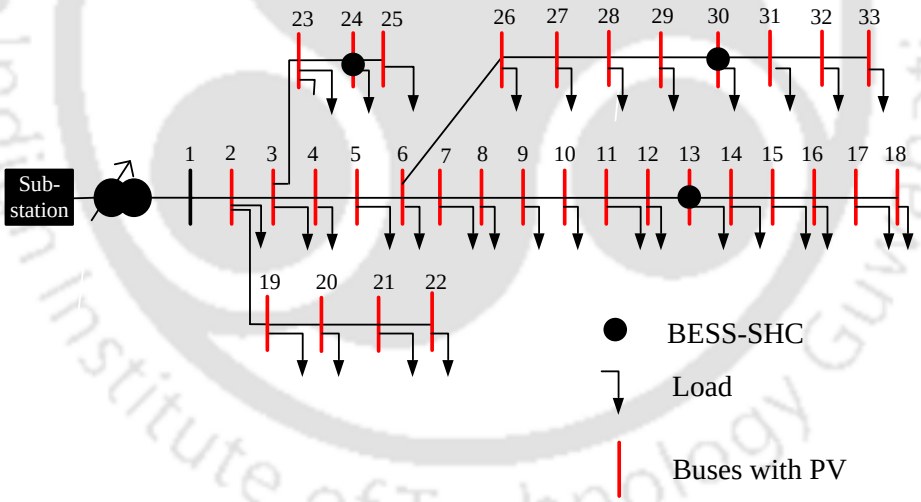

Fig. 5.2: Incorporation of PV and BESS-SHC in 33-bus distribution network

5.4 Results and discussion

The optimization problems are solved using MATLAB/Simulink on a system with a Ryzen 7-5800 CPU, 16GB of RAM, and a 1.9GHz processor. The approach for optimizing

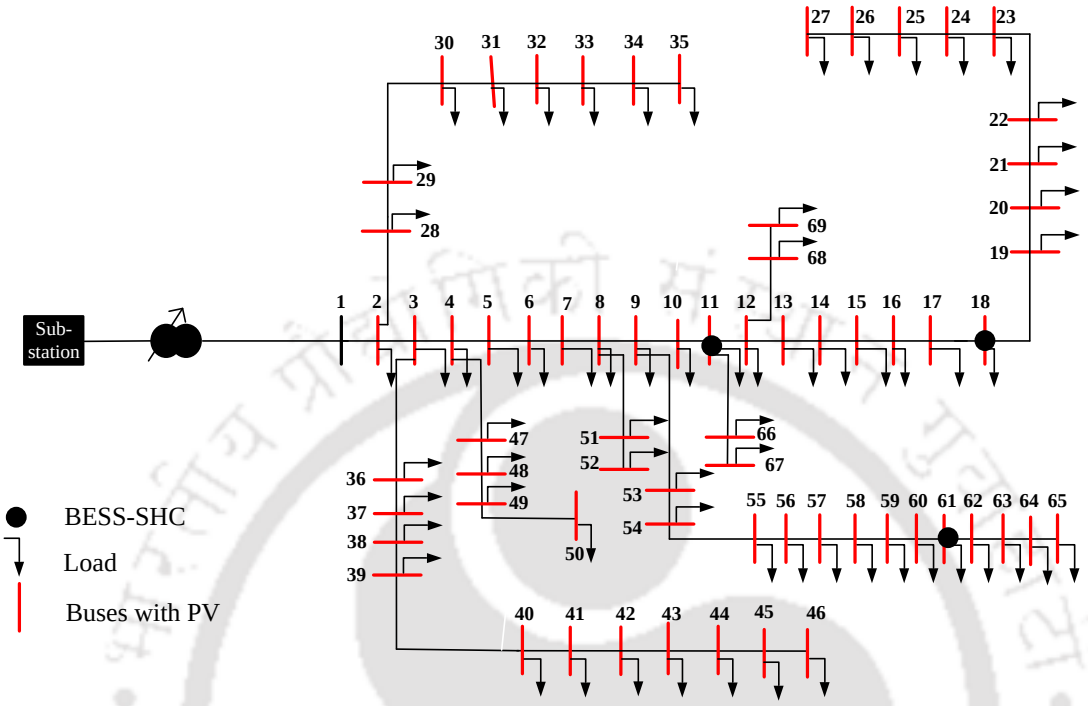

Fig. 5.3: Incorporation of PV and BESS-SHC in 69-bus distribution network

Table 5.1: Considered MO-GPRS-PSO parameters

Parameters	Considered values
Inertia weight, w	0.8
Acceleration coefficient, c_1	1.5
Acceleration coefficient, c_2	1.5
Population size, N_p	100
Surrogate threshold, s_{iter}	100
Maximum number of iterations, $MaxIt$	200

Table 5.2: Locations and ratings of BESS and SHC in the considered distribution networks

Parameters	33-bus network			69-bus network		
	Bus 13	Bus 24	Bus 30	Bus 11	Bus 18	Bus 61
BESS rated power (MW) [44]	0.880	1.190	1.150	0.564	0.420	1.878
BESS energy capacity (MWh) [44]	5.025	6.810	6.567	3.219	2.402	10.723
SHC capacity (MVA)	1.035	1.400	1.353	0.664	0.494	2.209
Maximum reactive power provided by SHC (MVAr)	0.545	0.736	0.713	0.349	0.260	1.164

Table 5.3: Solutions obtained in 33-bus distribution network

Parameters	Base-case Network	Case - A		Case - B		Case - C	
		Solution - A	Solution - B	Solution - A	Solution - B	Solution - A	Solution - B
Energy losses (kWh)	1930.7	1039.3	1282.2	678.39	872.46	355.69	588.57
PVHC (% of Base-case peak load demand)	-	94.94	149.78	135.89	189.24	152.27	196.89
PVHC (MW)	-	3.527	5.564	5.048	7.030	5.657	7.315
Total reactive power provided by SHC (MVArh)	-	0	0	47.894	47.894	25.8394	23.3281
Minimum bus voltage (pu)	0.9131	0.9334	0.9370	0.9599	0.9632	0.9570	0.9598
Maximum bus voltage (pu)	1.0	1.0061	1.0452	1.0261	1.0497	1.0251	1.0486

Table 5.4: Solutions obtained in 69-bus distribution network

Parameters	Base-case Network	Case - A		Case - B		Case - C	
		Solution - A	Solution - B	Solution - A	Solution - B	Solution - A	Solution - B
Energy losses (kWh)	2142.9	1456.6	1512.2	1175.3	1456.5	807.4	1044.7
PVHC (% of Base-case peak load demand)	-	140.55	168.68	161.97	212.52	181.96	215.77
PVHC (MW)	-	5.344	6.413	6.158	8.080	6.918	8.204
Total reactive power provided by SHC (MVArh)	-	0	0	42.552	42.552	21.342	19.605
Minimum bus voltage (pu)	0.9092	0.9254	0.9267	0.9471	0.9450	0.9478	0.9320
Maximum bus voltage (pu)	1.0	1.0314	1.0438	1.0359	1.0496	1.0373	1.0496

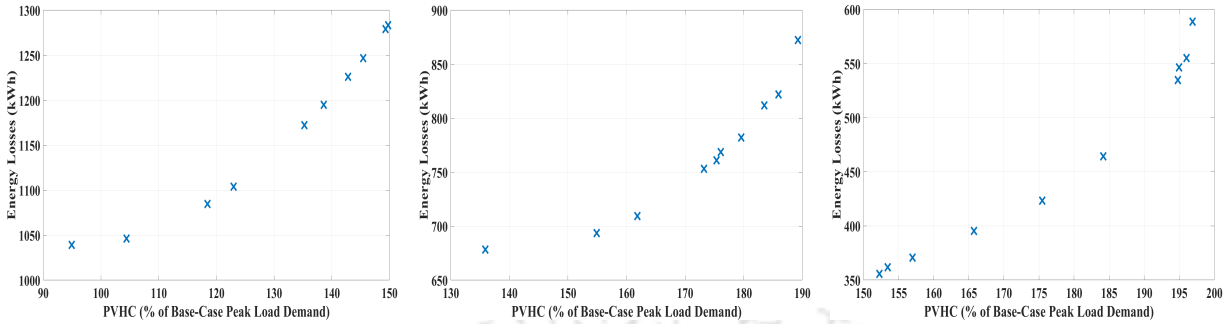

(a) (b) (c)

Fig. 5.4: PAF obtained using the SPEA2-MO-GPRS-PSO in (a) Case-A (b) Case-B (c) Cace-C, for 33-bus distribution network

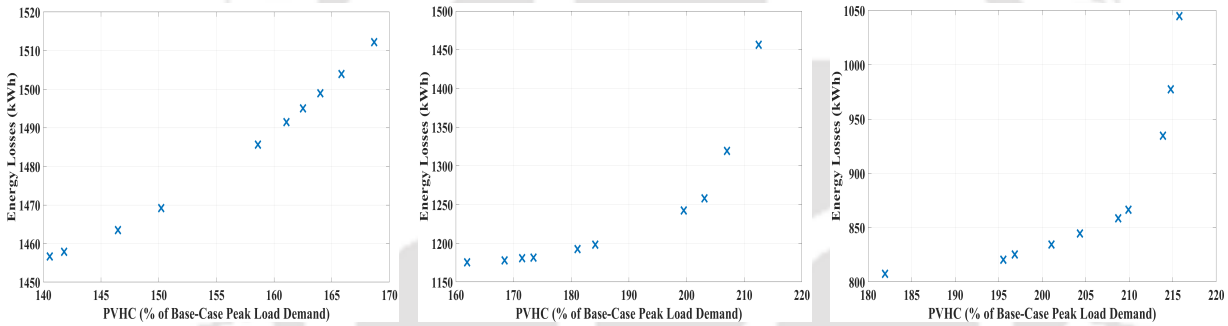

(a) (b) (c)

Fig. 5.5: PAF obtained using the SPEA2-MO-GPRS-PSO in (a) Case-A (b) Case-B (c) Cace-C, for 69-bus distribution network

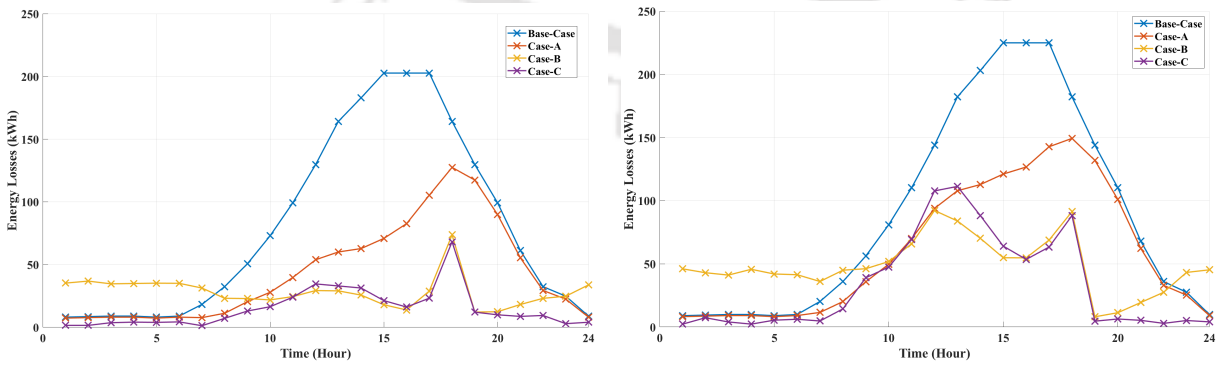

(a) (b)

Fig. 5.6: Energy losses obtained for Solution-A in all cases for (a) 33-bus network and (b) 69-bus network

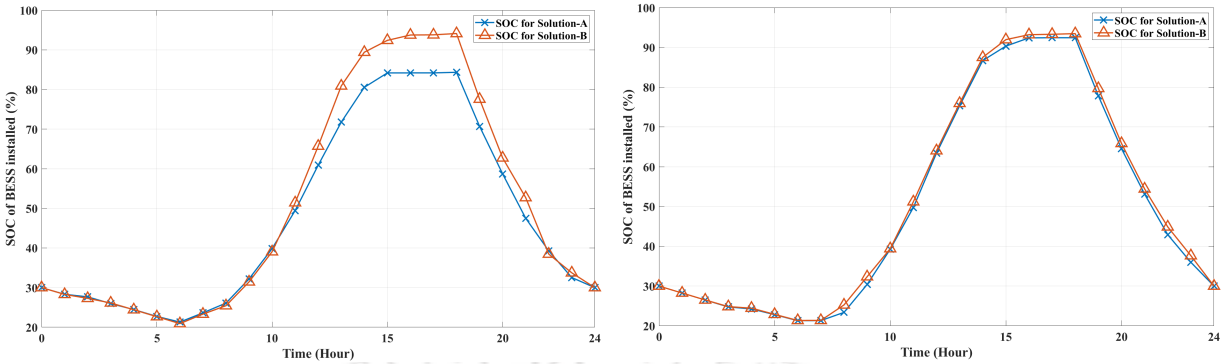

(a) (b)

Fig. 5.7: SOC of BESS in (a) Case-B (b) Case-C, for 33-bus network

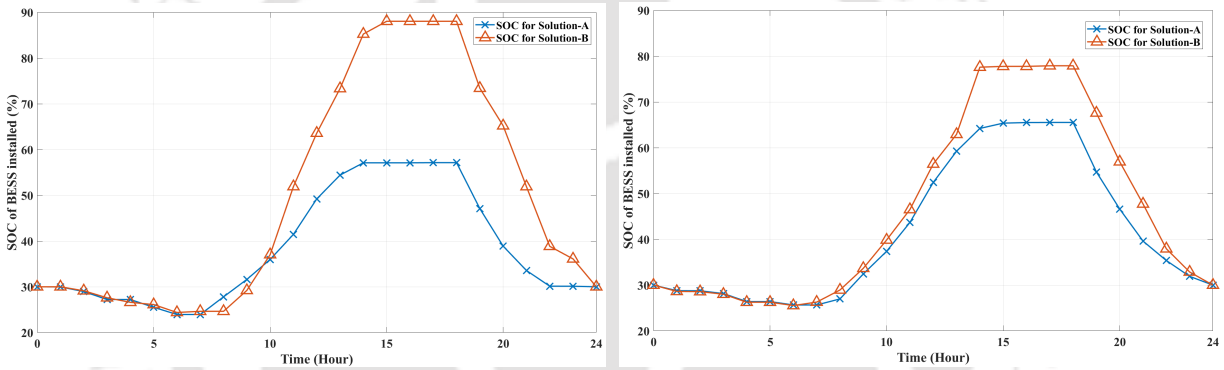

(a) (b)

Fig. 5.8: SOC of BESS in (a) Case-B (b) Case-C, for 69-bus network

PVHC and energy loss is validated on 33-bus and 69-bus radial distribution networks, shown in Figures 5.2 and 5.3.

Three case studies are conducted with different configurations of SHC and BESS units:

1. **Case-A:** This represents the base-case scenario without BESS or SHC units.

2. **Case-B:** BESS and SHC units are incorporated into the distribution network. During hours of available PV generation, the BESS stores active power. Meanwhile, it injects active power during PV non-generation hours, maintaining a constant or rated SHC VAr output. In this case, the optimization determines the optimal charging/discharging set-points for the BESS, accounting for time-varying load and PV

generation profiles.

3. **Case-C:** Similar to Case-B, Case-C also integrates BESS and SHCs into the distribution network. However, Case-C focuses explicitly on optimizing both the reactive power output of the SHC and the charging/discharging set-points of the BESS, considering the time-varying load and PV generation profiles.

To ensure network performance, bus voltage magnitude is maintained between 0.9 and 1.05 p.u [101]. Thermal limits for the 33-bus and 69-bus networks are in [102] and [99]. The daily load curve and PV generation profile are from [100], depicted in Figure 2.6. Initial and final SOC for BESS units in a day is set at 30%, with SOC limits from 20% to 100% [184], assuming 100% charging/discharging efficiency.

Table 5.2 presents the locations and specifications of BESS in both networks [44]. SHC ratings operate at a minimum power factor of 0.85, supplying reactive power [185]. Details on SHC rating and maximum reactive power capability are also in Table 5.2. After integrating these components, the extent of PV integration is determined through optimization. Each bus, except the substation, incorporates PV units uniformly. The optimization approach then regulates BESS charging/discharging and SHC operation to minimize energy losses and maximize PVHC within the network.

5.4.1 Analysis of energy losses in distribution networks

The results of optimizing the 33-bus and 69-bus distribution networks under different scenarios are summarized in Tables 5.3 and 5.4, respectively. The PAFs for these networks are depicted in Figures 5.4 and 5.5. Two solutions are considered in these tables 5.3 and 5.4.

- **Solution-A:** The extreme solution in PAF corresponds to the minimum energy losses
- **Solution-B:** The extreme solution in PAF corresponds to the maximum PVHC incorporated into the network.

In the 33-bus network, the base-case scenario shows energy losses of 1930.7 kWh. Optimization strategies in Case-A and Case-B significantly reduce energy losses. In Case-C, energy losses are reduced to 355.69 kWh, demonstrating the effectiveness of the optimization. This results in approximately 81.58% and 69.52% reduction in energy losses for Solution-A and Solution-B, respectively. Similarly, the 69-bus network's base case shows energy losses of 2142.9 kWh, significantly reduced in Case-A and Case-B. In Case-C, energy losses decrease to 807.4 kWh, highlighting the efficacy of the optimization technique.

Case-B shows lower energy losses in both networks than in Case-A due to the operational optimization of BESS charging/discharging and SHC-rated VAr injection. Case-C achieves even lower energy losses by optimizing SHC VAr injection for each hour based on load requirements. Figure 5.6 illustrates energy losses for Solution-A over 24 hours, showing Case-C's consistent superiority in minimizing energy losses. These findings emphasize the importance of optimization in reducing energy losses within distribution networks.

5.4.2 PVHC analysis in distribution networks

Table 5.3 shows that in the 33-bus network, both Case-A and Case-B exhibit notable PVHC values. Case-C shows a substantial increase in PVHC compared to the base-case and other scenarios, demonstrating the effectiveness of the optimization strategies. Similarly, Table 5.4 indicates PVHC improvements in the 69-bus network, with significant enhancements in Case-B compared to Case-A. The highest PVHC is achieved in Case-C, underscoring the impact of optimization techniques on increasing the network's capacity to accommodate PV units. The maximum PVHC levels without violating constraints are 7.315 kW for the 33-bus network and 8.204 kW for the 69-bus network. These results highlight the role of operational optimization in enhancing PVHC, promoting renewable energy integration, and advancing sustainable energy practices.

5.4.3 Reactive power provided by SHC

In Tables 5.3 and 5.4, the total reactive power supplied by SHCs is presented for different scenarios in the 33-bus and 69-bus distribution networks, respectively. In Case-B, SHCs provide rated VAr injection, improving system parameters compared to Case-A. In Case-C, SHCs reactive power injection is optimized hourly based on load demands, minimizing energy losses and enhancing PVHC. This highlights the importance of SHC integration and VAr optimization for network performance.

5.4.4 SOC profiles of the BESS

The hourly charge/discharge schedules for BESSs in the 33-bus and 69-bus networks are shown in Figures 5.7 and 5.8. These schedules illustrate optimal BESS operation, storing energy during PV generation and discharging during non-PV generation hours, thereby minimizing energy losses and maximizing PVHC. The BESS's SOC remains within prescribed limits throughout the day. Solution-B results in a higher maximum SOC than Solution-A, as Solution-A focuses on minimizing energy losses, prioritizing PV power supply during peak hours. Solution-B aims to maximize PVHC, leading to higher SOC storage.

Table 5.5: Comparative analysis between the proposed method and the previous method for the 33-bus distribution network

Parameters	**Previous approach [44]**	**Proposed approach**
Location of PV	13, 24, 30	uniformly distributed
Rating of PV (MW)	6.033	6.033
Location of BESS	13, 24, 30	13, 24, 30
Power rating of BESS (MW)	3.220	3.220
Energy capacity of BESS (MWh)	18.402	18.402
Location of SHCs	13, 24, 30	13, 24, 30
Total rating of SHCs (MVA)	3.220	3.788
Total reactive power provided by SHCs (MVArh)	- (Not optimized)	27.46
Energy losses (kWh)	717.90	384.96

5.4.5 Comparison of the proposed approach with the similar approach

Table 5.5 compares the proposed methodology with the previous approach [44] for the 33-bus network. The previous method designated specific PV installation locations, while the proposed method distributes PV uniformly across the network. For consistency, the PV rating, load, and generation profiles from the previous study are used in the comparison. The previous approach involves SHCs, in conjunction with the BESS, that provide only active power compensation. In contrast, the proposed approach incorporates SHCs rated at 3.788 MVA, which provides both active and reactive power compensation. This integration, along with the operational optimization of BESS and SHC, results in a 46.37% reduction in energy losses, reducing them to 384.96 kWh, thereby demonstrating the superiority of the proposed approach.

5.5 Summary

This chapter introduces a multi-objective planning approach based on SPEA2-MO-GPRS-PSO for optimizing PVHC and energy loss in distribution networks. A coordinated operational optimization method for BESS and SHCs is proposed to adapt to time-varying load demand and PV generation. The simulation results provide the following insights:

- The approach significantly reduces energy losses, achieving approximately 81.58% reduction for the 33-bus network and 62.32% for the 69-bus network in Case-C compared to base-case energy losses.

- In Case-C, the maximum PVHC levels reach 196.89% for the 33-bus network and 215.77% for the 69-bus network of the base-case peak load, without violating constraints.

- Case-C consistently exhibits lower energy losses and higher PVHC than Case-A and Case-B, demonstrating the effectiveness of optimizing BESS charging/discharging

alongside SHC VAr injection.

- The difference in BESS SOC storage between maximizing PVHC and minimizing energy losses highlights the trade-off between prioritizing PV power supply during peak hours and storing energy in the BESS.

Chapter 6

Multi-Objective Optimization for Allocating Series and Multiple PV-Integrated Shunt Compensators in Radial Distribution Networks

6.1 Introduction

The expanding integration of renewable energy sources may lead to distortions in voltage and current waveforms, causing various undesirable effects [186]. Compensators such as SEC and SHC are essential to address these power quality issues. SECs are used to reduce voltage fluctuations [5], while SHCs are employed to mitigate harmonic distortion in line currents [6].

Numerous strategies have been proposed in the literature to reduce voltage and current distortions in distribution networks. Effective control techniques and optimization methods are essential for managing these challenges [187]. Reference [188] presents a control method to minimize network disturbances caused by sensitive loads. Additionally,

reference [189] introduces an innovative dual control strategy designed to manage power oscillations in distribution networks that incorporate wind energy [190]. Furthermore, optimization techniques are required to minimize the compensator rating and determine its optimal placement within the network [191]. Optimization techniques are typically used to identify the optimal locations for SEC and SHC [192]. For effective mitigation of voltage sags at load points, SECs are ideally placed near the substation bus [193]. Conversely, SHCs should be located where harmonic distortions are most significant [78]. Detailed analysis of SEC and SHC placement and their effectiveness is provided in references [194, 195].

The existing literature primarily examines the use of single SEC and single SHC in distribution networks, which often leads to higher VA ratings. However, reference [196] proposes a hybrid compensator consisting of one SEC and multiple SHCs, effectively reducing network losses. Although this study does not employ an optimization technique, it manages to lower network losses despite a higher VA rating. While these studies use six compensators, there is potential to enhance distribution network performance by reducing the number of compensators while achieving minimal ratings and losses.

Based on the literature, this chapter presents the following contributions of the proposed approach:

- A multi-objective planning approach is introduced, which targets the reduction of power losses, the number of undervoltage nodes, and the total rating of compensators within the network.

- Formulated a method to reduce the number of compensators in the network by incorporating one SEC and three PV-SHCs, optimized using SPEA2-MO-GPRS-PSO.

The proposed planning approach has been validated using the 33-bus and 69-bus distribution networks.

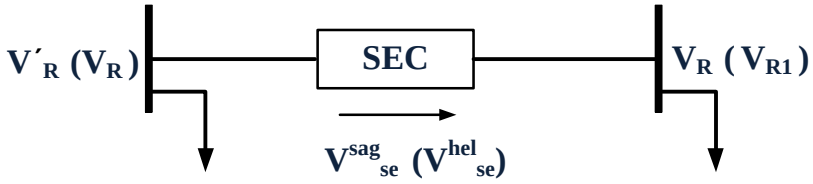

Fig. 6.1: Internal Block diagram of SEC

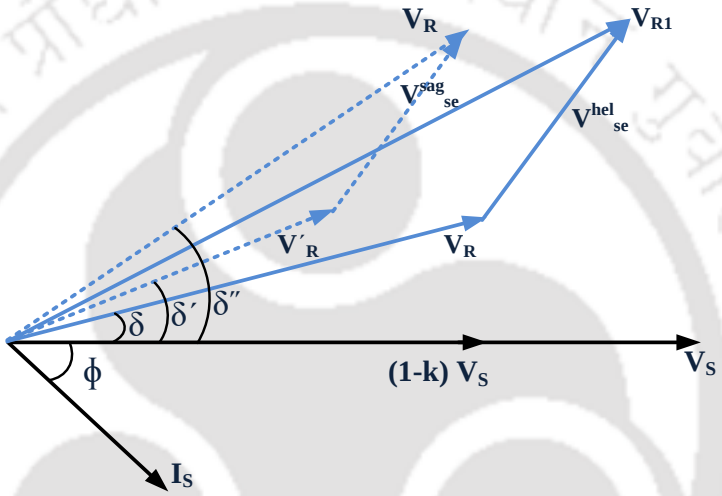

Fig. 6.2: Phasor diagram of SEC

6.2 Modelling of compensator

In this chapter, the proposed approach involves placing an SEC and multiple PV-SHCs within the distribution network.

6.2.1 Modelling of SEC

The SEC is designed to mitigate voltage sags by injecting voltage in series with the distribution network. During sag conditions, the SEC operates at its maximum rating, determined based on its ability to compensate for a maximum allowable sag of 0.8 [196].

The block diagram and phasor diagram corresponding to SEC are given in Fig. 6.1 and 6.2, respectively. From Fig.6.2, the series voltage to be injected during sag condition V_{se}^{sag}

is

$$V_{\text{se}}^{\text{sag}} = \sqrt{V_{\text{R}}^2 + V_{\text{R}}'^2 - 2V_{\text{R}}V_{\text{R}}' \cos(\delta'' - \delta')} \tag{6.1}$$

where $V_{\text{se}}^{\text{sag}}$ represents the maximum series voltage that the SEC can provide. V_{R} is the receiving end voltage under normal (healthy) conditions. V_{R}' is the receiving end voltage during a sag condition. δ' is the phase angle between the sending end voltage (V_{S}) and the receiving end voltage (V_{R}) before compensation during the sag condition. δ'' is the phase angle between V_{S} and V_{R} after compensation during the sag condition.

From Fig. 6.2,

$$V_{\text{R}} \cos\delta'' = V_{\text{R}}' \cos\delta' + V_{\text{se}}^{\text{sag}} \sin\varnothing \tag{6.2}$$

where $\varnothing$ represents the angle between V_{S} and sending end current V_{S} at the location of the SEC.

$$V_{\text{R}} \sin\delta'' = V_{\text{R}}' \sin\delta' + V_{\text{se}}^{\text{sag}} \cos\varnothing \tag{6.3}$$

By mapping V_{R} and V_{R}' onto I_S,

$$V_{\text{R}} \cos(\delta'' + \varnothing) = V_{\text{R}}' \cos(\delta' + \varnothing) \tag{6.4}$$

From Equations 6.2, 6.3 and 6.4,

$$\delta'' = \cos^{-1}\left\{\frac{V_{\text{R}}'}{V_{\text{R}}} \cos(\delta' + \varnothing)\right\} - \varnothing \tag{6.5}$$

VA rating of SEC is determined as

$$S_{\text{se}} = V_{\text{se}}^{\text{sag}} I_{\text{s}} \tag{6.6}$$

As the SEC is not connected across any PV sources, it can only provide reactive power to the network. Therefore, $V_{\text{se}}^{\text{sag}}$ is injected perpendicular to I_S. Accordingly, the total VA rating of the SEC is equal to the reactive power of the SEC.

$$Q_{\text{se}} = S_{\text{se}} \tag{6.7}$$

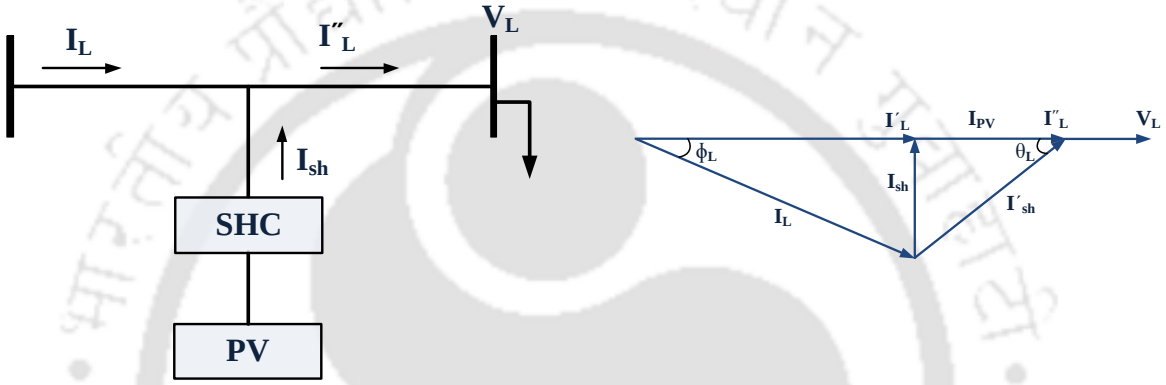

Fig. 6.3: (a) Internal Block Diagram (b) Phasor diagram of PV-SHC

6.2.2 Modelling of PV-SHC

The SHC mitigates harmonics in the line current by injecting an appropriate shunt current. In this work, the SHC is designed to integrate with a PV system, enabling active and reactive power compensation. As PV is connected to SHC, the fraction of line current (K_{PV}) can be provided by the PV itself. The current compensation by PV (I_{PV}) is evaluated as

$$I_{\text{PV}} = K_{\text{PV}}\ I_L \tag{6.8}$$

From fig. 6.3 (b),

$$\theta_L = \tan^{-1}\left(\frac{\sin\phi_L}{K_{\text{PV}}}\right) \tag{6.9}$$

$$I_{sh} = \frac{I_L \sin \phi_L}{\sin \theta_L} \tag{6.10}$$

where θ_L represents the angle between I_L and I_{sh}.

The VA rating of the PV-SHC is determined using Equation 2.7. The SHC is integrated with the PV unit and compensates active and reactive power.

Active and reactive power ratings of PV-SHC are determined as

$$P_{PV-SHC} = S_{sh} \cos \theta_L \tag{6.11}$$

$$Q_{PV-SHC} = S_{sh} \sin \theta_L \tag{6.12}$$

The PV unit is integrated into the SHC parallel to its DC link. The size of the PV array to be installed is determined based on the active power injection capability of the SHC.

$$PV_i = \frac{t_{oh}\ V_L\ I_{PV}}{24\ \text{CUF}_{PV}} \tag{6.13}$$

where t_{oh} is the operating hours of PV. CUF_{PV} is the considered Capacity Utilisation Factor of PV. Here, t_{oh} and CUF values are considered to be 5 and 0.18, respectively.

When multiple compensators are considered, adjusting the active and reactive power demands at all buses where compensators are installed is necessary. The modified active and reactive power demands at the location of a PV-SHC are given by:

$$P'_i(t) = P_i(t) - P_{PV-SHC(i)}(t) \tag{6.14}$$

$$Q'_i(t) = Q_i(t) - Q_{PV-SHC(i)}(t) \tag{6.15}$$

The modified reactive power demand at the location of SEC is

$$Q'_i(t) = Q_i(t) - Q_{se(i)}(t) \tag{6.16}$$

The FBS load flow algorithm, as discussed in Section 2.3, calculates the voltages and currents within the distribution network. Subsequently, the ratings for the SEC and PV-SHC are determined, and an evaluation is performed to identify the number of undervoltage nodes and to determine the power losses in the network.

6.3 Multi-objective optimization problem

This chapter presents a multi-objective approach to optimize the placement of SEC and PV-SHC in distribution networks. The objective is to simultaneously minimize network power losses, the number of undervoltage nodes, and the total VA rating of the compensators.

The optimization process considers the following objective functions:

$$\textit{Objective function 1:}\ \text{Minimize}\ \textit{Power Losses} = \sum_{ef \in \mathcal{Z}} PL_{ef} \tag{6.17}$$

$$\textit{Objective function 2:}\ \text{Minimize}\ \textit{Rating of Compensator} = S_{se} + \sum_{i=1}^{m} S_{sh_i} \tag{6.18}$$

$$\textit{Objective function 3:}\ \text{Minimize}\ \textit{Number of undervoltage nodes} = \sum_{i \in \mathcal{A}} N_i \tag{6.19}$$

where S_{SEC} and S_{SHC} represent the total rating of SEC and SHCs in the network, respectively. N_i represents a binary variable that equals 1 if node N_i is an undervoltage

node, and 0 otherwise.

The optimization aims to minimize these objective functions while adhering to certain constraints. These constraints ensure a power balance constraint, voltage, and thermal constraints and require the SEC and PV-SHCs to be located at different positions (Refer Equations 2.17-2.21).

The optimization process is conducted considering three cases:

- *Case A:* Optimization of objective functions 1 and 2 simultaneously.
- *Case B:* Optimization of objective functions 2 and 3 simultaneously.
- *Case C:* Optimization of objective functions 1, 2, and 3 simultaneously.

To minimize power losses, higher-rated compensators are typically required. Additionally, reducing the number of undervoltage nodes also demands higher-rated compensators. Consequently, minimizing power losses, reducing undervoltage nodes, and optimizing compensator ratings often conflict. To solve these conflicting objectives, a Pareto-based multi-objective optimization approach is employed. This approach produces a set of non-dominated solutions, where no solution is better or worse than another [197, 198]. The DNO can select the solution that best aligns with its specific requirements. Further details on the Pareto dominance principle are discussed in Section 5.2.4.

6.4 SPEA2-MO-GPRS-PSO based solution approach

This chapter employs the SPEA2-MO-GPRS-PSO algorithm to determine the optimal locations for SEC and PV-SHCs. The fundamental concepts of the GPRS-PSO algorithm and the SPEA2-based MO-GPRS-PSO approach are briefly outlined in sections 4.4.1 and 5.3, respectively. The incorporation of SEC and PV-SHCs into the FBSLF algorithm is detailed through Equations 6.14-6.16, while the comprehensive procedure of the FBSLF algorithm is described in Section 2.3.

N_p : Size of population
$MaxIt$: Maximum number of iterations
s_{iter}: Surrogate data storage iteration threshold
Begin
  Input bus data and line data of the distribution network
  Initialise input parameters for MO-GPRS-PSO
  Initialise position and velocity of particles for size N_p
  Determine objective functions values for corresponding locations
  Determine L_{best} and g_{best}
  iter = 1;
  While iter <= $MaxIt$
    Find out the fitness value for each particle of MO-GPRS-PSO
    Find the set of non-dominated solutions and store it in elite archive
    For p = 1:N_p
      Update position and velocity of particles
      Perform Forward-Backward Sweep load flow algorithm
      Calculate objective function values
      Penalise the objective functions, if constraints are violated
      Update L_{best} and g_{best} accordingly
        If $iter > s_{iter}$, Perform GPR Newton optimization
          For $local\_iterations = 1$ *to* 3
            Apply Newton's method to predict potential optima
            Evaluate the actual objective function value at the predicted optima
            If the predicted objective function value is lower, update g_{best}
          End For
        End If
      t = t + 1
    End For
  End While
  The final set of non-dominated solutions are the desired decision variables
End

Fig. 6.4: Pseudo code for the proposed SPEA2-MO-GPRS-PSO approach

The MO-GPRS-PSO-based planning algorithm employs the FBSLF subroutine to incorporate SEC and PV-SHCs into the distribution network. Each particle in this multi-objective approach is represented by the locations of the SEC and PV-SHCs. The pseudo-code for the SPEA2-MO-GPRS-PSO algorithm is illustrated in Figure 6.4. By optimizing the objectives simultaneously, the algorithm produces a set of non-dominated solutions.

Table 6.1: Network parameters from PAF using SPEA2-MO-GPRS-PSO for the 33-bus network after placing SEC and designed PV-SHCs (Scenario-1)

	Network parameters				
	Solution-1	**Solution-2**	**Solution-3**	**Solution-4**	**Solution-5**
SEC location	3	3	3	3	3
PV-SHC locations	9, 30, 6	14, 31, 30	14, 31, 13	16, 32, 15	18, 33, 16
SEC rating (MVA)	2.322	2.322	2.322	2.322	2.322
Overall SHC rating (MVA)	1.735	1.040	0.528	0.309	0.149
Total rating of compensator (MVA)	4.057	3.362	2.849	2.631	2.471
Network losses (kW)	98.74	114.7	131.4	149.3	165.9
Number of undervoltage nodes	2	6	15	16	17
Size of PV (kW)	625.63	296.29	222.55	132.69	64.01

Table 6.2: Network parameters from PAF using SPEA2-MO-GPRS-PSO for the 33-bus network after placing SEC and conventional PV-SHCs (Scenario-2)

	Network parameters				
	Solution-1	**Solution-2**	**Solution-3**	**Solution-4**	**Solution-5**
SEC location	3	3	3	3	3
PV-SHC locations	6, 30, 28	28, 29, 10	16, 30, 14	33, 14, 12	33, 16, 18
SEC rating (MVA)	2.322	2.322	2.322	2.322	2.322
Overall SHC rating (MVA)	0.701	0.457	0.247	0.151	0.059
Total rating of compensator (MVA)	3.023	2.779	2.569	2.473	2.381
Network losses (kW)	129.19	140.21	154.71	165.03	174.52
Number of undervoltage nodes	14	16	16	17	17
Size of PV (kW)	811.85	529.09	285.84	174.93	68.88

Table 6.3: Network parameters from PAF using SPEA2-MO-GPRS-PSO for the 69-bus network after placing SEC and designed PV-SHCs (Scenario-1)

	Network parameters				
	Solution-1	**Solution-2**	**Solution-3**	**Solution-4**	**Solution-5**
SEC location	3	3	3	3	3
PV-SHC locations	61, 58, 59	61, 20, 16	62, 17, 64	64, 62, 35	52, 27, 35
SEC rating (MVA)	2.796	2.796	2.796	2.796	2.796
Overall SHC rating (MVA)	1.863	1.446	0.67	0.289	0.018
Total rating of compensator (MVA)	4.659	4.24	3.466	3.085	2.814
Network losses (kW)	59.97	101.9	156.9	182.3	224.1
Number of undervoltage nodes	0	6	9	9	9
Size of PV (kW)	815.74	427.09	190.53	108.38	5.02

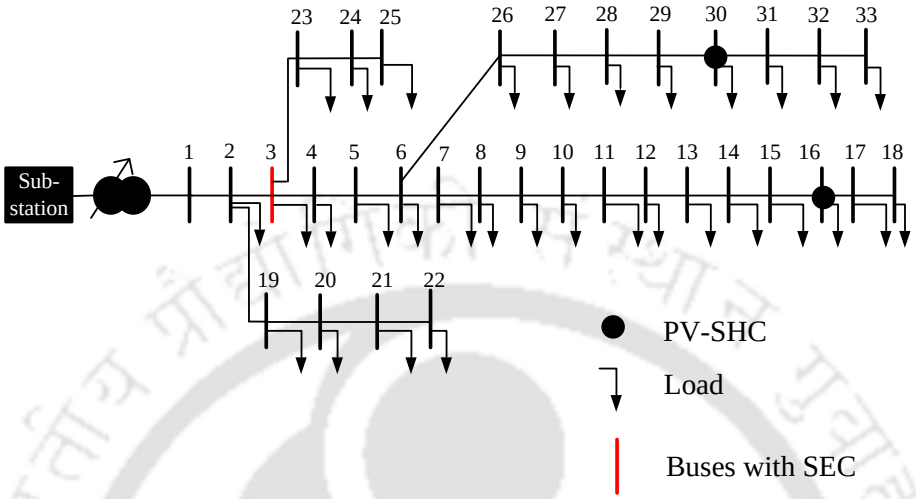

Fig. 6.5: Incorporation of SEC and PV-SHC in 33-bus distribution network

6.5 Results and discussion

The effectiveness of the proposed optimization approach is tested on the 33-bus and 69-bus radial distribution networks. Detailed information on the network data and single-line diagrams is provided in Appendix A. Figures 6.5 and 6.6 illustrate the single-line diagrams for one set of non-dominated solutions obtained through the Pareto-based approach. This methodology effectively reduces the compensator rating, number of undervoltage nodes,

Table 6.4: Network parameters from PAF using SPEA2-MO-GPRS-PSO for the 69-bus network after placing SEC and conventional PV-SHCs (Scenario-2)

	Network parameters				
	Solution-1	**Solution-2**	**Solution-3**	**Solution-4**	**Solution-5**
SEC location	3	3	3	3	3
PV-SHC locations	59, 60, 61	61, 60, 24	63, 61, 25	62, 63, 13	52, 35, 27
SEC rating (MVA)	2.796	2.796	2.796	2.796	2.796
Overall SHC rating (MVA)	0.888	0.555	0.34	0.176	0.004
Total rating of compensator (MVA)	3.68	3.35	3.14	2.97	2.8
Network losses (kW)	128.04	153.04	175.61	203.9	224.65
Number of undervoltage nodes	6	8	9	9	9
Size of PV (kW)	1028.3	642.43	393.53	203.34	5.02

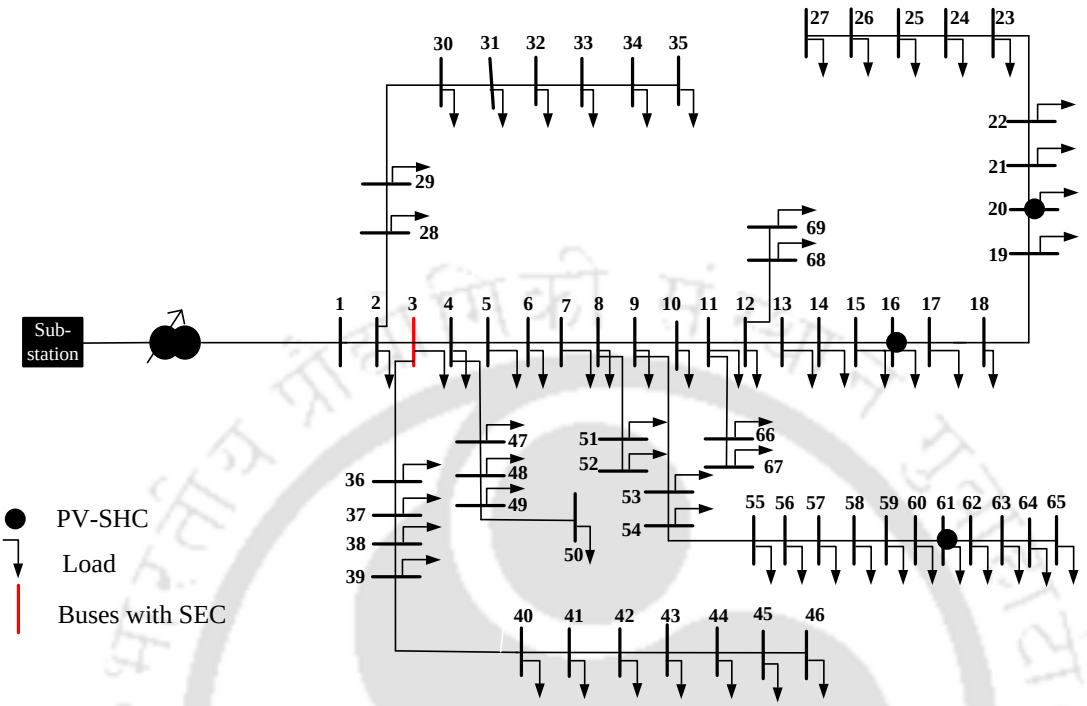

Fig. 6.6: Incorporation of SEC and PV-SHC in 69-bus distribution network

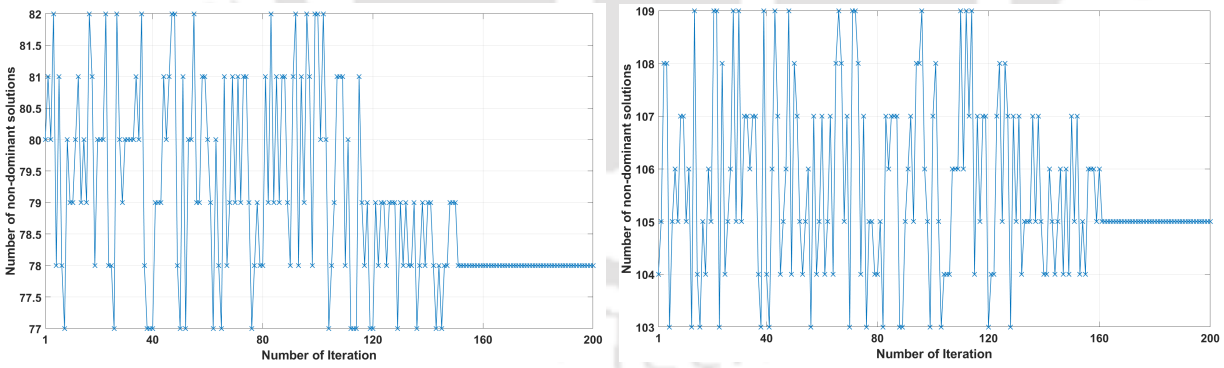

(a) (b)

Fig. 6.7: Convergence curves showing the number of non-dominated solutions obtained at each iteration for Case-A in the (a) 33-bus and (b) 69-bus networks using the SPEA2-MO-GPRS-PSO approach

and power losses within the network. In this study, a bus voltage magnitude below 0.95 pu is considered an undervoltage node [199].

This study considers two scenarios to analyze the objective functions:

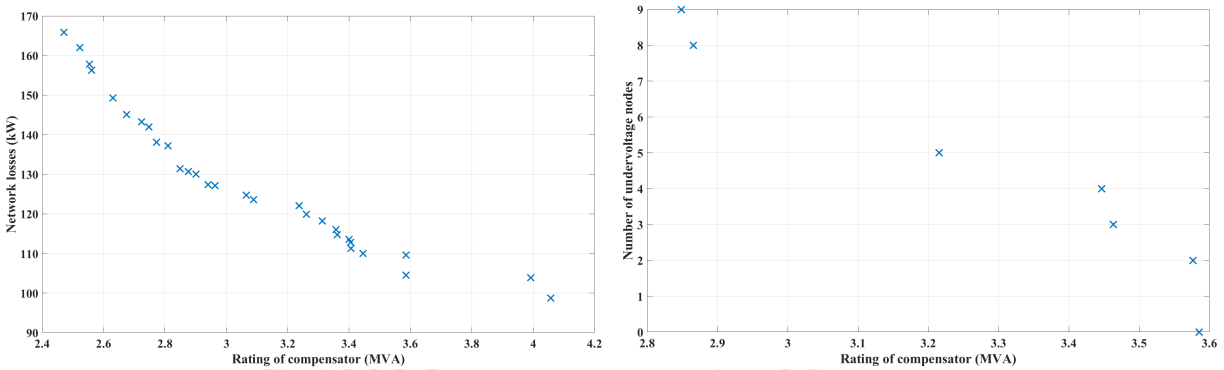

(a) (b)

Fig. 6.8: PAFs obtained for the 33-bus network using SPEA2-MO-GPRS-PSO when SEC and designed PV-SHCs considered for (a) Case-A (b) Case-B (Scenario-1)

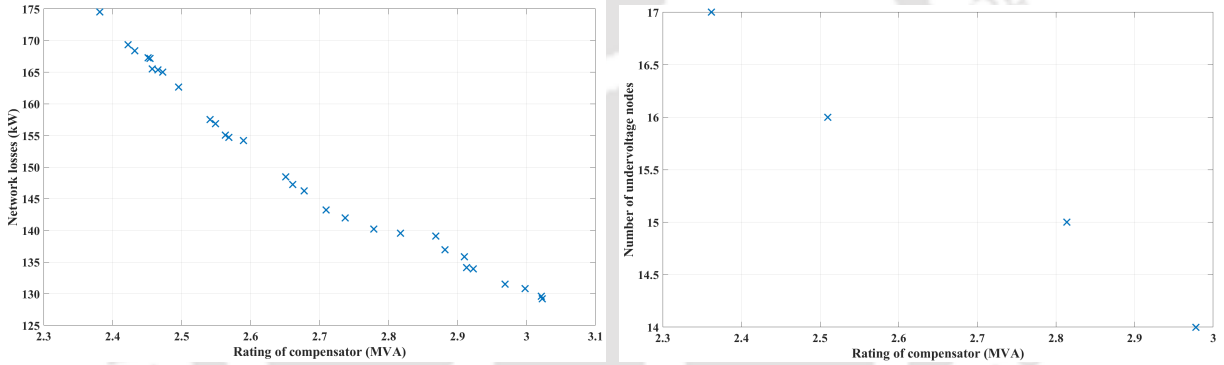

(a) (b)

Fig. 6.9: PAFs obtained for the 33-bus network using SPEA2-MO-GPRS-PSO when SEC and conventional PV-SHCs considered for (a) Case-A (b) Case-B (Scenario-2)

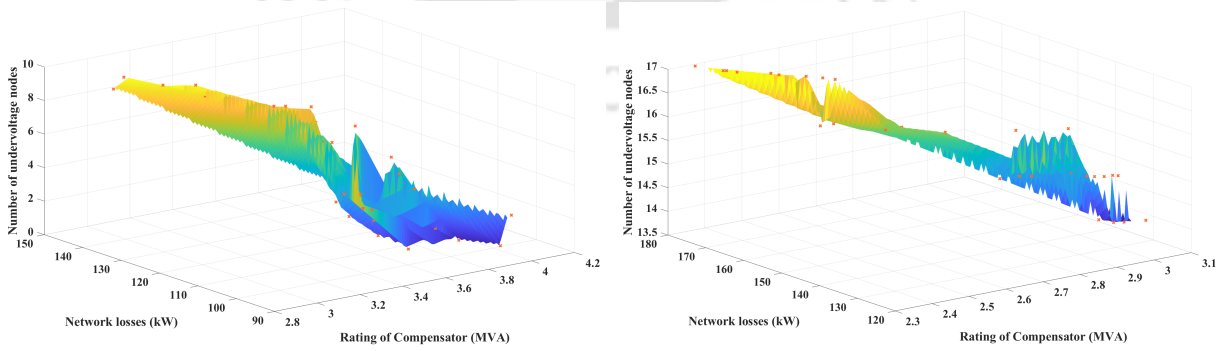

(a) (b)

Fig. 6.10: Pareto Approximate Surfaces obtained for the 33-bus network using SPEA2-MO-GPRS-PSO for Case-C in (a) Scenario-1 (b) Scenario-2

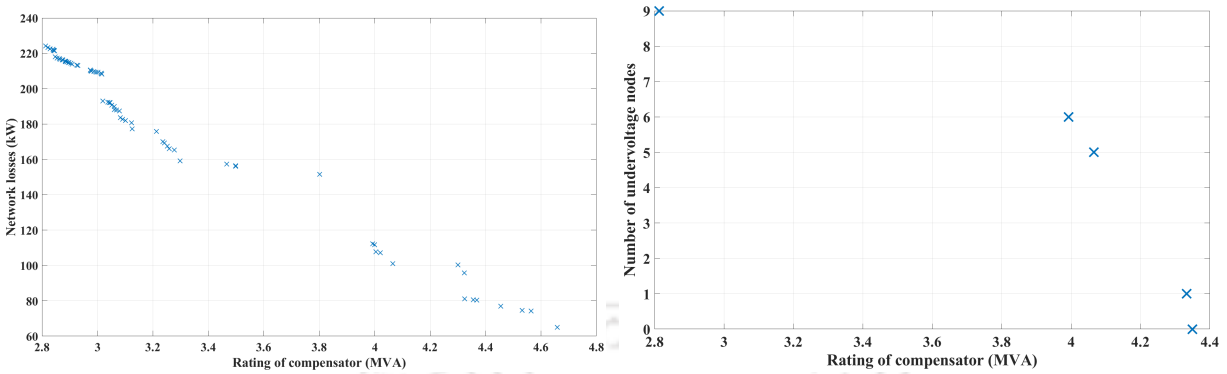

(a) (b)

Fig. 6.11: PAFs obtained for the 69-bus network using SPEA2-MO-GPRS-PSO when SEC and designed PV-SHCs considered for (a) Case-A (b) Case-B (Scenario-1)

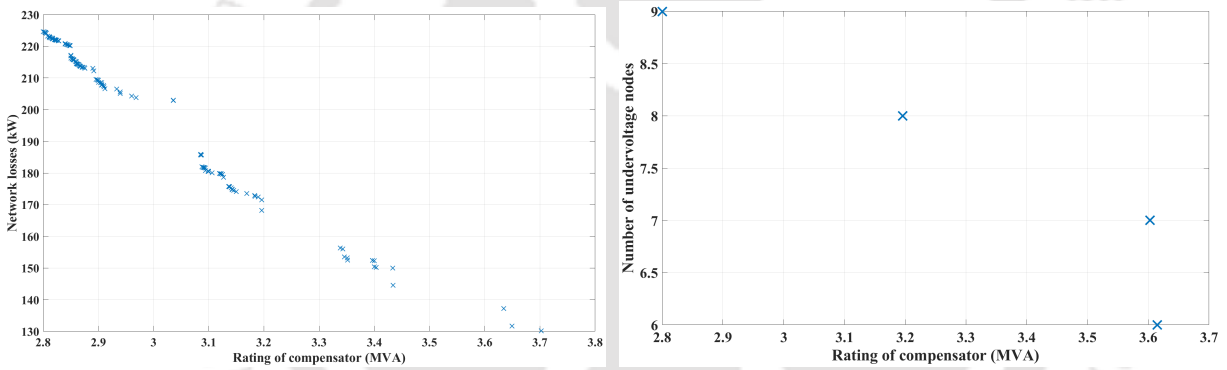

(a) (b)

Fig. 6.12: PAFs obtained for the 69-bus network using SPEA2-MO-GPRS-PSO when SEC and conventional PV-SHCs considered for (a) Case-A (b) Case-B (Scenario-2)

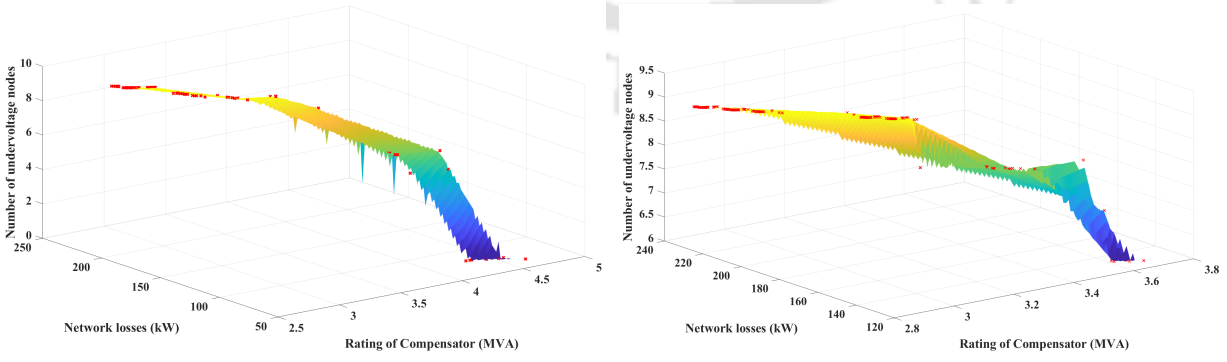

(a) (b)

Fig. 6.13: Pareto Approximate Surfaces obtained for the 69-bus network using SPEA2-MO-GPRS-PSO for Case-C in (a) Scenario-1 (b) Scenario-2

- *Scenario 1:* A single SEC is utilized, and designed PV-SHCs are implemented to mitigate harmonics and active and reactive power compensation.

- *Scenario 2:* A single SEC and conventional PV-SHCs are utilized only for active power compensation.

In multi-objective optimization, convergence plots differ from single-objective plots because the aim is to find a set of Pareto-optimal trade-offs among conflicting objectives rather than a single optimal solution. In this work, convergence is validated by analyzing the progression of non-dominated solutions obtained at each iteration. Figure 6.7 shows the convergence curves for the 33-bus and 69-bus networks using the SPEA2-MO-GPRS-PSO approach, illustrating how a diverse set of trade-offs is progressively identified.

6.5.1 Solutions obtained from PAF through multi-objective approach

In Scenario-1, the SEC is installed at bus 3, and the optimal locations for the PV-SHCs are subsequently identified. In this scenario, the PV-SHCs provide both active and reactive power compensation. The PAFs for Case-A and Case-B in Scenario-1 are illustrated in Figures 6.8 and 6.11 for the 33-bus and 69-bus networks, respectively. The solutions derived from the PAF for Case-A in these networks are quantitatively presented in Tables 6.1 and 6.3. These tables detail five solutions, highlighting the power losses, corresponding locations, and ratings of the SEC and PV-SHCs. The PAF features two extreme solutions, Solution-1 and Solution-5, which represent the endpoints of the PAF. The lowest network losses characterize Solution-1, while Solution-5 has a lower VA rating for the compensator but higher power losses. The intermediate solutions, 2, 3, and 4, offer a compromise between compensator rating and power losses. Additionally, the tables provide data on the number of undervoltage nodes and the PV rating for each solution.

In Scenario-2, conventional PV-SHCs operate at unity power factor, injecting only active power into the network. The optimal locations for PV-SHCs are determined using the

SPEA2-MO-GPRS-PSO approach, with the SEC placed at bus 3. The network parameters obtained from the PAF for Case-A are detailed in Tables 6.2 and 6.4 for the 33-bus and 69-bus networks, respectively. These tables include the locations of the compensators, objective function values related to power losses, and the VA ratings of the compensators for comparison. The PAFs for Scenario-2 corresponding to Case-A and Case-B are depicted in Figures 6.9 and 6.12 for the 33-bus and 69-bus networks, respectively. Additionally, the Pareto Approximate Surfaces for Case-C in both Scenario-1 and Scenario-2 for both networks are shown in Figures 6.10 and 6.13.

6.5.2 Performance comparison of scenario-1 and scenario-2

The findings from Table 6.1 and Table 6.2 reveal that Scenario-1 achieves significantly lower power losses compared to Scenario-2, with losses in Scenario-1 being nearly half of those in Scenario-2. This substantial loss reduction is primarily due to the combined reactive and active power compensation provided by the PV-SHCs in Scenario-1. In this scenario, the PV-SHC is designed to address harmonics and reactive power compensation, resulting in a higher overall SHC rating than Scenario-2. The placement of SHCs in both scenarios influences the subsequent sizing of PV units. As SHCs are sequentially placed, the size of the PV system depends on the level of active and reactive power compensation provided by the previously installed compensators. Consequently, although Scenario-2 requires a higher PV rating, Scenario-1 has a higher VA rating for the SHC. Implementing specially designed SHCs in Scenario-1 increases the overall rating and cost of the SHCs within the network, and it also offers the benefit of reducing the number of undervoltage nodes. Therefore, replacing conventional PV-SHCs with these designed PV-SHC units can effectively decrease harmonic content in the line current, provide necessary reactive power compensation, and ultimately reduce network losses and fewer undervoltage nodes. Similar outcomes are observed in the 69-bus network, as shown in Table 6.3 and Table 6.4.

The placement of SHCs in both scenarios influences the subsequent sizing of PV units.

As SHCs are sequentially installed, the size of the PV system is determined by the level of active and reactive power compensation provided by the previously installed compensators. Consequently, while Scenario-2 requires a higher PV rating, Scenario-1 necessitates a higher VA rating for the SHC. Implementing specially designed SHCs in Scenario-1 increases the overall rating and cost of the SHCs within the network, but it also effectively reduces the number of undervoltage nodes. Replacing conventional PV-SHCs with these specially designed PV-SHC units can significantly decrease harmonic content in the line current, provide essential reactive power compensation, and ultimately reduce network losses and the number of undervoltage nodes.

As shown in Figures 6.8 (b) and 6.9 (b), Scenario-2 reduces the number of undervoltage nodes in the 33-bus distribution network from 21 (in the base case) to 14. In contrast, Scenario-1, utilizing the designed PV-SHCs, eliminates undervoltage nodes. For the 69-bus network, the base case has 9 undervoltage nodes. Scenario-2 reduces this number to 6, while Scenario-1 eliminates the undervoltage nodes.

Table 6.5: Network parameters obtained from SPEA2-MO-GPRS-PSO for Scenario-1 and previous method in the 69-bus network

Parameters	**Obtained values**	
	Scenario-1	**[196]**
Network losses (kW)	59.97	150.9
Rating of compensator (MVA)	4.659	6.077
Number of undervoltage nodes	0	7
Location of SEC	3	3
Location of SHC	61, 58, 59	9, 19, 29, 37, 61
Total VA rating of SEC (MVA)	2.796	2.652
Total VA rating of SHC (MVA)	1.863	3.425
Total size of PV (kW)	815.74	-

6.5.3 Performance comparison of present approach with previous work

Table 6.5 highlights comparing the present study and previous similar approach [196]. In the earlier study [196], a 69-bus distribution network is analyzed without employing

any optimization techniques. This configuration involves placing one SEC and five SHCs, resulting in network losses of 150.9 kW and a compensator rating of 6.077 MVA.

In contrast, this study introduces a hybrid compensator approach comprising four compensators, including one SEC and three SHCs, strategically positioned within the network. These SHCs are integrated with PV units to provide active and reactive power compensation. This optimized configuration reduces network losses to 59.97 kW, and the compensator rating is significantly decreased to 4.66 MVA. This demonstrates a substantial improvement in losses and compensator rating compared to the previous study, offering cost advantages by lowering the overall compensator cost. Additionally, the new compensator configuration reduces the number of undervoltage nodes. Although integrating PV units increases the initial installation cost, it provides significant benefits by offering active power compensation and reducing power losses.

6.6 Summary

This research presents an optimization-based methodology to minimize compensator ratings, the number of undervoltage nodes, and power losses within the distribution network. The methodology optimizes these objectives by employing the SPEA2-MO-GPRS-PSO technique, generating a set of non-dominated solutions. It effectively identifies the optimal locations for SEC and PV-SHC units within the distribution network. The key findings from the study are summarized as follows:

- The proposed PV-SHCs reduce network power losses by 23.57% in the 33-bus network and by 53.16% in the 69-bus network, compared to conventional PV-SHCs.

- The implementation of PV-SHC units eliminates undervoltage nodes, reducing their number from 6 to 0 and 14 to 0 for the 33-bus and 69-bus networks, respectively, through combined active and reactive power compensation.

- The overall rating of the proposed compensator is 76.7% of the rating from a previously employed analytical method while also achieving reduced network power losses.
- Network power losses are reduced from 150.9 kW to 59.97 kW, representing a decrease of approximately 60% compared to the previous similar approach.

Chapter 7

Conclusion

The integration of DGs, ESS, and compensators plays a crucial role in transforming traditional distribution networks into active distribution systems. Proper planning of these integrations is essential for managing the increasing complexity of active distribution networks, characterized by time-varying renewable energy generation and load demands. In recent years, significant research has been conducted to optimize these integrations to improve overall network performance. Chapter-1 provides a systematic review of various approaches for incorporating DG, ESS, and compensators into distribution networks, organizing them according to specific objectives and methodologies highlighted in the literature. Additionally, the importance of CPD is highlighted for its ability to mitigate voltage sags, swells, and current harmonics in DG-integrated networks. Chapter-1 also discusses and classifies different strategies and techniques for integrating DG and CPD into distribution networks, categorizing them into four levels. Furthermore, integrating CPDs with advanced optimization techniques has become an essential area of research to maximize the effectiveness of DGs and ESS in these networks. Therefore, this thesis focuses on developing advanced optimization methods for the strategic placement and operation of DG, ESS, and compensators. The research aims to improve the operational performance of distribution networks by minimizing energy losses, reducing compensator ratings, maximizing economic

benefits, and increasing PVHC. The contributions of this thesis are summarized as follows:

- In Chapter-2, the modeling of SHCs in distribution networks and their integration using the FBS load flow algorithm is discussed. The primary goal is to minimize energy losses across time-varying varying load and PV generation scenarios. This is determined by optimally placing SHCs within the network using the PSO approach. Simulation studies are conducted on two test networks, namely the 33-bus and 69-bus networks, to evaluate the effectiveness of the SHC placement strategy in reducing energy losses under different levels of PV penetration. Furthermore, the research introduces a novel approach by evenly distributing PV generation capacity across all network buses, representing realistic conditions in urban areas with spatial limitations. The results highlight how the number of SHCs and the different levels of PV integration impact the overall performance of the distribution network. It is found that 2 SHCs are optimal for the 33-bus network, while 3 SHCs are optimal for the 69-bus network, showing that the number of SHCs needed depends on the network's size. The results indicate that optimal placement of SHCs in PV-integrated networks can reduce energy losses by 30-35% compared to those with PV integration alone.

- In Chapter-3, an economic evaluation assesses the combined placement of PV units and SHCs in distribution networks to maximize profit. This evaluation considers investment costs, revenue from PV generation, and cost savings from reduced network energy losses. The methodology identifies the optimal SHC placement for various levels of PV penetration, considering factors such as annual load growth, seasonal load variations, and PV generation profiles. The PSO algorithm is used to optimize SHC placement in PV-integrated networks. The results show that increased PV penetration leads to more significant savings in energy losses, with PV systems alone reducing energy losses by approximately 30-40% compared to non-PV conditions. Moreover, integrating multiple SHCs with PV units results in a 12-15% improvement

in profit compared to networks with only PV units, demonstrating the enhanced profitability of combining SHCs with PV systems. The chapter also highlights that the economic benefits are significantly influenced by the level of PV penetration and the strategic placement of SHCs, providing a comprehensive framework for economic evaluation and decision-making in distribution network management. This analysis underscores the importance of integrating SHCs with PV units to optimize financial and operational performance in distribution networks.

- In Chapter-4, the Parallel-MS-GPRS-PSO algorithm is introduced, specifically designed to optimize the operation of SHCs in PV-integrated distribution networks to minimize AEL costs. This algorithm operates within a multi-swarm framework, utilizing parallel computing for improved efficiency, incorporating knowledge-sharing mechanisms among swarms, and GPR-based Newton's optimization. It addresses the challenges of high-dimensional objective functions in power distribution systems, mainly focusing on the time-varying monthly load and PV generation curve variations. The Gaussian Probability Distribution technique estimates monthly load and PV generation curves across residential, commercial, and industrial sectors. The algorithm achieves significant reductions in AEL costs, ranging from 9 to 15% for the 33-bus network and 15 to 23% for the 69-bus network, demonstrating its effectiveness in reducing operational costs. Additionally, the algorithm's performance is evaluated on high-dimensional benchmark test functions, with comprehensive testing and statistical analysis confirming its superior performance. The chapter also provides a detailed analysis of the computational efficiency of various PSO variants, highlighting the trade-off between computation time and optimization quality. Although the Parallel-MS-GPRS-PSO algorithm requires longer computation times, it consistently delivers better optimization results, proving its effectiveness in solving high-dimensional problems. The method is highly adaptable to multi-dimensional optimization tasks, outperforming conventional PSO variants and other metaheuristic

approaches.

- In Chapter-5, a multi-objective optimization approach is presented to maximize PVHC and minimize energy losses in distribution networks simultaneously. The SPEA2-MO-GPRS-PSO algorithm is utilized for this optimization, utilizing the Pareto dominance principle to identify a set of non-dominated solutions. This method integrates SHCs and BESS in the distribution networks to provide active and reactive power compensation. The approach involves optimizing SHC VAr setpoints and BESS charging/discharging schedules in response to time-varying load demand and PV generation. The method achieves notable reductions in energy losses, approximately 81.58% for the 33-bus network and 62.32% for the 69-bus network, compared to base-case scenarios of 33-bus and 69-bus distribution networks, respectively. It also increases PVHC to 196.89% and 215.77% of the base-case peak load for the respective networks. The proposed method also demonstrates a 46.37% reduction in energy losses compared to the previous similar approach that provided only active power compensation through BESS-SHC. The results highlight the effectiveness of the proposed approach in optimizing the operations of both SHCs and BESS, achieving a trade-off between increasing PVHC and reducing energy losses.

- In Chapter-6, a multi-objective optimization approach is performed to determine the optimal placement of SEC and PV-SHC in distribution networks. The chapter briefly overviews the modeling for both SEC and PV-SHC. The primary goals of this optimization are to minimize power losses, the number of undervoltage nodes, and the total VA rating of compensators. The SPEA2-MO-GPRS-PSO algorithm addresses these objectives across three scenarios: minimizing power losses and compensator rating, minimizing power losses and undervoltage nodes, and minimizing all three objectives simultaneously. This method is validated on a 33-bus and 69-bus radial distribution network, where PV-SHCs are designed to provide both active and reactive

power compensation to reduce harmonic content in the line current. Meanwhile, the SEC mitigates voltage sags and swells through reactive power compensation. The optimization results demonstrate a significant reduction in power losses and the number of undervoltage nodes compared to the base-case network. Additionally, the chapter compares the proposed approach with previous similar work, noting a substantial decrease in network losses from 150.9 kW to 59.97 kW and a reduction in compensator rating from 6.077 MVA to 4.66 MVA. The results highlight notable improvements in network performance, including reduced power losses, lower compensator ratings, and the elimination of undervoltage nodes.

The major conclusions of the thesis are summarized as follows:

- Energy losses in PV-integrated distribution networks are significantly reduced through the optimal placement of SHCs for various levels of PV penetration. This results in a 30-35% reduction in energy losses compared to networks with PV systems alone.
- The results demonstrate that increasing the penetration of PV systems significantly reduces energy losses, with PV systems alone contributing to a 30-40% reduction in energy losses compared to scenarios without PV installations. Furthermore, the integration of SHCs with PV systems leads to a notable improvement in profitability, with an increase of 12-15% in profit over networks that only utilize PV systems.
- An operational optimization approach for SHCs minimizes the AEL costs in PV-integrated networks, particularly under time-varying load and PV generation conditions. This results in AEL cost reductions of 9-15% for the 33-bus network and 15-23% for the 69-bus network.
- A multi-objective planning approach, incorporating SPEA2-MO-GPRS-PSO, has been developed to simultaneously maximize PVHC and minimize energy losses in distribution networks. Additionally, the operational optimization of time-varying set-points for SHCs reactive power injection, as well as BESS charging and discharging,

results in significant reductions in energy losses—by 81.58% for the 33-bus network and 62.32% for the 69-bus network—compared to the base case.

- The optimal placement of SEC and multiple PV-SHC units simultaneously minimizes power losses, reduces the overall rating of compensators, and eliminates undervoltage nodes in the network. Specifically, the integration of PV-SHC units reduces network power losses by 53.16% and eliminates undervoltage nodes, decreasing their number from 6 to 0, through both real and reactive power compensation.

Numerous practical considerations can be integrated into the planning models. Future investigations should address the following aspects:

- **Development of planning approaches for unbalanced and mesh/ring distribution networks:** While the present study focuses on balanced radial distribution networks, future work can include unbalanced networks. Additionally, this study's methodologies and optimization techniques can be adapted for application in ring or meshed distribution networks. This adaptation necessitates developing and implementing advanced algorithms capable of managing the complexities of these diverse network configurations.

- **Coordinated control strategy for multiple SHCs and BESS units:** Multiple SHCs and BESS units are strategically placed throughout the network, necessitating a coordinated approach to adjust their internal settings and exchange VAR and charging/discharging data during fluctuations in load and generation. Chapters 4 and 5 provide a framework for determining variable VAR and charging/discharging set-points for SHCs and BESS units under varying load and generation conditions. However, specific control schemes for their inverters are not proposed. Therefore, there is a need for a coordinated control strategy to optimize SHC and BESS operations and achieve optimal objectives in distribution networks during time-varying

load and generation patterns. Specifically, in PV-integrated networks with BESS-SHC integration, a control scheme is essential to effectively coordinate the inverters of SHCs, PVs, and BESS units.

- **Incorporation of uncertainties in load and PV generation profiles:** The present research has focused on optimizing objective functions under time-varying load and PV generation profiles. Future efforts could involve developing techniques to predict uncertainties related to both load and PV generation patterns. This extension could utilize historical data and various forecasting methods to predict these uncertainties more effectively, necessitating further investigation.
- **Sensitivity analysis of SHCs to simulation parameters:** The operational effectiveness and performance of the proposed SHCs could potentially be affected by changes in simulation parameters. Thus, a thorough sensitivity analysis of SHCs to a wide range of simulation parameters is essential.

Bibliography

[1] IEA, "India energy outlook 2021," 2021 (https://www.iea.org/reports/india-energy-outlook-2021) (last access on January 2025).

[2] NITI, "Report on india renewable electricity roadmap 2030," 2015 (https://www.niti.gov.in/sites/default/files/2023-03/Report-onIndiaRenewableElectricityRoadmap2030.pdf) (last access on January 2025).

[3] MNRE, "National portal for rooftop solar," 2024 (https://pmsuryaghar.gov.in) (last access on January 2025).

[4] E. Hossain, M. R. Tür, S. Padmanaban, S. Ay, and I. Khan, "Analysis and mitigation of power quality issues in distributed generation systems using custom power devices," *IEEE Access*, vol. 6, pp. 16816–16833, 2018.

[5] A. M. Rauf and V. Khadkikar, "An enhanced voltage sag compensation scheme for dynamic voltage restorer," *IEEE Transactions on Industrial Electronics*, vol. 62, no. 5, pp. 2683–2692, 2015.

[6] R. T. Hock, Y. R. de Novaes, and A. L. Batschauer, "A voltage regulator for power quality improvement in low-voltage distribution grids," *IEEE Transactions on Power Electronics*, vol. 33, no. 3, pp. 2050–2060, 2018.

[7] B. Han, B. Bae, H. Kim, and S. Baek, "Combined operation of unified power-quality conditioner with distributed generation," *IEEE Transactions on Power Delivery*, vol. 21, no. 1, pp. 330–338, 2006.

[8] A. Patel, S. K. Yadav, H. D. Mathur, S. Bhanot, and R. C. Bansal, "Optimum sizing of pv based upqc-dg with improved power angle control," *Electric Power Systems Research*, vol. 182, p. 106259, 2020.

[9] G. M. Pelz, S. A. O. da Silva, and L. P. Sampaio, "Distributed generation integrating a photovoltaic-based system with a single- to three-phase upqc applied to rural or remote areas supplied by single-phase electrical power," *International Journal of Electrical Power & Energy Systems*, vol. 117, p. 105673, 2020.

[10] S. K. Khadem, M. Basu, and M. F. Conlon, "Intelligent islanding and seamless reconnection technique for microgrid with upqc," *IEEE Journal of Emerging and Selected Topics in Power Electronics*, vol. 3, no. 2, pp. 483–492, 2015.

[11] S. Chakraborty and M. G. Simoes, "Experimental evaluation of active filtering in a single-phase high-frequency ac microgrid," *IEEE Transactions on Energy Conversion*, vol. 24, no. 3, pp. 673–682, 2009.

[12] S. Poongothai and S. Srinath, "Power quality enhancement in solar power with grid connected system using upqc," *Microprocessors and Microsystems*, vol. 79, p. 103300, 2020.

[13] S. Lakshmi Kanthan Bharathi and S. Selvaperumal, "Mgwo-pi controller for enhanced power flow compensation using unified power quality conditioner in wind turbine squirrel cage induction generator," *Microprocessors and Microsystems*, vol. 76, p. 103080, 2020.

[14] P. G. Khorasani, M. Joorabian, and S. G. Seifossadat, "Smart grid realization with introducing unified power quality conditioner integrated with dc microgrid," *Electric Power Systems Research*, vol. 151, pp. 68–85, 2017.

[15] A. Ajami and M. Armaghan, "Fixed speed wind farm operation improvement using current-source converter based upqc," *Energy Conversion and Management*, vol. 58, pp. 10–18, 2012.

[16] K. Sarker, D. Chatterjee, and S. Goswami, "Grid integration of photovoltaic and wind based hybrid distributed generation system with low harmonic injection and power quality improvement using biogeography-based optimization," *Renewable Energy Focus*, vol. 22-23, pp. 38–56, 2017.

[17] B. S. Goud and B. L. Rao, "Power Quality Enhancement in Grid-Connected PV/Wind/Battery Using UPQC: Atom Search Optimization," *Journal of Electrical Engineering & Technology*, vol. 16, pp. 821–835, Mar. 2021.

[18] A. A. E. Fergany and H. M. Hasanien, "Single and multi-objective optimal power flow using grey wolf optimizer and differential evolution algorithms," *Electric Power Components and Systems*, vol. 43, no. 13, pp. 1548–1559, 2015.

[19] A. R. Reisi, M. H. Moradi, and H. Showkati, "Combined photovoltaic and unified power quality controller to improve power quality," *Solar Energy*, vol. 88, pp. 154–162, 2013.

[20] Y. Bouzelata, E. Kurt, R. Chenni, and N. Altın, "Design and simulation of a unified power quality conditioner fed by solar energy," *International Journal of Hydrogen Energy*, vol. 40, no. 44, pp. 15267–15277, 2015.

[21] K. Palanisamy, D. Kothari, M. K. Mishra, S. Meikandashivam, and I. Jacob Raglend, "Effective utilization of unified power quality conditioner for interconnecting pv mod-

ules with grid using power angle control method," *International Journal of Electrical Power & Energy Systems*, vol. 48, pp. 131–138, 2013.

[22] Y. Thangaraj and K. Ravi, "Multi-objective simultaneous placement of dg and dstatcom using novel lightning search algorithm," *Journal of Applied Research and Technology*, vol. 15, 2017.

[23] D. K R and K. Ravi, "Optimal size and siting of multiple dg and dstatcom in radial distribution system using bacterial foraging optimization algorithm," *Ain Shams Engineering Journal*, vol. 7, 2015.

[24] Y. Thangaraj and K. Ravi, "Multi-objective simultaneous dg and dstatcom allocation in radial distribution networks using cuckoo searching algorithm," *Alexandria Engineering Journal*, vol. 57, 2018.

[25] S. Lakshmi and S. Ganguly, "Multi-objective planning for the allocation of pv-bess integrated open upqc for peak load shaving of radial distribution networks," *Journal of Energy Storage*, vol. 22, pp. 208–218, 2019.

[26] M. Purlu and B. E. Turkay, "Optimal allocation of renewable distributed generations using heuristic methods to minimize annual energy losses and voltage deviation index," *IEEE Access*, vol. 10, pp. 21455–21474, 2022.

[27] A. Ahmed, M. F. N. Khan, I. Khan, H. Alquhayz, M. A. Khan, and A. T. Kiani, "A novel framework to determine the impact of time varying load models on wind dg planning," *IEEE Access*, vol. 9, pp. 11342–11357, 2021.

[28] S. Lakshmi and S. Ganguly, "Modelling and allocation of open-upqc-integrated pv generation system to improve the energy efficiency and power quality of radial distribution networks," *IET Renewable Power Generation*, vol. 12, no. 5, pp. 605–613, 2018.

[29] S. Lakshmi and S. Ganguly, "An on-line operational optimization approach for open unified power quality conditioner for energy loss minimization of distribution networks," *IEEE Transactions on Power Systems*, vol. 34, no. 6, pp. 4784–4795, 2019.

[30] H. A. Taha, M. H. Alham, and H. K. M. Youssef, "Multi-objective optimization for optimal allocation and coordination of wind and solar dgs, besss and capacitors in presence of demand response," *IEEE Access*, vol. 10, pp. 16225–16241, 2022.

[31] Y. Li, B. Feng, G. Li, J. Qi, D. Zhao, and Y. Mu, "Optimal distributed generation planning in active distribution networks considering integration of energy storage," *Applied Energy*, vol. 210, pp. 1073–1081, 2018.

[32] G. W. Chang, N. C. Chinh, and C. Sinatra, "Equilibrium optimizer-based approach of pv generation planning in a distribution system for maximizing hosting capacity," *IEEE Access*, vol. 10, pp. 118108–118122, 2022.

[33] E. Zulu, R. Hara, and H. Kita, "An efficient hybrid particle swarm and gradient descent method for the estimation of the hosting capacity of photovoltaics by distribution networks," *Energies*, vol. 16, no. 13, 2023.

[34] B. Khan, K. Redae, E. Gidey, O. P. Mahela, I. B. Taha, and M. G. Hussien, "Optimal integration of dstatcom using improved bacterial search algorithm for distribution network optimization," *Alexandria Engineering Journal*, vol. 61, no. 7, pp. 5539–5555, 2022.

[35] Y. Li, K. Li, Z. Yang, Y. Yu, R. Xu, and M. Yang, "Stochastic optimal scheduling of demand response-enabled microgrids with renewable generations: An analytical-heuristic approach," *Journal of Cleaner Production*, vol. 330, p. 129840, 2022.

[36] X. Xu, D. Niu, L. Peng, S. Zheng, and J. Qiu, "Hierarchical multi-objective optimal planning model of active distribution network considering distributed generation and

demand-side response," *Sustainable Energy Technologies and Assessments*, vol. 53, p. 102438, 2022.

[37] B. C. Sujatha, A. Usha, and R. S. Geetha, "Dynamic fuzzy learning based hybrid gwo-csa for optimal planning of pv, bess and dstatcom with network reconfiguration," *Discover Applied Sciences*, vol. 6, no. 2, 2024.

[38] T. Adefarati and R. Bansal, "Reliability, economic and environmental analysis of a microgrid system in the presence of renewable energy resources," *Applied Energy*, vol. 236, pp. 1089–1114, 2019.

[39] T. Yuvaraj, S. Arun, T. Suresh, and M. Thirumalai, "Minimizing the impact of electric vehicle charging station with distributed generation and distribution static synchronous compensator using psr index and spotted hyena optimizer algorithm on the radial distribution system," *e-Prime - Advances in Electrical Engineering, Electronics and Energy*, vol. 8, p. 100587, 2024.

[40] T. F. Agajie, B. Khan, J. M. Guerrero, and O. prakash Mahela, "Reliability enhancement and voltage profile improvement of distribution network using optimal capacity allocation and placement of distributed energy resources," *Computers & Electrical Engineering*, vol. 93, p. 107295, 2021.

[41] P. D. Huy, V. K. Ramachandaramurthy, J. Y. Yong, K. M. Tan, and J. B. Ekanayake, "Optimal placement, sizing and power factor of distributed generation: A comprehensive study spanning from the planning stage to the operation stage," *Energy*, vol. 195, p. 117011, 2020.

[42] R. Sanjay, T. Jayabarathi, T. Raghunathan, V. Ramesh, and N. Mithulananthan, "Optimal allocation of distributed generation using hybrid grey wolf optimizer," *IEEE Access*, vol. 5, pp. 14807–14818, 2017.

[43] E. Ali, S. Abd Elazim, and A. Abdelaziz, "Ant lion optimization algorithm for optimal location and sizing of renewable distributed generations," *Renewable Energy*, vol. 101, pp. 1311–1324, 2017.

[44] M. Khasanov, S. Kamel, C. Rahmann, H. M. Hasanien, and A. Al-Durra, "Optimal distributed generation and battery energy storage units integration in distribution systems considering power generation uncertainty," *IET Generation, Transmission & Distribution*, vol. 15, no. 24, pp. 3400–3422, 2021.

[45] B. S. Shravan Kumar Yadav and A. Prabhakaran, "Optimal placement of upqc in distribution network using hybrid approach," *Cybernetics and Systems*, vol. 54, no. 7, pp. 1014–1036, 2023.

[46] M. Amini and A. Jalilian, "Optimal sizing and location of open-upqc in distribution networks considering load growth," *International Journal of Electrical Power & Energy Systems*, vol. 130, 2021.

[47] M. Kandasamy, R. Thangavel, T. Arumugam, S. Kumaravel, S. Aruchamy, W.-W. Kim, and Z. W. Geem, "Strategic incorporation of dstatcom and distributed generations in balanced and unbalanced radial power distribution networks considering time varying loads," *Energy Reports*, vol. 9, pp. 4345–4359, 2023.

[48] A. Ali, M. F. Shaaban, and H. F. Sindi, "Optimal operational planning of res and hess in smart grids considering demand response and dstatcom functionality of the interfacing inverters," *Sustainability*, vol. 14, no. 20, 2022.

[49] Y. Li, J. Peng, H. Jia, B. Zou, B. Hao, T. Ma, and X. Wang, "Optimal battery schedule for grid-connected photovoltaic-battery systems of office buildings based on a dynamic programming algorithm," *Journal of Energy Storage*, vol. 50, p. 104557, 2022.

[50] E. S. Oda, A. M. A. E. Hamed, A. Ali, A. A. Elbaset, M. A. E. Sattar, and M. Ebeed, "Stochastic optimal planning of distribution system considering integrated photovoltaic-based dg and dstatcom under uncertainties of loads and solar irradiance," *IEEE Access*, vol. 9, pp. 26541–26555, 2021.

[51] C. M. Castiblanco-Pérez, D. E. Toro-Rodríguez, O. D. Montoya, and D. A. Giral-Ramírez, "Optimal placement and sizing of d-statcom in radial and meshed distribution networks using a discrete-continuous version of the genetic algorithm," *Electronics*, vol. 10, no. 12, 2021.

[52] J. Sanam, "Optimization of planning cost of radial distribution networks at different loads with the optimal placement of distribution statcom using differential evolution algorithm," *Soft Computing*, vol. 24, no. 17, pp. 13269–13284, 2020.

[53] M. Ebeed, M. Hashem, M. Aly, S. Kamel, F. Jurado, E. A. Mohamed, and A. M. Abd El Hamid, "Optimal integrating inverter-based pvs with inherent dstatcom functionality for reliability and security improvement at seasonal uncertainty," *Solar Energy*, vol. 267, p. 112200, 2024.

[54] M. I. Akbar, S. A. A. Kazmi, O. Alrumayh, Z. A. Khan, A. Altamimi, and M. M. Malik, "A novel hybrid optimization-based algorithm for the single and multi-objective achievement with optimal dg allocations in distribution networks," *IEEE Access*, vol. 10, pp. 25669–25687, 2022.

[55] A. Ebrahimnejad, M. Tavana, and V. Charles, "Analytics under uncertainty: a novel method for solving linear programming problems with trapezoidal fuzzy variables," *Soft Computing*, vol. 26, no. 1, pp. 327–347, 2022.

[56] R. R. Jha and A. Dubey, "Network-level optimization for unbalanced power distribution system: Approximation and relaxation," *IEEE Transactions on Power Systems*, vol. 36, no. 5, pp. 4126–4139, 2021.

[57] S. Pirouzi, M. A. Latify, and G. R. Yousefi, "Conjugate active and reactive power management in a smart distribution network through electric vehicles: A mixed integer-linear programming model," *Sustainable Energy, Grids and Networks*, vol. 22, p. 100344, 2020.

[58] H. Akulker and E. Aydin, "Optimal design and operation of a multi-energy microgrid using mixed-integer nonlinear programming: Impact of carbon cap and trade system and taxing on equipment selections," *Applied Energy*, vol. 330, p. 120313, 2023.

[59] T. Yang, Y. Guo, L. Deng, H. Sun, and W. Wu, "A linear branch flow model for radial distribution networks and its application to reactive power optimization and network reconfiguration," *IEEE Transactions on Smart Grid*, vol. 12, no. 3, pp. 2027–2036, 2021.

[60] C. Yang and X. Wang, "A steam injection distribution optimization method for sagd oil field using lstm and dynamic programming," *ISA Transactions*, vol. 110, pp. 198–212, 2021.

[61] K. M. Ang, W. H. Lim, N. A. M. Isa, S. S. Tiang, and C. H. Wong, "A constrained multi-swarm particle swarm optimization without velocity for constrained optimization problems," *Expert Systems with Applications*, vol. 140, p. 112882, 2020.

[62] Prashant, A. S. Siddiqui, M. Sarwar, A. Althobaiti, and S. S. M. Ghoneim, "Optimal location and sizing of distributed generators in power system network with power quality enhancement using fuzzy logic controlled d-statcom," *Sustainability*, vol. 14, no. 6, 2022.

[63] M. Najafi Ashtiani, A. Toopshekan, F. Razi Astaraei, H. Yousefi, and A. Maleki, "Techno-economic analysis of a grid-connected pv/battery system using the teaching-learning-based optimization algorithm," *Solar Energy*, vol. 203, pp. 69–82, 2020.

[64] V. F. Yu, H. Susanto, P. Jodiawan, T.-W. Ho, S.-W. Lin, and Y.-T. Huang, "A simulated annealing algorithm for the vehicle routing problem with parcel lockers," *IEEE Access*, vol. 10, pp. 20764–20782, 2022.

[65] A. Selim, S. Kamel, and F. Jurado, "Optimal allocation of distribution static compensators using a developed multi-objective sine cosine approach," *Computers & Electrical Engineering*, vol. 85, p. 106671, 2020.

[66] A. Selim, S. Kamel, and F. Jurado, "Efficient optimization technique for multiple dg allocation in distribution networks," *Applied Soft Computing*, vol. 86, p. 105938, 2020.

[67] Y. Lee, A. Resiga, S. Yi, and C. Wern, "The optimization of machining parameters for milling operations by using the nelder–mead simplex method," *Journal of Manufacturing and Materials Processing*, vol. 4, no. 3, 2020.

[68] G. Bonvin, S. Demassey, and A. Lodi, "Pump scheduling in drinking water distribution networks with an lp/nlp-based branch and bound," *Optimization and Engineering*, vol. 22, no. 3, pp. 1275–1313, 2021.

[69] D. Gong, Z. Zhang, Q. Shi, A. van den Hengel, C. Shen, and Y. Zhang, "Learning deep gradient descent optimization for image deconvolution," *IEEE Transactions on Neural Networks and Learning Systems*, vol. 31, no. 12, pp. 5468–5482, 2020.

[70] P. D. Khanh, B. S. Mordukhovich, V. T. Phat, and D. B. Tran, "Globally convergent coderivative-based generalized newton methods in nonsmooth optimization," *Mathematical Programming*, vol. 205, no. 1, pp. 373–429, 2024.

[71] Y. Tian, H. Chen, H. Ma, X. Zhang, K. C. Tan, and Y. Jin, "Integrating conjugate gradients into evolutionary algorithms for large-scale continuous multi-objective optimization," *IEEE/CAA Journal of Automatica Sinica*, vol. 9, no. 10, pp. 1801–1817, 2022.

[72] R. Shaikh, A. Stojcevski, M. Seyedmahmoudian, and J. Chandran, "A multi-objective approach for optimal sizing and placement of distributed generators and distribution static compensators in a distribution network using the black widow optimization algorithm," *Sustainability*, vol. 16, no. 11, 2024.

[73] S. Kumar, K. K. Mandal, and N. Chakraborty, "Optimal dg placement by multi-objective opposition based chaotic differential evolution for techno-economic analysis," *Applied Soft Computing*, vol. 78, pp. 70–83, 2019.

[74] M. Pesaran H.A., M. Nazari-Heris, B. Mohammadi-Ivatloo, and H. Seyedi, "A hybrid genetic particle swarm optimization for distributed generation allocation in power distribution networks," *Energy*, vol. 209, p. 118218, 2020.

[75] K. Govindan, F. Salehian, H. Kian, S. T. Hosseini, and H. Mina, "A location-inventory-routing problem to design a circular closed-loop supply chain network with carbon tax policy for achieving circular economy: An augmented epsilon-constraint approach," *International Journal of Production Economics*, vol. 257, p. 108771, 2023.

[76] S. Roy Ghatak, S. Sannigrahi, and P. Acharjee, "Multi-objective approach for strategic incorporation of solar energy source, battery storage system, and dstatcom in a smart grid environment," *IEEE Systems Journal*, vol. 13, no. 3, pp. 3038–3049, 2019.

[77] I. Ben Hamida, S. B. Salah, F. Msahli, and M. F. Mimouni, "Optimal network reconfiguration and renewable dg integration considering time sequence variation in load and dgs," *Renewable Energy*, vol. 121, pp. 66–80, 2018.

[78] S. Lakshmi and S. Ganguly, "Simultaneous optimisation of photovoltaic hosting capacity and energy loss of radial distribution networks with open unified power quality conditioner allocation," *IET Renewable Power Generation*, vol. 12, no. 12, pp. 1382–1389, 2018.

[79] V. Vita, "Development of a decision-making algorithm for the optimum size and placement of distributed generation units in distribution networks," *Energies*, vol. 10, no. 9, 2017.

[80] M. Dalawir, M. Azzouz, and A. Azab, "Optimal allocation of wind-based distributed generators and statcoms using a hierarchical stochastic programming approach," *Electric Power Systems Research*, vol. 237, p. 110960, 2024.

[81] A. Nieto, V. Vita, and T. I. Maris, "Power quality improvement in power grids with the integration of energy storage systems," *International Journal of Engineering and Technical Research*, vol. 5, pp. 438–443, 07 2016.

[82] W. E. K. Almoataz Y. Abdelaziz, Yasser G. Hegazy and M. M. Othman, "A multi-objective optimization for sizing and placement of voltage-controlled distributed generation using supervised big bang–big crunch method," *Electric Power Components and Systems*, vol. 43, no. 1, pp. 105–117, 2015.

[83] T. Aziz and N. Ketjoy, "Pv penetration limits in low voltage networks and voltage variations," *IEEE Access*, vol. 5, pp. 16784–16792, 2017.

[84] R. Torquato, D. Salles, C. Oriente Pereira, P. C. M. Meira, and W. Freitas, "A comprehensive assessment of pv hosting capacity on low-voltage distribution systems," *IEEE Transactions on Power Delivery*, vol. 33, no. 2, pp. 1002–1012, 2018.

[85] T. Stetz, F. Marten, and M. Braun, "Improved low voltage grid-integration of photovoltaic systems in germany," *IEEE Transactions on Sustainable Energy*, vol. 4, no. 2, pp. 534–542, 2013.

[86] S. Lakshmi and S. Ganguly, "Modelling and allocation planning of voltage-sourced converters to improve the rooftop pv hosting capacity and energy efficiency of distribution networks," *IET Generation, Transmission & Distribution*, vol. 12, 09 2018.

[87] D. Kaliaperumal Rukmani, Y. Thangaraj, U. Subramaniam, S. Ramachandran, R. Madurai Elavarasan, N. Das, L. Baringo, and M. Imran Abdul Rasheed, "A new approach to optimal location and sizing of dstatcom in radial distribution networks using bio-inspired cuckoo search algorithm," *Energies*, vol. 13, no. 18, 2020.

[88] F. Iqbal, M. T. Khan, and A. S. Siddiqui, "Optimal placement of dg and dstatcom for loss reduction and voltage profile improvement," *Alexandria Engineering Journal*, vol. 57, no. 2, pp. 755–765, 2018.

[89] G. Isha and P. Jagatheeswari, "Optimal allocation of dstatcom and pv array in distribution system employing fuzzy-lightning search algorithm," *Automatika*, vol. 62, pp. 339–352, 10 2021.

[90] S. Ganguly and D. Samajpati, "Distributed generation allocation on radial distribution networks under uncertainties of load and generation using genetic algorithm," *IEEE Transactions on Sustainable Energy*, vol. 6, no. 3, pp. 688–697, 2015.

[91] A. Noori, Y. Zhang, N. Nouri, and M. Hajivand, "Multi-objective optimal placement and sizing of distribution static compensator in radial distribution networks with variable residential, commercial and industrial demands considering reliability," *IEEE Access*, vol. 9, pp. 46911–46926, 2021.

[92] A. Gupta and A. Kumar, "Optimal placement of d-statcom using sensitivity approaches in mesh distribution system with time variant load models under load growth," *Ain Shams Engineering Journal*, vol. 9, 2016.

[93] H. S. Elnaz Shahryari and M. Moradzadeh, "Probabilistic and multi-objective placement of d-statcom in distribution systems considering load uncertainty," *Electric Power Components and Systems*, vol. 46, no. 1, pp. 27–42, 2018.

[94] S. Ghosh and D. Das, "Method of load flow solution of radial distribution network," *Generation, Transmission and Distribution, IEE Proceedings-*, vol. 146, pp. 641 – 648, 12 1999.

[95] J. A. M. Rupa and S. Ganesh, "Power flow analysis for radial distribution system using backward/forward sweep method," *International Journal of Electrical and Computer Engineering*, vol. 8, pp. 1621–1625, 2015.

[96] R. Poli, J. Kennedy, and T. M. Blackwell, "Particle swarm optimization," *Swarm Intelligence*, vol. 1, pp. 33–57, 1995.

[97] Y. Shi and R. C. Eberhart, "A modified particle swarm optimizer," *1998 IEEE International Conference on Evolutionary Computation Proceedings. IEEE World Congress on Computational Intelligence*, pp. 69–73, 1998.

[98] M. Baran and F. Wu, "Network reconfiguration in distribution systems for loss reduction and load balancing," *IEEE Transactions on Power Delivery*, vol. 4, no. 2, pp. 1401–1407, 1989.

[99] J. S. Savier and D. Das, "Impact of network reconfiguration on loss allocation of radial distribution systems," *IEEE Transactions on Power Delivery*, vol. 22, no. 4, pp. 2473–2480, 2007.

[100] A. Dutta, S. Ganguly, and C. Kumar, "Mpc-based coordinated voltage control in active distribution networks incorporating cvr and dr," *IEEE Transactions on Industry Applications*, vol. 58, no. 4, pp. 4309–4318, 2022.

[101] D. B. Prakash and C. R. Lakshminarayana, "Multiple dg placements in distribution system for power loss reduction using pso algorithm," *Procedia Technology*, vol. 25, pp. 785–792, 2016.

[102] S. Wang, S. Chen, L. Ge, and L. Wu, "Distributed generation hosting capacity evaluation for distribution systems considering the robust optimal operation of oltc and svc," *IEEE Transactions on Sustainable Energy*, vol. 7, no. 3, pp. 1111–1123, 2016.

[103] N. Kanwar, N. Gupta, K. Niazi, and A. Swarnkar, "Improved cat swarm optimization for simultaneous allocation of dstatcom and dgs in distribution systems," *Journal of Renewable Energy*, pp. 1–10, 2015.

[104] S. Devi and M. Geethanjali, "Optimal location and sizing determination of distributed generation and dstatcom using particle swarm optimization algorithm," *International Journal of Electrical Power & Energy Systems*, vol. 62, pp. 562–570, 2014.

[105] A. Noori, Y. Zhang, N. Nouri, and M. Hajivand, "Hybrid allocation of capacitor and distributed static compensator in radial distribution networks using multi-objective improved golden ratio optimization based on fuzzy decision making," *IEEE Access*, vol. 8, pp. 162180–162195, 2020.

[106] R. Panigrahi, S. K. Mishra, S. C. Srivastava, A. K. Srivastava, and N. N. Schulz, "Grid integration of small-scale photovoltaic systems in secondary distribution network—a review," *IEEE Transactions on Industry Applications*, vol. 56, no. 3, pp. 3178–3195, 2020.

[107] M. Karimi, H. Mokhlis, K. Naidu, S. Uddin, and A. Bakar, "Photovoltaic penetration issues and impacts in distribution network – a review," *Renewable and Sustainable Energy Reviews*, vol. 53, pp. 594–605, 2016.

[108] S. Sakar, M. E. Balci, S. H. Abdel Aleem, and A. F. Zobaa, "Increasing pv hosting capacity in distorted distribution systems using passive harmonic filtering," *Electric Power Systems Research*, vol. 148, pp. 74–86, 2017.

[109] I. R. de Parijos Junior, M. A. B. Galhardo, T. O. Costa, J. T. Pinho, S. Williamson, and W. N. Macêdo, "Influence of photovoltaic microgeneration on the demand profile

and its effects on the grid power quality," *Electric Power Systems Research*, vol. 214, p. 108935, 2023.

[110] T. Yuvaraj, K. Devabalaji, and K. Ravi, "Optimal placement and sizing of dstatcom using harmony search algorithm," *Energy Procedia*, vol. 79, pp. 759–765, 2015.

[111] A. R. Gupta and A. Kumar, "Impact of various load models on d-statcom allocation in dno operated distribution network," *Procedia Computer Science*, vol. 125, pp. 862–870, 2018.

[112] A. M. Shaheen, R. A. El Sehiemy, A. Ginidi, A. M. Elsayed, and S. F. Al-Gahtani, "Optimal allocation of pv-statcom devices in distribution systems for energy losses minimization and voltage profile improvement via hunter-prey-based algorithm," *Energies*, vol. 16, no. 6, 2023.

[113] M. Kashem, A. Le, M. Negnevitsky, and G. Ledwich, "Distributed generation for minimization of power losses in distribution systems," in *2006 IEEE Power Engineering Society General Meeting*, 2006.

[114] M. Mohammadi, S. Hosseinian, and G. Gharehpetian, "Ga-based optimal sizing of microgrid and dg units under pool and hybrid electricity markets," *International Journal of Electrical Power & Energy Systems*, vol. 35, no. 1, pp. 83–92, 2012.

[115] M. A. Darfoun and M. E. E. Hawary, "Multi-objective optimization approach for optimal distributed generation sizing and placement," *Electric Power Components and Systems*, vol. 43, no. 7, pp. 828–836, 2015.

[116] R. Singh and S. Goswami, "Optimum allocation of distributed generations based on nodal pricing for profit, loss reduction, and voltage improvement including voltage rise issue," *International Journal of Electrical Power & Energy Systems*, vol. 32, no. 6, pp. 637–644, 2010.

[117] M. Zellagui, A. Lasmari, S. Settoul, R. A. El Sehiemy, C. Z. El Bayeh, and R. Chenni, "Simultaneous allocation of photovoltaic dg and dstatcom for techno-economic and environmental benefits in electrical distribution systems at different loading conditions using novel hybrid optimization algorithms," *International Transactions on Electrical Energy Systems*, vol. 31, no. 8, p. e12992, 2021.

[118] J. Sanam, S. Ganguly, A. Panda, and C. Hemanth, "Optimization of energy loss cost of distribution networks with the optimal placement and sizing of dstatcom using differential evolution algorithm," *Arabian Journal for Science and Engineering*, vol. 42, pp. 2851–2865, 07 2017.

[119] A. Amin, M. Ebeed, L. Nasrat, M. Aly, E. M. Ahmed, E. A. Mohamed, H. H. Alnuman, and A. M. Abd El Hamed, "Techno-economic evaluation of optimal integration of pv based dg with dstatcom functionality with solar irradiance and loading variations," *Mathematics*, vol. 10, no. 14, 2022.

[120] IRENA, "Renewable power generation costs in 2021," 2022 (https://www.irena.org/publications/2022/Jul/Renewable-Power-Generation-Costs-in-2021) (last access on September 2024).

[121] N. Khalesi, N. Rezaei, and M. R. Haghifam, "Dg allocation with application of dynamic programming for loss reduction and reliability improvement," *International Journal of Electrical Power & Energy Systems*, vol. 33, no. 2, pp. 288–295, 2011.

[122] S. C. Hsieh, "Economic evaluation of the hybrid enhancing scheme with dstatcom and active power curtailment for pv penetration in taipower distribution systems," *IEEE Transactions on Industry Applications*, vol. 51, no. 3, pp. 1953–1961, 2015.

[123] S. Biswas, S. Goswami, and A. Chatterjee, "Optimal distributed generation placement in shunt capacitor compensated distribution systems considering voltage sag

and harmonics distortions," *Generation, Transmission & Distribution, IET*, vol. 8, pp. 783–797, 05 2014.

[124] H. HassanzadehFard and A. Jalilian, "Optimal sizing and location of renewable energy based dg units in distribution systems considering load growth," *International Journal of Electrical Power & Energy Systems*, vol. 101, pp. 356–370, 2018.

[125] S. Roy Ghatak, S. Sannigrahi, and P. Acharjee, "Comparative performance analysis of dg and dstatcom using improved pso based on success rate for deregulated environment," *IEEE Systems Journal*, vol. 12, no. 3, pp. 2791–2802, 2018.

[126] S. Kansal, B. Tyagi, and V. Kumar, "Cost–benefit analysis for optimal distributed generation placement in distribution systems," *International Journal of Ambient Energy*, vol. 38, no. 1, pp. 45–54, 2017.

[127] Y. Jin, H. Wang, T. Chugh, D. Guo, and K. Miettinen, "Data-driven evolutionary optimization: An overview and case studies," *IEEE Transactions on Evolutionary Computation*, vol. 23, no. 3, pp. 442–458, 2019.

[128] Y. Cui, Z. Geng, Q. Zhu, and Y. Han, "Review: Multi-objective optimization methods and application in energy saving," *Energy*, vol. 125, pp. 681–704, 2017.

[129] A. Keane, L. F. Ochoa, C. L. T. Borges, G. W. Ault, A. D. Alarcon-Rodriguez, R. A. F. Currie, F. Pilo, C. Dent, and G. P. Harrison, "State-of-the-art techniques and challenges ahead for distributed generation planning and optimization," *IEEE Transactions on Power Systems*, vol. 28, no. 2, pp. 1493–1502, 2013.

[130] M. Thirunavukkarasu, Y. Sawle, and H. Lala, "A comprehensive review on optimization of hybrid renewable energy systems using various optimization techniques," *Renewable and Sustainable Energy Reviews*, vol. 176, p. 113192, 2023.

[131] R. Chaurasia, S. Gairola, and Y. Pal, "Optimal planning and performance estimation of renewable energy model for isolated hilly indian area," *Energy Systems*, vol. 14, pp. 357–390, May 2023.

[132] A. M. Shaheen, R. A. El Sehiemy, A. Ginidi, A. M. Elsayed, and S. F. Al-Gahtani, "Optimal allocation of pv-statcom devices in distribution systems for energy losses minimization and voltage profile improvement via hunter-prey-based algorithm," *Energies*, vol. 16, no. 6, 2023.

[133] S. Choudhury, G. T. Varghese, S. Mohanty, V. R. Kolluru, M. Bajaj, V. Blazek, L. Prokop, and S. Misak, "Energy management and power quality improvement of microgrid system through modified water wave optimization," *Energy Reports*, vol. 9, pp. 6020–6041, 2023.

[134] H. P. C, K. Subbaramaiah, and P. Sujatha, "Optimal dg unit placement in distribution networks by multi-objective whale optimization algorithm & its techno-economic analysis," *Electric Power Systems Research*, vol. 214, p. 108869, 2023.

[135] R. Veramalla, S. R. Arya, V. Gundeboina, B. Jampana, R. Chilipi, and S. Madasthu, "Meta-heuristics algorithms for optimization of gains for dynamic voltage restorers to improve power quality and dynamics," *Optimal Control Applications and Methods*, vol. 44, no. 2, pp. 1006–1025, 2022.

[136] A. Khare and S. Rangnekar, "A review of particle swarm optimization and its applications in solar photovoltaic system," *Applied Soft Computing*, vol. 13, no. 5, pp. 2997–3006, 2013.

[137] M. M'dioud, R. Bannari, and I. Elkafazi, "A novel pso algorithm for dg insertion problem," *Energy Systems*, vol. 15, no. 1, pp. 325–351, 2024.

[138] M. Pushkarna, H. Ashfaq, R. Singh, and R. Kumar, "An optimal placement and sizing of type-iv dg with reactive power support using upqc in an unbalanced distribution

system using particle swarm optimization," *Energy Systems*, vol. 15, no. 1, pp. 353–370, 2024.

[139] Y. Lu, B. Li, S. Liu, and A. Zhou, "A population cooperation based particle swarm optimization algorithm for large-scale multi-objective optimization," *Swarm and Evolutionary Computation*, vol. 83, p. 101377, 2023.

[140] H. Garg, "A hybrid pso-ga algorithm for constrained optimization problems," *Applied Mathematics and Computation*, vol. 274, pp. 292–305, 2016.

[141] Y. Song, Y. Liu, H. Chen, and W. Deng, "A multi-strategy adaptive particle swarm optimization algorithm for solving optimization problem," *Electronics*, vol. 12, no. 3, 2023.

[142] K. Meng, H. G. Wang, Z. Dong, and K. P. Wong, "Quantum-inspired particle swarm optimization for valve-point economic load dispatch," *IEEE Transactions on Power Systems*, vol. 25, no. 1, pp. 215–222, 2010.

[143] X. Zhang, X. Wang, Q. Kang, and J. Cheng, "Differential mutation and novel social learning particle swarm optimization algorithm," *Information Sciences*, vol. 480, pp. 109–129, 2019.

[144] A. Madani, A. Engelbrecht, and B. Ombuki-Berman, "Cooperative coevolutionary multi-guide particle swarm optimization algorithm for large-scale multi-objective optimization problems," *Swarm and Evolutionary Computation*, vol. 78, p. 101262, 2023.

[145] Q. Qin, S. Cheng, Q. Zhang, L. Li, and Y. Shi, "Particle swarm optimization with interswarm interactive learning strategy," *IEEE Transactions on Cybernetics*, vol. 46, no. 10, pp. 2238–2251, 2016.

[146] Z. Lv, D. Niu, S. Li, and H. Sun, "Multi-surrogate assisted pso with adaptive speciation for expensive multimodal multi-objective optimization," *Applied Soft Computing*, vol. 147, p. 110724, 2023.

[147] S. C. Chu, X. Yuan, J. S. Pan, B. S. Lin, and Z. J. Lee, "A multi-strategy surrogate-assisted social learning particle swarm optimization for expensive optimization and applications," *Applied Soft Computing*, vol. 162, p. 111876, 2024.

[148] D. Luo, J. Huang, G. Su, and H. Tao, "A dynamic gaussian process surrogate model-assisted particle swarm optimisation algorithm for expensive structural optimisation problems," *European Journal of Environmental and Civil Engineering*, vol. 27, no. 1, pp. 416–436, 2023.

[149] B. H. Nguyen, B. Xue, and M. Zhang, "A constrained competitive swarm optimiser with an svm-based surrogate model for feature selection," *IEEE Transactions on Evolutionary Computation*, pp. 1–1, 2022.

[150] H. Carreon-Ortiz, F. Valdez, and O. Castillo, "Comparative study of type-1 and interval type-2 fuzzy logic systems in parameter adaptation for the fuzzy discrete mycorrhiza optimization algorithm," *Mathematics*, vol. 11, no. 11, 2023.

[151] J. Kim, S. Lee, and H. Jang, "Lessons from residential electricity demand analysis on the time of use pricing experiment in south korea," *Energy Economics*, vol. 113, p. 106224, 2022.

[152] M. A. Arasomwan and A. O. Adewumi, "On the performance of linear decreasing inertia weight particle swarm optimization for global optimization," *The Scientific World Journal*, vol. 2013, 2013.

[153] J. Zhang and X. Ding, "A multi-swarm self-adaptive and cooperative particle swarm optimization," *Engineering Applications of Artificial Intelligence*, vol. 24, no. 6, pp. 958–967, 2011.

[154] C. Sun, Y. Jin, R. Cheng, J. Ding, and J. Zeng, "Surrogate-assisted cooperative swarm optimization of high-dimensional expensive problems," *IEEE Transactions on Evolutionary Computation*, vol. 21, no. 4, pp. 644–660, 2017.

[155] J. Tian, Y. Tan, J. Zeng, C. Sun, and Y. Jin, "Multiobjective infill criterion driven gaussian process-assisted particle swarm optimization of high-dimensional expensive problems," *IEEE Transactions on Evolutionary Computation*, vol. 23, no. 3, pp. 459–472, 2019.

[156] J. Tian, M. Hou, H. Bian, and J. Li, "Variable surrogate model-based particle swarm optimization for high-dimensional expensive problems," *Complex & Intelligent Systems*, vol. 9, pp. 3887–3935, Aug 2023.

[157] M. Yu, J. Liang, K. Zhao, and Z. Wu, "An arbf surrogate-assisted neighborhood field optimizer for expensive problems," *Swarm and Evolutionary Computation*, vol. 68, p. 100972, 2022.

[158] H. Chen, W. Li, and W. Cui, "Surrogate-assisted evolutionary algorithm with hierarchical surrogate technique and adaptive infill strategy," *Expert Systems with Applications*, vol. 232, p. 120826, 2023.

[159] J. Kůdela and R. Matousek, "Combining lipschitz and rbf surrogate models for high-dimensional computationally expensive problems," *Information Sciences*, vol. 619, pp. 457–477, 2023.

[160] M. Shafiullah, S. D. Ahmed, and F. A. Al-Sulaiman, "Grid integration challenges and solution strategies for solar pv systems: A review," *IEEE Access*, vol. 10, pp. 52233–52257, 2022.

[161] G. Notton, M. L. Nivet, C. Voyant, C. Paoli, C. Darras, F. Motte, and A. Fouilloy, "Intermittent and stochastic character of renewable energy sources: Consequences,

cost of intermittence and benefit of forecasting," *Renewable and Sustainable Energy Reviews*, vol. 87, pp. 96–105, 2018.

[162] S. M. Ismael, S. H. Abdel Aleem, A. Y. Abdelaziz, and A. F. Zobaa, "State-of-the-art of hosting capacity in modern power systems with distributed generation," *Renewable Energy*, vol. 130, pp. 1002–1020, 2019.

[163] Z. M. Zenhom, S. H. E. A. Aleem, A. F. Zobaa, and T. A. Boghdady, "A comprehensive review of renewables and electric vehicles hosting capacity in active distribution networks," *IEEE Access*, vol. 12, pp. 3672–3699, 2024.

[164] B. Ahmadi, O. Ceylan, and A. Ozdemir, "Reinforcement of the distribution grids to improve the hosting capacity of distributed generation: Multi-objective framework," *Electric Power Systems Research*, vol. 217, p. 109120, 2023.

[165] F. Capitanescu, L. F. Ochoa, H. Margossian, and N. D. Hatziargyriou, "Assessing the potential of network reconfiguration to improve distributed generation hosting capacity in active distribution systems," *IEEE Transactions on Power Systems*, vol. 30, no. 1, pp. 346–356, 2015.

[166] X. Xu, Z. Xu, X. Lyu, and J. Li, "Optimal svc placement for maximizing photovoltaic hosting capacity in distribution network," *IFAC-PapersOnLine*, vol. 51, no. 28, pp. 356–361, 2018.

[167] T. Gush, C.-H. Kim, S. Admasie, J.-S. Kim, and J.-S. Song, "Optimal smart inverter control for pv and bess to improve pv hosting capacity of distribution networks using slime mould algorithm," *IEEE Access*, vol. 9, pp. 52164–52176, 2021.

[168] S. S. AlKaabi, V. Khadkikar, and H. H. Zeineldin, "Incorporating pv inverter control schemes for planning active distribution networks," *IEEE Transactions on Sustainable Energy*, vol. 6, no. 4, pp. 1224–1233, 2015.

[169] A. Escalera, M. Prodanovic, E. D. Castronuovo, and J. Roldan-Perez, "Contribution of active management technologies to the reliability of power distribution networks," *Applied Energy*, vol. 267, p. 114919, 2020.

[170] M. Taghavi, H. Delkhosh, M. Moghaddam, and A. Sheikhi, "Hosting capacity enhancement of hybrid ac/dc distribution network based on static and dynamic reconfiguration," *IET Generation, Transmission & Distribution*, vol. 17, no. 17, pp. 3765–3780, 2023.

[171] R. Torquato, D. Salles, C. Oriente Pereira, P. C. M. Meira, and W. Freitas, "A comprehensive assessment of pv hosting capacity on low-voltage distribution systems," *IEEE Transactions on Power Delivery*, vol. 33, no. 2, pp. 1002–1012, 2018.

[172] S. Ganguly and S. Lakshmi, "Simultaneous optimization of photovoltaic hosting capacity and energy loss of radial distribution networks with open unified power quality conditioner allocation," *IET Renewable Power Generation*, vol. 12, 07 2018.

[173] S. Lakshmi and S. Ganguly, "Modelling and allocation planning of voltage-sourced converters to improve the rooftop pv hosting capacity and energy efficiency of distribution networks," *IET Generation, Transmission & Distribution*, vol. 12, 09 2018.

[174] J. Xiao, Y. Li, X. Qiao, Y. Tan, Y. Cao, and L. Jiang, "Enhancing hosting capacity of uncertain and correlated wind power in distribution network with anm strategies," *IEEE Access*, vol. 8, pp. 189115–189128, 2020.

[175] A. Rabiee and S. M. Mohseni-Bonab, "Maximizing hosting capacity of renewable energy sources in distribution networks: A multi-objective and scenario-based approach," *Energy*, vol. 120, pp. 417–430, 2017.

[176] F. Ding and B. Mather, "On distributed pv hosting capacity estimation, sensitivity study, and improvement," *IEEE Transactions on Sustainable Energy*, vol. 8, no. 3, pp. 1010–1020, 2017.

[177] T. S. Ustun, J. Hashimoto, and K. Otani, "Impact of smart inverters on feeder hosting capacity of distribution networks," *IEEE Access*, vol. 7, pp. 163526–163536, 2019.

[178] A. S. Abbas, A. A. A. El Ela, R. A. El Sehiemy, and K. K. Fetyan, "Assessment and enhancement of uncertain renewable energy hosting capacity with/out voltage control devices in distribution grids," *IEEE Systems Journal*, vol. 17, no. 2, pp. 1986–1994, 2023.

[179] F. Peprah, S. Gyamfi, M. Amo-Boateng, and E. Effah-Donyina, "Impact assessment of grid tied rooftop pv systems on lv distribution network," *Scientific African*, vol. 16, p. e01172, 2022.

[180] Z. Sherinov and A. Unveren, "Multi-objective imperialistic competitive algorithm with multiple non-dominated sets for the solution of global optimization problems," *Soft Computing*, vol. 22, pp. 8273–8288, December 2018.

[181] R. H. Stewart, T. S. Palmer, and B. DuPont, "A survey of multi-objective optimization methods and their applications for nuclear scientists and engineers," *Progress in Nuclear Energy*, vol. 138, p. 103830, 2021.

[182] S. Zhu, L. Xu, E. D. Goodman, and Z. Lu, "A new many-objective evolutionary algorithm based on generalized pareto dominance," *IEEE Transactions on Cybernetics*, vol. 52, no. 8, pp. 7776–7790, 2022.

[183] S. Ganguly, "Multi-objective planning for reactive power compensation of radial distribution networks with unified power quality conditioner allocation using particle swarm optimization," *IEEE Transactions on Power Systems*, vol. 29, no. 4, pp. 1801–1810, 2014.

[184] S. Lakshmi and S. Ganguly, "Coordinated operational optimization approach for pv inverters and besss to minimize the energy loss of distribution networks," *IEEE Systems Journal*, vol. 16, no. 1, pp. 1228–1238, 2022.

[185] J. McDowell, R. Walling, W. Peter, E. Von Engeln, E. Seymour, R. Nelson, L. Casey, A. Ellis, and C. Barker, "Reactive power interconnection requirements for pv and wind plants : recommendations to nerc," 2012.

[186] M. Cohen and D. Callaway, "Effects of distributed pv generation on california's distribution system, part 1: Engineering simulations," *Solar Energy*, vol. 128, pp. 126–138, 2016. Special issue: Progress in Solar Energy.

[187] V. Khadkikar, "Enhancing electric power quality using upqc: A comprehensive overview," *IEEE Transactions on Power Electronics*, vol. 27, no. 5, pp. 2284–2297, 2012.

[188] S. Devassy and B. Singh, "Performance analysis of solar pv array and battery integrated unified power quality conditioner for microgrid systems," *IEEE Transactions on Industrial Electronics*, vol. 68, no. 5, pp. 4027–4035, 2021.

[189] R. H. Yang and J. X. Jin, "Unified power quality conditioner with advanced dual control for performance improvement of dfig-based wind farm," *IEEE Transactions on Sustainable Energy*, vol. 12, no. 1, pp. 116–126, 2021.

[190] J. Yu, Y. Xu, Y. Li, and Q. Liu, "An inductive hybrid upqc for power quality management in premium-power-supply-required applications," *IEEE Access*, vol. 8, pp. 113342–113354, 2020.

[191] T. Yuvaraj, K. Devabalaji, and K. Ravi, "Optimal placement and sizing of dstatcom using harmony search algorithm," *Energy Procedia*, vol. 79, pp. 759–765, 2015.

[192] A. Amin, M. Ebeed, L. Nasrat, M. Aly, E. M. Ahmed, E. A. Mohamed, H. H. Alnuman, and A. M. Abd El Hamed, "Techno-economic evaluation of optimal integration of pv based dg with dstatcom functionality with solar irradiance and loading variations," *Mathematics*, vol. 10, no. 14, 2022.

[193] M. Brenna, R. Faranda, and E. Tironi, "A new proposal for power quality and custom power improvement: Open upqc," *IEEE Transactions on Power Delivery*, vol. 24, no. 4, pp. 2107–2116, 2009.

[194] H. Hafezi, G. D'Antona, A. Dedè, D. Della Giustina, R. Faranda, and G. Massa, "Power quality conditioning in lv distribution networks: Results by field demonstration," *IEEE Transactions on Smart Grid*, vol. 8, no. 1, pp. 418–427, 2017.

[195] A. Teke, M. E. Meral, M. U. Cuma, M. Tumay, and K. C. Bayindir, "Open unified power quality conditioner with control based on enhanced phase locked loop," *IET Generation, Transmission & Distribution*, vol. 7, no. 3, pp. 254–264, 2013.

[196] M. Amini and A. Jalilian, "Modelling and improvement of open-upqc performance in voltage sag compensation by contribution of shunt units," *Electric Power Systems Research*, vol. 187, 07 2020.

[197] A. Mousa, M. E. Shorbagy, and W. A. E. Wahed, "Local search based hybrid particle swarm optimization algorithm for multiobjective optimization," *Swarm and Evolutionary Computation*, vol. 3, pp. 1–14, 2012.

[198] M. V. Patil and A. J. Kulkarni, "Pareto dominance based multiobjective cohort intelligence algorithm," *Information Sciences*, vol. 538, pp. 69–118, 2020.

[199] S. Ganguly, "Impact of unified power-quality conditioner allocation on line loading, losses, and voltage stability of radial distribution systems," *IEEE Transactions on Power Delivery*, vol. 29, no. 4, pp. 1859–1867, 2014.

Appendix A

This Appendix provides a comprehensive collection of simulation data for all the test networks examined, including bus data, line data, base MVA, base kV, and other relevant parameters. The bus data outlines the active and reactive power demands at each bus within the network, while the line data details the connections between buses, including the resistance and reactance of the network's lines.

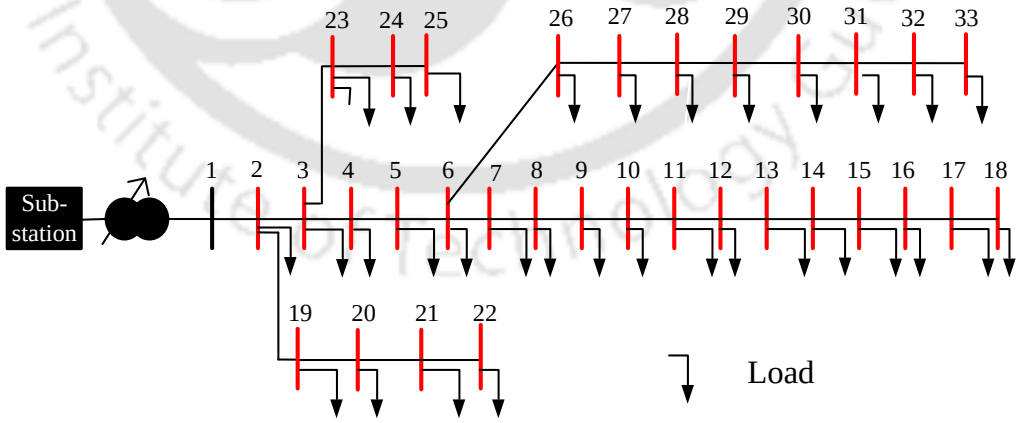

Fig. A.1: 33-bus distribution network

Table A.1: Load data and Line data of the 33-bus distribution network

Load Data			Line Data				
Bus No.	**Active Power (kW)**	**Reactive Power (kVAr)**	**Branch No.**	**From Bus**	**To Bus**	**Resistance (Ω)**	**Reactance (Ω)**
1	0	0	1	1	2	0.0922	0.0470
2	100	60	2	2	3	0.4930	0.2511
3	90	40	3	3	4	0.3660	0.1864
4	120	80	4	4	5	0.3811	0.1941
5	60	30	5	5	6	0.8190	0.7070
6	60	20	6	6	7	0.1872	0.6188
7	200	100	7	7	8	0.7114	0.2351
8	200	100	8	8	9	1.0300	0.7400
9	60	20	9	9	10	1.0440	0.7400
10	60	20	10	10	11	0.1966	0.0650
11	45	30	11	11	12	0.3744	0.1238
12	60	35	12	12	13	1.4680	1.1550
13	60	35	13	13	14	0.5416	0.7129
14	120	80	14	14	15	0.5910	0.5260
15	60	10	15	15	16	0.7463	0.5450
16	60	20	16	16	17	1.2890	1.7210
17	60	20	17	17	18	0.7320	0.5740
18	90	40	18	2	19	0.1640	0.1565
19	90	40	19	19	20	1.5042	1.3554
20	90	40	20	20	21	0.4095	0.4784
21	90	40	21	21	22	0.7089	0.9373
22	90	40	22	3	23	0.4512	0.3083
23	90	50	23	23	24	0.8980	0.7091
24	420	200	24	24	25	0.8960	0.7011
25	420	200	25	6	26	0.2030	0.1034
26	60	25	26	26	27	0.2842	0.1447
27	60	25	27	27	28	1.0590	0.9337
28	60	20	28	28	29	0.8042	0.7006
29	120	70	29	29	30	0.5075	0.2585
30	200	600	30	30	31	0.9744	0.9630
31	150	70	31	31	32	0.3105	0.3619
32	210	100	32	32	33	0.3410	0.5302
33	60	40	–	–	–	–	–

A.1 Simulation data for the 33-bus radial distribution network

The 33-bus radial distribution network consists of a single feeder connected to one substation. Bus 1 is the substation bus, with all other buses designated as load buses. The simulation data for this network is sourced from [98]. Detailed bus and line data for the network are presented in Table A.1. The network operates with a base capacity of 100 MVA and a base voltage of 12.66 kV. The single-line diagram of the 33-bus network is provided in Fig. A.1.

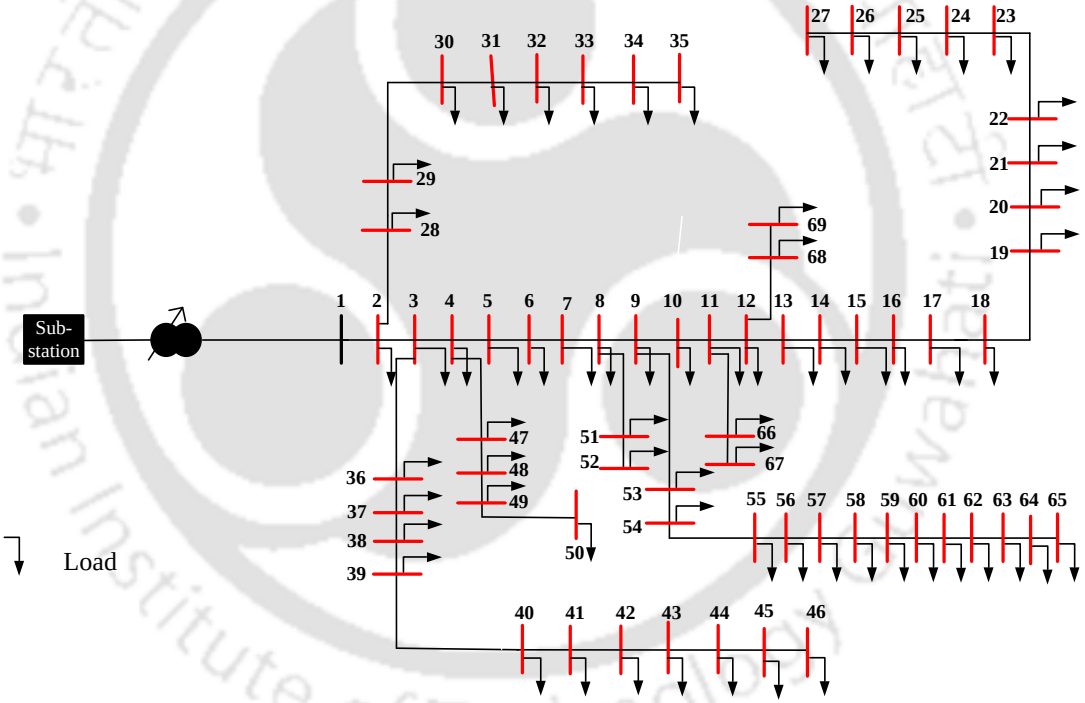

Fig. A.2: 69-bus distribution network

A.2 Simulation data for the 69-bus radial distribution network

The 69-bus radial distribution network comprises a single feeder connected to a substation. In this network, Bus 1 serves as the substation bus, with all other buses designated

Table A.2: Line data of the 69-bus distribution network

From Bus	To Bus	Resistance (Ω)	Reactance (Ω)	From Bus	To Bus	Resistance (Ω)	Reactance (Ω)
1	2	0.0005	0.0012	3	36	0.0044	0.0108
2	3	0.0005	0.0012	36	37	0.0640	0.1565
3	4	0.0015	0.0036	37	38	0.1053	0.1230
4	5	0.0251	0.0294	38	39	0.0304	0.0355
5	6	0.3660	0.1864	39	40	0.0018	0.0021
6	7	0.3810	0.1941	40	41	0.7283	0.8509
7	8	0.0922	0.0470	41	42	0.3100	0.3623
8	9	0.0493	0.0251	42	43	0.0410	0.0478
9	10	0.8190	0.2707	43	44	0.0092	0.0116
10	11	0.1872	0.0619	44	45	0.1089	0.1373
11	12	0.7114	0.2351	45	46	0.0009	0.0012
12	13	1.0300	0.3400	4	47	0.0034	0.0084
13	14	1.0440	0.3450	47	48	0.0851	0.2083
14	15	1.0580	0.3496	48	49	0.2898	0.7091
15	16	0.1966	0.0650	49	50	0.0822	0.2011
16	17	0.3744	0.1238	8	51	0.0928	0.0473
17	18	0.0047	0.0016	51	52	0.3319	0.1114
18	19	0.3276	0.1083	9	53	0.1740	0.0886
19	20	0.2106	0.0690	53	54	0.2030	0.1034
20	21	0.3416	0.1129	54	55	0.2842	0.1447
21	22	0.0140	0.0046	55	56	0.2813	0.1433
22	23	0.1591	0.0526	56	57	1.5900	0.5337
23	24	0.3463	0.1145	57	58	0.7837	0.2630
24	25	0.7488	0.2475	58	59	0.3042	0.1006
25	26	0.3089	0.1021	59	60	0.3861	0.1172
26	27	0.1732	0.0572	60	61	0.5075	0.2585
3	28	0.0044	0.0108	61	62	0.0974	0.0496
28	29	0.0640	0.1565	62	63	0.1450	0.0738
29	30	0.3978	0.1315	63	64	0.7105	0.3619
30	31	0.0702	0.0232	64	65	1.0410	0.5302
31	32	0.3510	0.1160	11	66	0.2012	0.0611
32	33	0.8390	0.2816	66	67	0.0047	0.0014
33	34	1.7080	0.5646	12	68	0.7394	0.2444
34	35	1.4740	0.4873	68	69	0.0047	0.0016

Table A.3: Load data of the 69-bus distribution network

Bus No.	Active Power (kW)	Reactive Power (kVAr)	Bus No.	Active Power (kW)	Reactive Power (kVAr)
1	0	0	36	26	18.55
2	0	0	37	26	18.55
3	0	0	38	0	0
4	0	0	39	24	17
5	0	0	40	24	17
6	2.6	2.2	41	1.2	1
7	40.4	30	42	0	0
8	75	54	43	6	4.3
9	30	22	44	0	0
10	28	19	45	39.22	26.3
11	145	104	46	39.22	26.3
12	145	104	47	0	0
13	8	5	48	79	56.4
14	8	5.5	49	384.7	274.5
15	0	0	50	384.7	274.5
16	45.5	30	51	40.5	28.3
17	60	35	52	3.6	2.7
18	60	35	53	4.35	3.5
19	0	0	54	26.4	19
20	1	0.6	55	24	17.2
21	114	81	56	0	0
22	5	3.5	57	0	0
23	0	0	58	0	0
24	28	20	59	100	72
25	0	0	60	0	0
26	14	10	61	1244	888
27	14	10	62	32	23
28	26	18.6	63	0	0
29	26	18.6	64	227	162
30	0	0	65	59	42
31	0	0	66	18	13
32	0	0	67	18	13
33	14	10	68	28	20
34	19.5	14	69	28	20
35	6	4	-	-	-

as load buses. The simulation data for the 69-bus network is obtained from [99]. The bus and line data are detailed in Tables A.3 and A.2, respectively. The network operates with a base power of 10 MVA and a base voltage of 12.66 kV. The single-line diagram of the 69-bus network is provided in Fig. A.2.

List of Publications

Journal Publications:

1. Vamsi Priya Goli and Sanjib Ganguly, "Multi-swarm surrogate model assisted PSO algorithm to minimize distribution network energy losses," *Applied Soft Computing* (Elseveir), vol. 159, p. 111616, 2024. (DOI: https://doi.org/10.1016/j.asoc.2024.111616)

2. Vamsi Priya Goli and Sanjib Ganguly, "Cost-Benefit Analysis of Multiple Shunt Compensators Allocation in PV-Integrated Distribution Networks for Profit Maximization," *Electric Power Components and Systems* (Taylor & Francis), 2024. (In Press) (DOI: https://doi.org/10.1080/15325008.2024.2309226)

3. Vamsi Priya Goli and Sanjib Ganguly, "Energy Loss Minimization for Photovoltaic Integrated Distribution Networks with the Optimal Placement of Multiple Shunt Compensators," *Energy Systems* (Springer), 2024. (Accepted)

Conference Publications:

1. Vamsi Priya Goli and Sanjib Ganguly, "Multi-Objective Optimisation Approach for Energy Loss Minimization of Distribution Networks using Single Series and Multiple Shunt Compensators," in *2022 IEEE Calcutta Conference (CALCON)*, Calcutta, India, pp. 117–121, 2022.

2. Vamsi Priya Goli and Sanjib Ganguly, "Modelling of series and multiple shunt com-

pensators to minimize power losses in Photovoltaic integrated power distribution networks," in *2023 IEEE Guwahati Subsection Conference (GCON)*, Guwahati, India, pp. 1–5, 2023.

3. Vamsi Priya Goli and Sanjib Ganguly, "Optimal allocation of series and multiple PV-integrated shunt compensators to minimize power loss and under-voltage nodes of radial distribution networks," in *2023 11th National Power Electronics Conference (NPEC)*, Guwahati, India, pp. 1–6, 2023.

Journals Under Review:

1. Vamsi Priya Goli and Sanjib Ganguly, "Operational Optimization of BESS and Shunt Compensators for Simultaneous Optimization of Energy Losses and Photovoltaic Hosting Capacity in Radial Distribution Networks," *Journal of Energy Storage* (Elseveir), 2024. (Under Review)

2. Vamsi Priya Goli and Sanjib Ganguly, "Economic Assessment of Multiple Shunt Compensators Allocation in Photovoltaic Integrated Power Distribution Networks," *IET journal of Energy Conversion and Economics*, 2024. (Under Review)

Author's Biography

Vamsi Priya Goli (Student Member, IEEE) received her undergraduate degree in Electrical and Electronics Engineering at JNTU College of Engineering, Vizianagaram, India, in 2018. She obtained her Master's degree in Power Electronics and Power Systems from the National Institute of Technology Goa, India, in 2020. She is pursuing her doctoral degree at the Department of Electronics and Electrical Engineering, Indian Institute of Technology Guwahati. Her research interests include custom power devices, distributed generation, distribution network planning and optimization, multi-objective optimization, and evolutionary algorithms.